Synthesis, electrochemical, kinetic and thermodynamic properties of new ferrocene-containing betadiketonato rhodium(I) complexes with biomedical applications

A dissertation submitted in accordance with the requirements for the degree

Magister Scientiae

in the

Department of Chemistry

Faculty of Science

at the

University of Free State

by

Palesa Klaas

Supervisor

Prof. J.C. Swarts

Co-supervisor

Dr. J. Conradie

November 2002

Acknowledgements

My sincere gratitude to God Almighty for His grace, strength and wisdom that carried me through this study.

I would like to thank my supervisor, Prof. J.C. Swarts, for the support, excellent guidance and the valuable time devoted in the course of this study. To my co-supervisor, Dr. J. Conradie, I thank her for the willingness to render assistance whenever called upon.

I am most grateful to my parents and family for their prayers, concern and valuable encouragement during the years of my study. To my friend and colleagues for the support they showed, I am grateful.

I wish to acknowledge the National Research Foundation for the financial support over the period of this study.

Palesa Klaas

Contents

List of Abbreviations

Ligands

CO	carbonyl ligand or carbon monoxide
cod	1,5-cyclooctadiene
Fc	ferrocenyl ligand
Fc^+	ferrocenium
Hacac	2,4-pentanedione, acetylacetone
Hba	1-phenyl-1,3-butanedione
Hbfcm	1-ferrocenyl-3-phenyl-1,3-propanedione
Hbzaa	3-benzyl-2,4-pentanedione
Hcupf	N-hydroxy-N-nitroso-benzeneamine, cupferron
Hdbm	1,3-diphenyl-1,3-propanedione
Hdfcm	1,3-diferrocenyl-1,3-propanedione
Hdfhd	1,1,1,2,2,3,3,7,7,7-decafluoro-4,6-heptanedione
Hdmavk	dimethylaminovinylketone
Hfca	1-ferrocenyl-1,3-butanedione
Hfch	2-ferrocenoyl-1-etanal
Hfcdma	1-ferrocenyl-5-methyl-1,3-pentanedione
Hfcp	1-ferrocenyl-1,3-pentanedione
Hfctca	1-ferrocenyl-4,4,4-trichloro-1,3-butanedione
Hfctfa	1-ferrocenyl-4,4,4-trifluoro-1,3-butanedione
Hfctma	1-ferrocenyl-5,5-dimethyl-1,3-pentanedione
Hfod	1,1,1,2,2,3,3-heptafluoro-7,7-dimethyl-4,6-octanedione
Hhfaa	1,1,1,5,5,5-hexafluoro-2,4-pentanedione
Hpta	1,1,1-trifluoro-5,5-dimethyl-2,4-hexanedione
Hsacac	thioacetylacetone
Htfaa	1,1,1-trifluoro-2,4-pentanedione
Hthd	2,2,6,6-tetramethyl-3,5-heptanedione
Htmhd	2,6-dimethyl-3,5-heptanedione
Htrop	tropolone
Htta	2-thenoyltrifluoroacetone
L-L'-BID	mono anionic bidentate ligand
phen	1,10-phenanthroline
PEt_3	triethylphosphine
PPh_3	triphenylphosphine

Solvents

CH_3CN	acetonitrile
DMF	dimethyl formamide
DMSO	dimethyl sulfoxide
THF	tetrahydrofuran

Spectroscopy

A	absorbance
ε	molar extinction coefficient
ν(C=O)	infrared stretching frequency of carbonyl
IR	infrared spectroscopy
NMR	nuclear magnetic resonance
pK_a	-log K_a, K_a = acid dissociation constant
T	temperature
UV/Vis	ultraviolet/visible spectroscopy

Cyclic voltammetry

CV	cyclic voltammetry
$E^{o/}$	formal reduction potential
E_{pa}	peak anodic potential
E_{pc}	peak cathodic potential
ΔE_p	difference of peak anodic and peak cathodic potentials
i_{pa}	peak anodic current
i_{pc}	peak cathodic current
$TBAPF_6$	tetrabutylammonium hexafluorophosphate

Cytotoxic studies

A_{2780}	human ovarian cancer cell line
DNA	deoxyribonucleic acid
HeLa	human cervix epitheloid cancer cell line
IC_{50}	mean drug concentration causing 50% cell death
PHA	phytohaemaglutin stimulated human mononuclear lymphocytes

List of figures

List of schemes

List of tables

CHAPTER 1

INTRODUCTION

1.1 The platinum group metals in catalytic processes

Rhodium, iridium, palladium, platinum, silver and gold are commonly known as the platinum group metals. The chemistry[1] of these elements have common features, but there are also wide variations including different stabilities of oxidation states and stereochemistry. There is little similarity to cobalt, copper and nickel except in some compounds of π-acid ligands such as CO and in stoichiometries of compounds. Platinum group metals have a strong tendency to form bonds to carbon, especially with alkenes and alkynes.

These metals, especially rhodium, iridium, palladium and platinum are extensively used as catalysts in industry. The catalytic fume converters in use in automobile exhausts use platinum metal as catalyst. One of the biggest uses of Pt is as Pt-Re or Pt-Ge on alumina catalysts in the production of crude petroleum from methane gas. Both palladium and platinum are capable of absorbing large volumes of molecular hydrogen. Complexes of the platinum group metals are mostly used in homogeneous catalytic processes such as hydroformylation and alcohol carbonylation. This is a consequence of these metals being capable of undergoing oxidative addition reactions with e.g. alkyl halides and also CO insertion reactions. In comparing the activities of various metal carbonyls in hydroformylation reactions, rhodium carbonyls show a very high activity. Rhodium carbonyls are approximately a thousand times more active than cobalt carbonyls, the second most active metal carbonyl in CO insertion reactions.[2] The catalytic cycle of hydroformylation[2] of C_2H_4 by $HRh(CO)_3$ to produce CH_3CH_2CHO, (the oxo process) serves as an example:

$$H_2C{=}CH_2 + HRh(CO)_3 \longrightarrow C_2H_5Rh(CO)_3$$
$$C_2H_5Rh(CO)_3 + CO \longrightarrow C_2H_5CORh(CO)_3$$
$$C_2H_5CORh(CO)_3 + H_2 \longrightarrow C_2H_5CORh(H_2)(CO)_3$$
$$C_2H_5CORh(H_2)(CO)_3 \longrightarrow C_2H_5CHO + HRh(CO)_3$$

1.2 The platinum group metals in medical applications

Cisplatin, $[Pt(NH_3)_2Cl_2]$, one of the most widely used metal-containing chemotherapeutic drugs,[3] has been found to have many side effects during chemotherapy. These include the inability to distinguish between healthy and cancerous cells,[4] high toxicity to the kidney and bone marrow,[5]

loss of appetite,[6] high rate of excretion from the body,[7] low aqueous solubility and development of drug resistance after continued drug dosage.[8] More recent studies have characterised some aspects of antineoplastic properties of co-ordination metal complexes, other than platinum compounds. The compounds examined include rhodium(I) and iridium(I) derivatives of the type $[M(chel)(L\text{-}L)]^{+/0}$ (chel = pyridinalimine (N-N-R), acetylacetonate; L-L = 1,5-hexadiene, 1,5-cyclooctadiene, norbornadiene) on mouse Lewis lung carcinoma.[9] It was also found that complexes of rhodium(I) are more active than the corresponding isomorph of iridium(I) complexes. A significant increase in the antitumour activity was also obtained with $[Rh^{I}(chel)(L\text{-}L)]^{+/0}$ complexes having a acetylacetonato moiety instead of chelating agents, (chel), such as piperidine, bipyridine and phenanthroline.[10, 11, 12] The presence of the diolefenic ligand, (L-L), 1,5-cyclooctadiene, conferred more favourable antitumour properties than norbornadiene and 1,5-hexadiene.[11] This discovery raised a question if antitumour activity of rhodium(I) can further be increased by small variations in the β- diketonato ligands in rhodium complexes of the type $[Rh^{I}(\beta\text{-diketonato})(cod)]$.

1.3 Metallocenes in anticancer applications

In 1984 Kopf-Maier reported on the antineoplastic activity of some ferricenium salts against Ehrlich Ascites tumour cell lines, which are very resistant to classical antitumour agents.[13, 14] Some of these ferricenium salts showed more favourable 50% lethal dosage (LD_{50}) values than cisplatin. Experiments involving the combination of ferricenium tetrachloroferrate and cisplatin showed the combination of the effects of the drugs to be additive.[15] Tests involving combinations of platinum complexes and other chemotherapeutic drugs, showed highly desirable synergistic activity (therapeutic effects better than adding the individual effects of each component in the drug mixture) during the treatment of mice with advanced L1210 leukaemia.[16]

Molecules with a rhodium(I) and ferrocenyl fragment within the same molecule hold the promise of displaying synergistic effects in chemotherapy without the need of administering two or more types of antineoplastic drugs simultaneously to a tumour-bearing mammal. Hence, new ferrocene containing rhodium(I) complexes have been synthesised, characterised and evaluated as antineoplastic agents in this laboratory.[17] These complexes were of the type [Rh(FcCOCHCOR)(cod)] with R = CH_3, CF_3, CCl_3, Ph (phenyl) and Fc (ferrocenyl). The CF_3 analogue was by far the best complex evaluated to date. A need still remains to investigate other

metallocene-containing β-diketonato complexes with different metallocenes and other R groups to find the rhodium(I) complex with the best chemotherapeutic activity.

1.4 Aims of this study

Considering this background, the following goals were set for this study:

(a) The synthesis of new ferrocene containing β-diketones of the type $FcCOCH_2COR$, with Fc = ferrocenyl and R =H, CH_3, CH_2CH_3, $CH(CH_3)_2$ and $C(CH_3)_3$

(b) The complexation of β-diketones with $[Rh_2Cl_2(cod)_2]$ giving complexes of the type [Rh(FcCOCHCOR)(cod)]

(c) The determination of the group electronegativities of CH_2CH_3, $CH(CH_3)_2$ and $C(CH_3)_3$

(d) The characterisation of β-diketone ligands in terms of pK_a-values, keto-enol equilibrium constants and the rate of conversion between keto and enol isomers.

(e) An electrochemical study utilising cyclic voltammetry to determine the formal reduction potentials of the iron core and of the rhodium(I) nucleus in the free β-diketones and in the complexes [Rh(FcCOCHCOR)(cod)]

(f) To study the kinetics of substitution of $(FcCOCHCOR)^-$ with 1,10-phenanthroline from [Rh(FcCOCHCOR)(cod)] complexes using stopped-flow techniques.

(g) The determination of the cytotoxic properties of the new ligands and rhodium(I) complexes of goals (a) and (b).

(h) The determination of the relationships between the physical quantities such as group electronegativities, rate constants, reduction potentials, pK_a-values and carbonyl stretching frequencies.

1.5 References

[1] Cotton, F.A., Wilkinson, G. and Gaus, P.L., *Basic Inorg. Chem.*, John Wiley & Sons, New York, 1976, **3rd Ed,** 597.

[2] Imyanitov, N.S., *Rhodium Express*, **8-11,** 11 (1995).

[3] Sherman, S.E. and Lippard, S.J., *Chem. Rev.*, **87,** 1153 (1987).

[4] Woodsman, R.J., Venditti, J.M. and Schepartz, S.A., *Proc. Am. Assoc.Cancer Res.*, **12,** 24 (1971).

[5] Rozenswerg, M., van Hoff, D.D., Slavik, M. and Chrisholm, J., *Ann. Int. Med.*, **86,** 803 (1977).

[6] Burchenal, J.H., Kalaher, K., O'Toole, T. and Chrislom, J., *Cancer Res.*, **37,** 3455 (1977).

[7] Drobnik, J. and Horacek, P., *Chem-Bio. Interact.*, **7,** 223 (1973).

[8] Wolf, W. and Manaka, R.C., *J. Clin. Hemotol. Oncol.*, **7,** 79 (1977).

[9] Sava, G., Zorzet, S. and Perissin, L., *Inorg. Chim. Acta,* **137,** 69 (1987)

[10] Giraldi, T., Sava, G., Bertoli, G. and Menstroni, G., *Cancer Res.,* **37,** 2662 (1977).

[11] Giraldi, T., Sava, G., Menstroni, G., Zassinovich, G. and Stolfa, D., *Chem. Biol. Interact.,* **22,** 231 (1978).

[12] Giraldi, T., Sava, G., Menstroni, G. and Zassinovich, G., *Chem. Biol. Interact.,* **9,** 389, (1974).

[13] Kopf-Maier, P., Kopf, H. and Neuse, E.W., *Cancer Res. Clin. Incol.,* **108,** 336 (1984).

[14] Kopf-Maier, P.Z, Naturforsch.C. Biochem. Biophys. Biol. Virol., **40C,** 843 (1985).

[15] Neuse, E.W. and Kanzawa, *Appl. Organomet. Chem.,* **4,** 19 (1990).

[16] Gale, G.R., Atkins, L.M. and Meischen, S.J., *Cancer Treat. Rep.*, **61,** 445 (1977).

[17] Swarts, J.C. and van Rensburg, C.E.J., Provisional P.C.T. country patent, deposit no. 2007167 for Dec 2001.

CHAPTER 2

LITERATURE SURVEY AND FUNDAMENTAL ASPECTS

2 The chemistry of β-diketones

2.1.1 Synthesis

Under certain conditions, a ketone having an α-hydrogen atom may be acylated with an ester, an acid anhydride, or an acid chloride to form a β-diketone.[1] The reaction, also known as Claisen condensation, involves the replacement of an α-hydrogen atom of a ketone by an acyl group:

$$RCOX + HCH_2COR \longrightarrow RCOCH_2COR + HX$$

(X = OR, OCOR, Cl)

The acylation of ketones may also result in oxygen acylation rather than carbon acylation to form O-acyl derivatives. These may be rearranged thermally to give a β-diketone.[2] Although Lewis acids such as BF_3 can be used to promote β-diketone formation, the acylation of ketones with esters is generally affected by means of a basic reagent such as sodium ethoxide, sodium amide,[3] sodium hydride[4] or sodium, a process that probably involves a three-step ionic mechanism. For example, the condensation of acetone with ethyl acetate[1] utilising sodium ethoxide or sodium amide as the basic initiator, involves in the first step the removal of a α-hydrogen of the ketone to form the acetonato anion. The second step may be formulated as the addition of the acetonato anion to the carbonyl carbon of the ethyl acetate, followed by the release of the ethoxide anion to form acetylacetone.

$$CH_3COCH_3 + Na^{+-}OC_2H_5 \rightleftharpoons Na^+(CH_2COCH_3)^- + C_2H_5OH \qquad (1)$$

$$\begin{array}{l} Na^+(CH_2COCH_3)^- \\ + \\ CH_3COOC_2H_5 \end{array} \rightleftharpoons \begin{array}{l} O^-Na^+ \\ | \\ CH_3CCH_2COCH_3 \\ | \\ OC_2H_5 \end{array} \rightleftharpoons \begin{array}{l} CH_3COCH_2COCH_3 \\ + \\ Na^{+-}OC_2H_5 \end{array} \longrightarrow \begin{array}{l} Na^+(CH_3COCH_2COCH_3)^- \\ + \\ C_2H_5OH \end{array} \qquad (2)$$

With ethoxide anion, the equilibrium in the first step is probably on the side of the unchanged ketone (i.e. to the left). However, with $NaNH_2$, an equivalent of ketone is converted essentially completely to its anion and ammonia, NH_3, is produced rather than ethanol, C_2H_5OH. The pK_a of β-diketones is so low (e.g. pK_a of Hacac is 8.95) that it is invariably isolated as the salt (see final step in (2)) and must be regenerated by acidification.

The equilibrium of the overall reaction is shifted in the direction of the condensation product by the precipitation of the β-diketone as its sodium salt. When sodium ethoxide is used as the condensing agent, the equilibrium may be shifted still further in the same direction (i.e. to the right) through the removal by distillation of the alcohol formed during the reaction. The presence of excess sodium amide, compared with the amount of ketone used, as illustrated in **Table 2.1** has been found to have a favourable influence on the yield of the β-diketone. The yields of β-diketones with two equivalents of sodium amide to one equivalent of ketone are twice those compared with equivalents of the base and ketone.

Table 2.1: Yields of β-diketones[3] from ethyl esters and methyl ketones in the presence of sodium amide

Ethyl Ester, moles	Ketone/ 0.3 mol	$NaNH_2$/ mol	β-diketone	Yield/ %
Propionate, 0.3	Methyl ethyl	0.3	Dipropionylmethane	30
Propionate, 0.6	Methyl ethyl	0.6	Dipropionylmethane	57
n-Butyrate, 0.3	Methyl n-propyl	0.3	Dibutyrylmethane	33
n-Butyrate, 0.6	Methyl n-propyl	0.6	Dibutyrylmethane	68
n-Butyrate, 0.3	Methyl isobutyl	0.3	Butyrylisovalerylmethane	44
n-Butyrate, 0.6	Methyl isobutyl	0.6	Butyrylisovalerylmethane	80

It can also be observed that the ester reacts mainly with the ketone anion rather than an extra equivalent of amide ion. The evolution of ammonia when sodium amide is used, may not be particularly important, since the amide ion is strong enough to convert most ketones completely to their anions. Hauser and Adams[3] reported that sodium amide is superior as compared to either sodium metal or sodium ethoxide for the acylation of aliphatic methyl ketones with aliphatic esters other than ethyl acetate.

For the preparation of a ferrocene-containing β-diketone, $FcCOCH_2COCH_3$, (Hfca[5], with Fc = ferrocenyl), the use of the sterically hindered base lithium diisopropylamide, $LiNPr^i_2$, was favoured. The chemistry behind the use of this base is similar to the one of the other bases described above, except that higher yields of Hfca were obtained with $LiNPr^i_2$ and the reaction was faster than the alkoxide method.

2.1.2 Keto-enol tautomerism

Although β-diketones are commonly represented in the ketonic form, most of them exist as keto and enol isomers, which are in equilibrium with each other. The enol isomer can exist as two tautomers and are stabilised by a hydrogen bridge as shown on **Scheme 2.1**. Structurally the enol form possess a *cis* configuration and a *syn* conformation and is pseudo aromatic. The kinetics of conversion from one enol form to the other is very fast, with a rate constant approaching 10^6 s^{-1}. Kwon and Moon[6] investigated this conversion in selected β-diketones using ^{17}O NMR. It was observed that the equilibrium constant is highly dependent on the character and the position of the R groups.

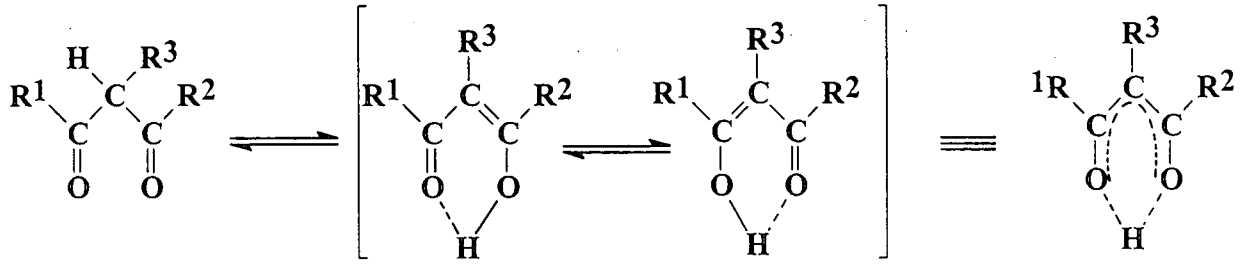

Keto form **Enol forms**

Scheme 2.1: Schematic representation of tautomerism of β-diketones with the enol forms showing pseudo aromatic character

The hydrogen atom of the CHR^3 group (a substituted methine group) in the keto form is very acidic because of the adjacent withdrawing C=O groups. Observed pK_a' values for several β-diketones are listed in **Table 2.2**. The keto-enol tautomerism of a wide variety of β-diketones has been studied over many years, by techniques such as bromine titration,[7] polarographic measurements,[8] energy of enolization,[9, 10] UV,[11] infra red[12] and NMR spectroscopy. [13, 14] It has been generally accepted that the enolic form is favoured in non-polar solvents and simultaneous conjugation and chelation through hydrogen bonding is responsible for the stability of the enol tautomer. From a ^1H NMR study recently performed by Du Plessis,[15] the percentages of enolised tautomers in deuterated chloroform solutions of some β-diketones were found to be very high (> 85%) (**Table 2.2**).

Table 2.2: pK_a values and % enol tautomers of various β-diketones.

β-Diketones	R^1	R^2	pK_a'	% Enol
Hacac	CH_3	CH_3	8.95[15]	91
Htfaa	CH_3	CF_3	6.30[16]	>99
Hba	CH_3	C_6H_5	8.55[15]	92
Hdbm	C_6H_5	C_6H_5	9.35[16]	>99
Hhfaa	CF_3	CF_3	4.43[16]	100
Htmhd	$CH(CH_3)_2$	$CH(CH_3)_2$	11.77[17]	98
Hfca	Fc	CH_3	10.01[15]	86
Hfctfa	Fc	CF_3	6.53[15]	>99
Hbfcm	Fc	C_6H_5	10.41[15]	≈95
Hdfcm	Fc	Fc	13.1[15]	>99

The proportion of the enol tautomers generally increases when an electron withdrawing group, for example, fluorine, is substituted for hydrogen at an α-position relative to a carbonyl group in β-diketones, or when the ligands contain an aromatic ring.[18] Substitution by a bulky group such as an alkyl, at α-position tend to produce steric hindrance between R^3 and R^1 (or R^2) groups (**Scheme 2.1**) particularly in the enol tautomer, and this together with inductive effects of the alkyl groups often brings about a large decrease in the enol proportion.[19]

Regarding β-diketones with a ferrocenyl group, enolization in solution was found to be predominantly away from the aromatic ferrocenyl group. Two different driving forces that control the conversion from β-diketone into an enolic isomer were postulated.[15] These forces were labelled as electronic- and resonance driving forces. In the former, the formation of the preferred enol isomer is controlled by the electronegativity of the R^1 and R^2 substituents on the β-diketone:

$$R^1\text{–(HO)C=CH–CO–}R^2 \rightleftharpoons R^1\text{–CO–CH}_2\text{–CO–}R^2 \rightleftharpoons R^1\text{–CO–CH=C(OH)–}R^2$$

(I) **(k)** **(II)**

When the electronegativity of R^1 is greater than that of R^2 the carbon atom of the carbonyl group adjacent to R^2 on the β-diketone, **k**, will be less positive in character than the carbon atom of the other carbonyl, implying that enol **(II)** will dominate. However, many β-diketones were described that did not follow the enolisation pattern predicted by the electronic driving force.[15, 22] All the cited exceptions had aromatic R^1 or R^2 side groups and hence it was stated that the electronic driving force will always take second priority compared with the resonance driving force.

The resonance driving force implies that the formation of different canonical forms of a specific isomer will lower the energy of this specific isomer enough to allow it to dominate over the existence of other isomers that may be favoured by electronic effects.

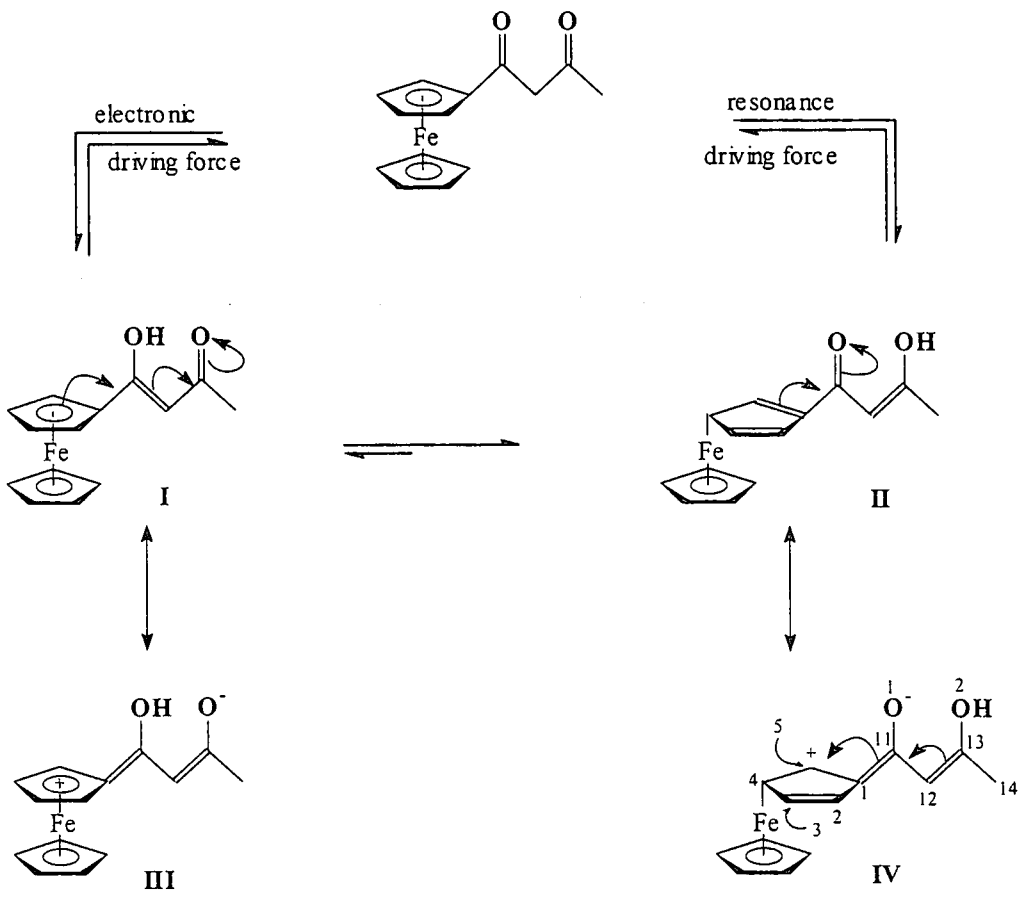

Scheme 2.2: Electronic considerations in terms of electronegativity, χ (χ_{methyl} = 2.34, $\chi_{ferrocenyl}$ = 1.87), favour I as the enol form of Hfca. However, structure II was shown by crystallography and NMR spectroscopy to be dominant, implying that the equilibrium between I and II lies far to the right. A dihedral angle of 4.9(2)° between aromatic ferrocenyl group and the pseudo-aromatic β-diketone core implies that the energy lowering canonical forms such as IV make a noticeable contribution to the overall existence of Hfca. For clarity, the ferrocenyl group in II and IV is shown just in canonical forms but in both cases the iron atom can be bound in any of the five cyclopentadienyl carbon atoms as indicated in I. Likewise, the positive charge of IV is not confined to the single position shown, but rather oscillates between C(2) and C(5) (it cannot be on C(1), atom numbers are indicated to individual atoms) to give rise to four different canonical forms as indicated in III.

Indirect evidence for the existence of these canonical forms is found in crystal structure determinations of the enol forms of Hfctfa[20] and Hfca[21] as discussed elsewhere.[15, 20] The two cited examples cover the cases where the group electronegativity, χ_R, of R^1 and R^2 are fairly similar (in

Hfca) or very much different (in Hfctfa). This resonance driving force is valid when both R^1 and R^2 groups are aromatic groups or if one or neither R^1 nor R^2 are aromatic, provided resonance stabilisation via different canonical forms are still possible.

In addition, it was noted that under certain conditions the keto isomer of Hfca could be observed in large quantities by proton NMR, while under other conditions the keto isomer of the same compound is much less pronounced. The explanation for these apparent differences was postulated to the β-diketone concentration of the solution studied, because at very low concentration hydrogen-bonding stabilisation of the enol form should be absent. Although it has been shown that very low concentrations slightly favour the keto form in solution, this did not adequately explain why in some cases the keto form of concentrated solutions is observed in appreciable quantities (> 80%), while in other cases not (< 5%).[22] In a follow-up kinetic investigation it was found that the rate of conversion from keto to enol isomers for simple ferrocene-containing β-diketones is very slow ($t_{1/2}$ = 4.4 hours for Hfca). Many β-diketones are isolated by isolating the solid Li salt, R^1–CO–$\overline{C}$HLi$^+$–CO–R^2 from solution, followed by acidification. This means that the first product that is obtained during a synthetic procedure, must be the keto isomer, because the lithium salt exists as a keto isomer. If the ^{1}H NMR is obtained very quickly after isolation and acidification (i.e. within minutes), it follows that the keto content will be high. However, if the ^{1}H NMR is obtained several days after synthesis, time would have elapsed to allow conversion of the keto form to the equilibrium content. Consequently the keto form will be much less dominant. It is interesting to observe that in the solid state, the enol form is the only stable isomer (i.e. no keto form) for the ferrocene-containing β-diketones studied in reference 22, while in solution, the equilibrium positions allows keto isomers in percentages up to 32%.

Cyclic β-diketones have been shown to have different enolisation behaviour as compared to acyclic β-diketones. Acyclic enolised β-diketones form intra molecular hydrogen bonding while cyclic enolised β-diketones form inter molecular hydrogen bonding (**Figure 2.1**). The tendency for enolization is greater in cyclopentanediones than in cyclohexanediones.

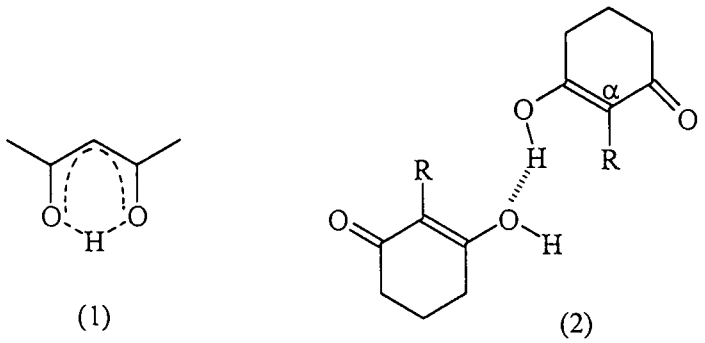

Figure 2.1: The structures of (1) acetylacetone demonstrating intra molecular hydrogen bonding of acyclic β-diketones and (2) R-substituted cyclohexanediones demonstrating inter molecular hydrogen bonding of cyclic β-diketones. Bulky R substituents on the α position of cyclic β-diketones discourage enolisation.

It is of importance to note that bulkier α-alkyl groups such as isopropyl and sec-butyl depress the percentage of enol form to zero, whereas smaller primary α-alkyl substituents favour enolization in cyclic β-diketones. The presence of a bulky α-group may be expected to force the carbonyl oxygen atoms of the cyclic β-diketone further apart from each other thus causing distorted sp^2 hybridised orbital shapes and overlaps in the enol form, and hence disfavours enolisation. Yogev and Mazur[23] have shown that cyclohexanediones exist predominantly as the keto tautomers in very dilute solutions of non-polar solvents.

2.2 Metal β-diketonates

2.2.1 Introduction

Under appropriate conditions the enolic hydrogen atom of a β-diketonato ligand can be replaced by a metal cation to produce a six-membered pseudo-aromatic chelate ring (**Scheme 2.3**).

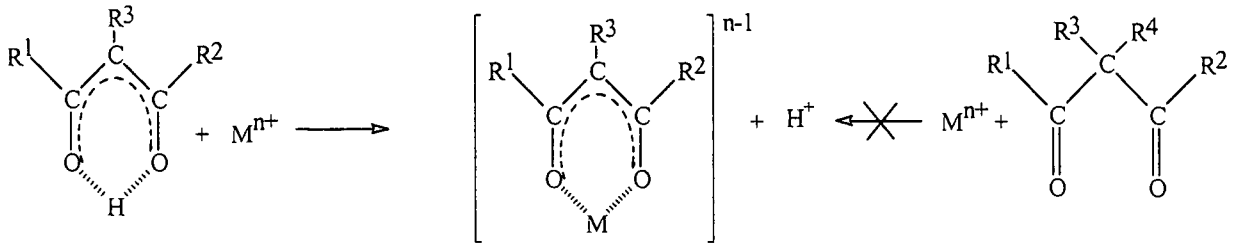

Scheme 2.3: Schematic representation of pseudo-aromatic chelate ring of metal β-diketonates, will only form only if the β-diketone is enolizable.

It should be noted that metal co-ordination is not possible if both hydrogen atoms of the methine carbon atom in β-diketones are replaced by an allyl or another group, (i.e. both R^3 and $R^4 \neq H$), because the β-diketone cannot exist in the enol form.

2.2.2. Classification of metal β-diketonates

Metal β-diketonates are classified based on the mode of binding between ligand and metal cation. The β-diketone may be bonded to the metal through the oxygen; the carbon; both carbon and oxygen and through the olefinic bond. The difference in the affinity of the metal for carbon, or for oxygen, is the main factor that determines the formation of different types of metal β-diketonato complexes.[24] An extensive study on oxygen-bonded β-diketonato complexes has shown that the β-ketonato anion $R^1COC(R^3)=C(R^2)O^-$ may act as a ligand in several ways, *viz.*, unidentate, bidentate and neutral ligand.

The β-ketonato ligand can act as a unidentate ligand to form simple salts with highly electropositive metals. An example[25] of such system is shown in **Figure 2.2**, whereby the silicon atom has adopted a tetrahedral conformation and the acetylacetonato is behaving as a unidentate ligand.

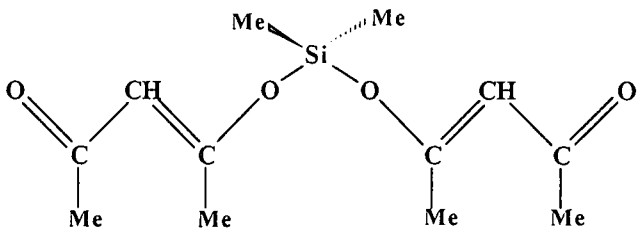

Figure 2.2: Behaviour of acetylacetonato as a unidentate ligand[25]

The second classification, which is the usual bonding mode of β-diketonato ligands, is shown in **Figure 2.3.** Here, a metal replaces the enolic hydrogen, forming a six-membered chelate ring and the β-diketonato now acts as a bidentate ligand. Based on physicochemical characteristics, the possibility of resonance forms for the anion, with resultant electron cloud delocalization in the resulting chelate ring can cause the ring to have a certain amount of aromatic character, hence the term "pseudo-aromatic" is used in this study.

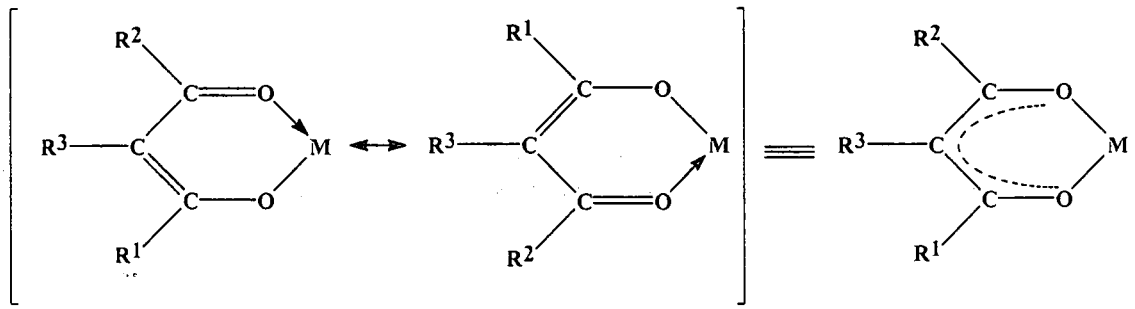

Figure 2.3: β-Ketonato as bidentate ligand

This type of oxygen bonding has been extensively studied. For example, the crystal structure[26] of [Rh(acac)(CO)(PPh_3)], **Figure 2.4** shows that the average C-C (1.392(12)Å), C-O (1.275(8)Å) and Rh-O (2.058(5)Å) bond distances of the β-diketone ring are approximately the same. This confirms a delocalization of electrons in the ring which supports the aromatic nature of the β-diketonato ring.

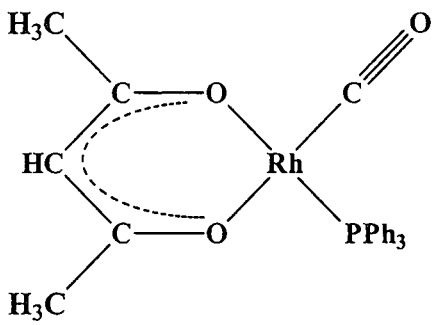

Figure 2.4: The structure of [Rh(acac)(CO)(PPh_3)]

In the above diagrams, all β-diketonato ligands had a –1 charge after H^+ abstraction.

Another class of oxygen bonded β-diketonato complexes is where the keto form act as neutral ligands. An example[27] of this rather rare bonding mode is [$Co(NH_3)_2(Hacac)_2$], **Figure 2.5**. Two neutral keto oxygens act as donor atoms forming an octahedral structure.

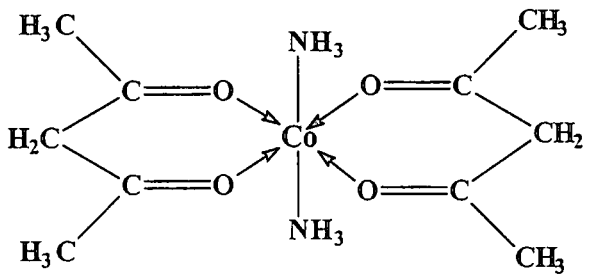

Figure 2.5: Acetylacetonato acting as a neutral ligand

Carbon-bonded β-diketonato complexes are usually those of non-metals,[28] sulphur, tellurium, selenium and metals, mercury[29] and gold.[30] In these complexes, the carbonyl groups do not participate in the bonding. Some examples are illustrated in **Figure 2.6**.

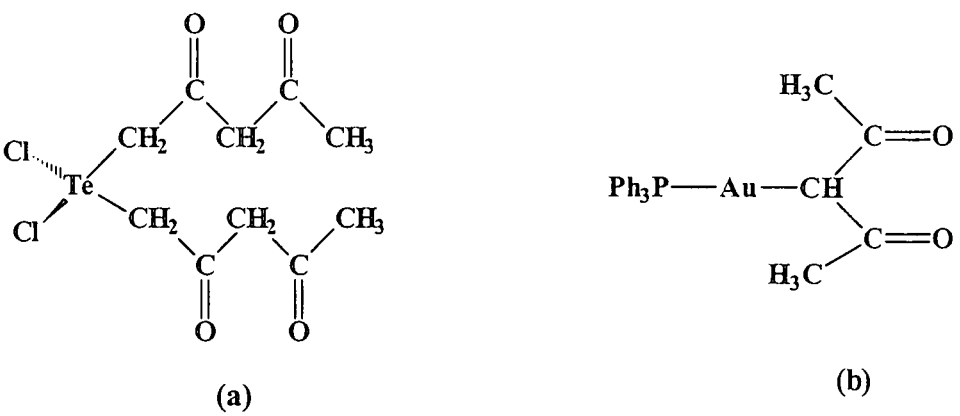

Figure 2.6: Structures of carbon-bonded β-diketonato complexes bonded to (a) a non-metal[31] and (b) a metal[30]

The metal-carbon bond in these complexes is quite stable since they were prepared in alkaline medium. However, certain factors have been found to influence the formation of carbon-bonded β-diketonato complexes. The electronegativities of the bonding groups have been found to play an influential role in the formation of carbon-bonded β-diketonato complexes. The presence of high electronegative groups in these complexes is known to favour their formation. Research results[32] show an increase in the formation of carbon-bonded complexes for 5d transition metals as compared to 4d transition state.

The last two classifications of metal β-diketonates in which the metal atom is bonded to the methine carbon of the β-diketonato ligand and in which the metal is bonded to the olefinic part of the β-

diketonato ligand as illustrated in **Figure 2.7** and **Figure 2.8** respectively. In both these cases, the mode of bonding is accompanied by M–O-bonding to a second β-diketonato ligand. The former class of compounds is also quite common, stable and soluble in organic solvents.

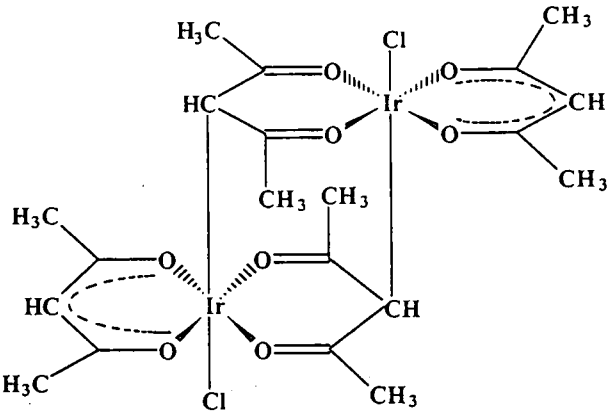

Figure 2.7: A simultaneously methine carbon-bonded and oxygen-bonded β-diketonato complex, $[Ir_2(acac)_4Cl_2]$[33]

Although no X-ray crystallographic evidence has yet been established for the existence of metal-olefin bonds in metal β-diketonates, it has been generally accepted that such bonding does exist.[34] These complexes are also soluble in organic solvents.

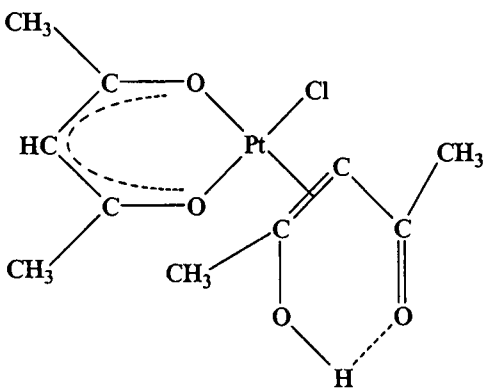

Figure 2.8: Hypothetical complex showing simultaneous oxygen-bonded and olefin bonded β-diketonato co-ordination[35]

2.2.3 Properties of the β-diketonato complexes

2.2.3.1 Physical properties

The most important physical properties of β-diketonates are those based on their volatility, thermal stability and vapour pressure. Conditions that influence these properties are given below:[36]

- The substitution of hydrogen with fluorine in the β-diketone ligand greatly increases the volatility and thermal stability of resultant β-diketonato complexes. For example,[37] the volatility characteristics of non-fluorinated β-diketonato complexes of the type $[Ln(RCOCHCOR')_3 \cdot nH_2O]$, (Ln = lanthanide) were found to be less than those of fluorinated complexes (**Table 2.3**) and hence the thermal stability decreases with non-fluorinated complexes.
- A decrease in solvation effects and interaction between molecules due to the effective shielding of the metal ions by ligands, increases their volatility. The larger the R and R′ groups on the β-diketonato ligand, the greater the stability of the complex and its volatility. This was observed in reactions[38] of the type

$$\underset{\text{more volatile}}{Ln(RCOCHCOR')_3(OH_2)} \rightarrow \underset{\text{less volatile}}{Ln(RCOCHCOR')_2OH} + RCOCH_2COR'$$

In hfaa chelates the above reaction occurs more readily than in dfhd chelates (abbreviations are described in **Table 2.3**). The bulkiness of the dfhd ligands results in some steric crowding and hence a lower reactivity, of the co-ordinated water molecule. This manifests a relatively greater stability of $Ln(dfhd)_3(OH_2)$ complex. **Table 2.3** also compares some complexes on this basis.

Table 2.3: Comparative effects of fluorination degree and ligand size in β-diketonato complexes of the type [Ln(RCOCHCOR′)$_3$·nH$_2$O], Ln = lanthanide

β-diketone	R	R′	Volatility characteristics
Hacac	CH_3	CH_3	Negligible volatile
Htfaa	CH_3	CF_3	Slightly volatile
Hhfaa	CF_3	CF_3	Sublimes with slight decomposition
Hpta	$C(CH_3)_3$	CF_3	Sublimes without decomposition
Hfod	$C(CH_3)_3$	n-C_3F_7	Sublimes easily without decomposition
Hthd	$C(CH_3)_3$	$C(CH_3)_3$	Sublimes easily without decomposition
Hdfhd	CF_3	n-C_3F_7	Sublimes with slight decomposition

- A decrease in the radius of the central metal ion increases the volatility of metal chelates for a given class of metals with a common ligand. Sievers and co-workers[39] observed an increase of chelate volatility with decreasing ionic radius of the trivalent metal ions for the complex [Ln(fod)$_3$], Ln = Sm, Eu, Gd, Tb, Dy, Ho, Er, Tm, Yb and Lu, and fod = $(H_3C)_3C$-$COCHCOC_3F_7$.
- The substitution of a group other than hydrogen in the α-position of the β-diketone ligand decreases the volatility and the thermal stability of metal chelates. For example,[40] substitution of the hydrogen atom in the α-position with bromine for the complex [Cr(acac)$_3$] to give [Cr(Br-acac)$_3$], reduced the volatility of the chelate. At about 200°C the [Cr(Br-acac)$_3$] complex was found to be decomposing instead of subliming.

2.2.3.2 Chemical Properties

Because metal β-diketonates possess pseudo-aromaticity, they are known to undergo electrophilic substitution reactions. However, steric hindrance has been observed to cause electrophilic substitution reactions to proceed sluggishly. The wide variety of electrophilic substitution reactions in the metal β-diketonato system can be classified under the following headings: halogenation,[41] nitration,[42] diazotization,[43] thiocyanation,[44] acylation,[45] formylation[46] and other electrophilic reactions.[47] The general reaction for the electrophilic substitution reaction is shown in **Figure 2.9**. The most widely studied β-diketonato chelates which undergo electrophilic substitution reactions, are those of the tris(β-diketonato) chelates of Co(III),[48] Cr(III)[49] and Rh(III),[46] which are kinetically

stable. Amongst a variety of β-diketonato systems studied, the most extensive investigations have been carried out on electrophilic substitution reactions of metal acetylacetonates.

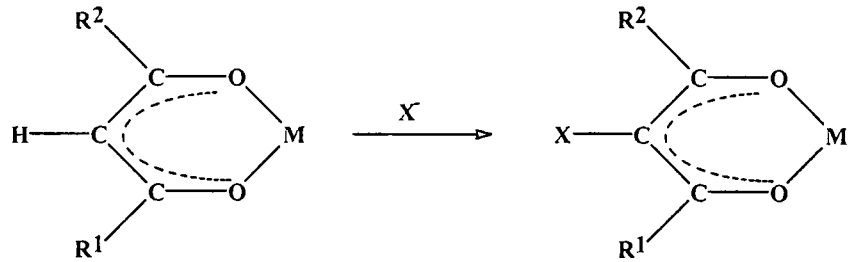

Figure 2.9: Electrophilic substitution of metal β-diketonates

2.2.4 Ferrocene-containing β-diketones and their rhodium(I) complexes

Studies[15] in this laboratory on different ferrocene-containing β-diketones of the type $FcCOCH_2COR$, with R = H, CH_3, CF_3, CCl_3, Ph and Fc have been conducted. These compounds were characterised by using ^1H NMR and cyclic voltammetry. Rhodium complexes of the type [Rh(FcCOCHCOR)(cod)] were obtained for these β-diketones by reaction with $[Rh_2Cl_2(cod)_2]$. Oxidative addition, insertion and substitution reactions were conducted on these rhodium complexes. The influence of the R group on rate constants, pK_a' values, formal reduction potentials and cytotoxicity activity, was also determined.

2.3 Substitution reactions of square-planar complexes

2.3.1 Introduction

Square planar metal complexes are complexes in which the metal has dsp^2-hybridized orbitals resulting in a planar geometry around the metallic nucleus for the ML_4 entity. Substitution reactions in such complexes occur by the replacement of a ligand (a leaving group) on the square-planar compound by a substituent (the incoming group) as also shown in the following scheme:

$$[L_nM\text{-}X] + Y \rightarrow [L_nM\text{-}Y] + X$$

where M = metal ion and L = ancillary non-participating kinetically inert ligand, X = the leaving group and Y = the entering group. Y can also be a solvent species. In ligand substitution reactions, the metal co-ordination number, the oxidation state and the number of valence electrons remain unchanged.

Substitution reactions or ligand exchange are usually divided into three main groups: nucleophilic substitutions, electrophilic substitutions and oxidative additions followed by reductive elimination.[50] By far the greatest number of known square-planar complexes are formed by transition metal ions with a d^8-electron configuration near the end of the transition series, for example, Rh(I), Ir(I), Pd(II), Pt(II) and Au(III). These reactions have been extensively studied, because they are normally fast and the availability of methods for following fast reactions, e.g. stopped-flow kinetic technique, has made it possible for a number of mechanistic studies of these complexes. Substitution reactions involve the transition between 18-electron and 16-electron species as encountered in catalytic processes.

2.3.2 Mechanisms of substitution reactions

There are three mechanisms by which substitution reactions can occur, namely dissociative mechanism, an associative mechanism, or a hybrid of these two, the so-called interchange processes.

2.3.2.1 Dissociative mechanism

This kind of mechanism resembles S_N1 substitution (in organic chemistry) whereby the leaving group first dissociates from the co-ordination sphere of the metal, thereby reducing the number of ligands bonded to the central metal ion. Thereafter, the entering group reacts with the newly formed transition state to form the final product.

$$[L_nM\text{-}X] \xrightarrow{k} [L_nM] + X \quad \text{(slow step)}$$

$$[L_nM] + Y \longrightarrow [L_nM\text{-}Y] \quad \text{(fast step)}$$

The intermediate (transition) state, $[L_nM]$, is co-ordinatively unsaturated and very reactive. Reactions involving dissociation may proceed either with retention of stereochemistry or with racemization, depending upon the rate of trapping of the intermediate by the incoming ligand.[51] **Scheme 2.4** illustrates the dissociative process for an octahedral complex. If the second step is very rapid, the 16-electron intermediate has no time to reorganise and $[L_nM\text{-}Y]$ has the same stereochemistry as $[L_nM\text{-}X]$. However, if the second step is slow, the first-formed square pyramidal structure may rearrange to a trigonal bipyramidal, which permits racemization.[51]

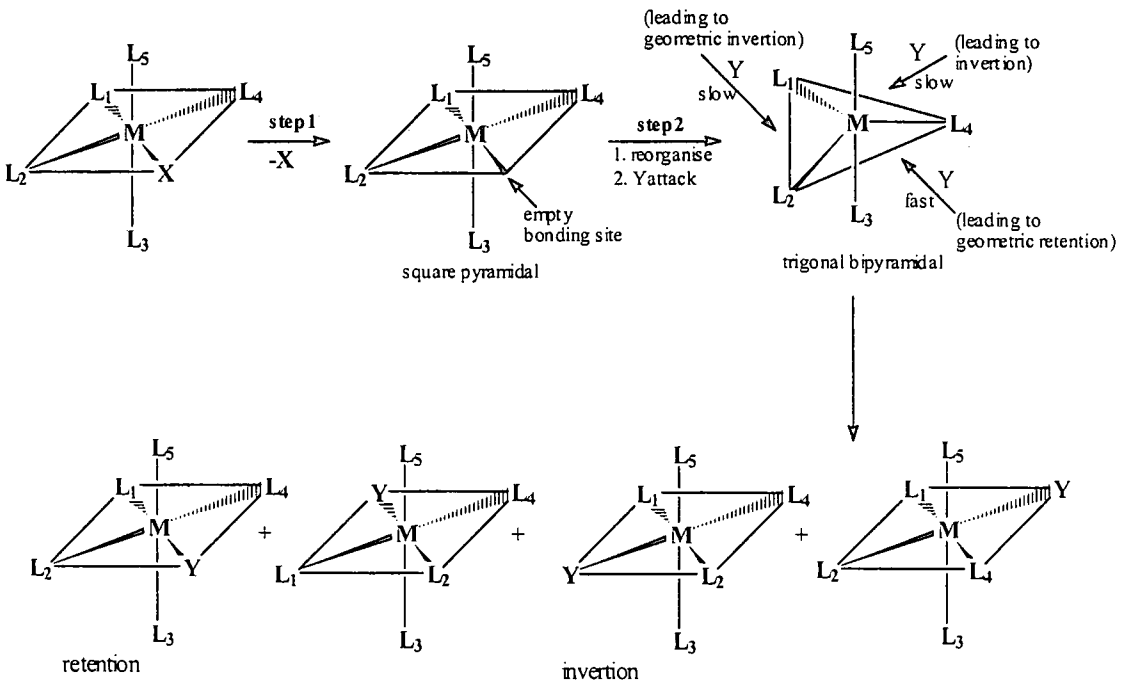

Scheme 2.4: A schematic representation of the stereochemistry of the product of a substitution reaction of an octahedral complex following a dissociative mechanism. A fast process result in retaining of stereochemistry, while with a slow process the first-formed square pyramidal structure may rearrange to a trigonal bipyramidal structure leading to inverted stereochemistry.

2.3.2.2 The associative mechanism

This mechanism resembles the S_N2 substitution reaction in organic chemistry. Associative mechanism is favoured for electron-deficient complexes (e.g. 16 or 17 electron compounds e.g. rhodium complexes) but is not totally excluded for 18 electron compounds.[51] In this mechanism, the incoming ligand initially attaches to the metal ion, leading to an intermediate with an increase in the number of co-ordinated ligands on the metal. This intermediate subsequently undergoes a further reaction to detach the leaving group to finally give the substituted product. The associative mechanism often involves solvent co-ordination, especially if the solvent is polar, or has a tendency

to solvate (e.g. acetonitrile or DMSO). However, if the solvent is non-polar or non-solvative (e.g. hexane), the substitution reaction proceed without solvent participation. **Scheme 2.5** summarises these two paths while at the same time attempt to visualise intermediates that are associated with an associative mechanism.

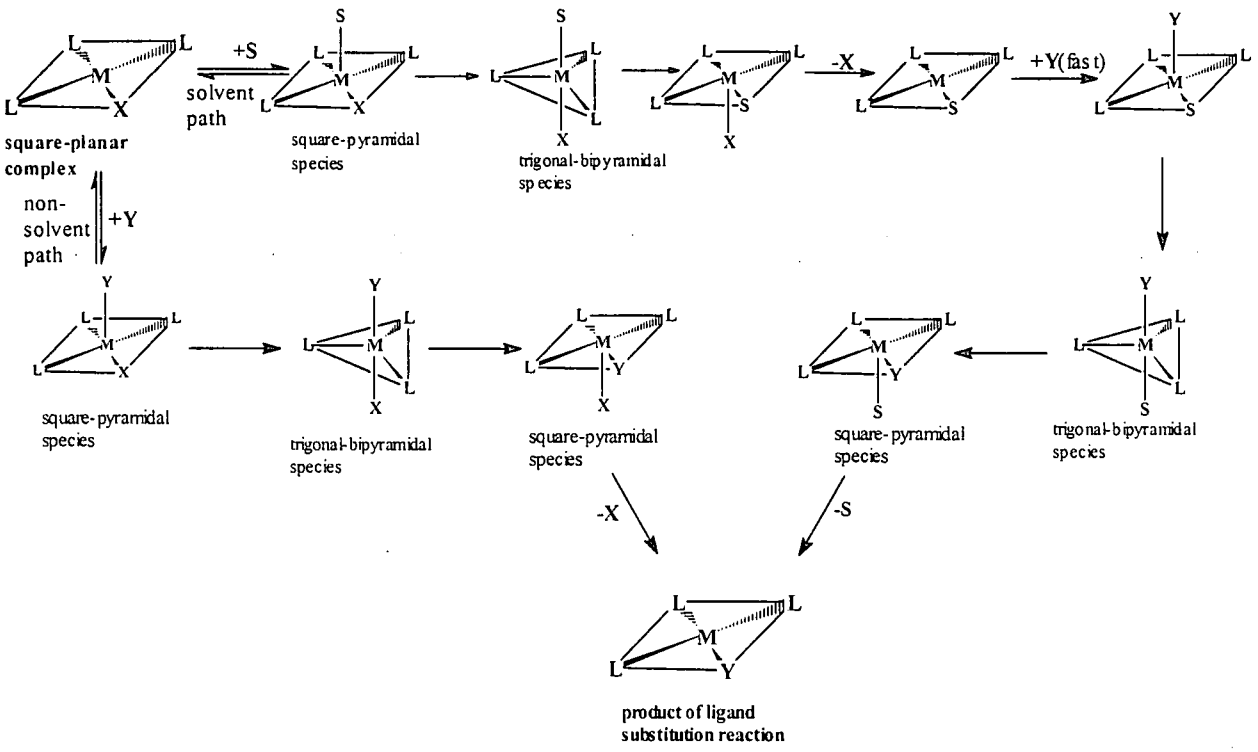

Scheme 2.5: Schematic representation of the direct (non-solvent path) and solvent pathway of the associative mechanism of substitution reaction of square planar complexes [ML_3X]. S = solvent and Y = incoming ligand

Reactions on square planar complexes that are associative, involve a nucleophilic attack of the entering ligand Y on the metal with the 5-coordinate adduct passing through the square-pyramidal and trigonal-bipyramidal stages,[50] **Scheme 2.5**. As the entering group approaches the complex, the symmetry of its donor orbital is usually appropriate for overlap with the unoccupied metal p_z, p_x and p_y orbitals. Y at this stage can move in any the four possible directions. Thermodynamically, it is generally expected that Y will move towards the group trans to the leaving group.[52] The reaction then undergoes geometrical changes, that is a transformation from square pyramidal to trigonal-bipyramidal and again to square-pyramidal as illustrated in **Scheme 2.5**. As this study is concerned with substitution in [Rh(β-diketonato)(cod)] square planar complexes, attention will hereafter be mainly focused on such complexes.

The general rate law for a substitution process is summarised in **Equation 2.1**.[52]

$$\text{Rate} = k_s[\text{complex}] + k_2[Y][\text{complex}] \qquad \textbf{Equation 2. 1}$$

$$= (k_s + k_2[Y])[\text{complex}] \qquad (= k_2[Y][\text{complex}] \text{ if } k_s = 0)$$

$$= k_{obs}[\text{complex}]$$

with $k_{obs} = k_s + k_2[Y]$. k_s is the rate constant of the solvent pathway and k_2 the rate constant of the direct pathway for the substitution of X with Y. For the rate law of **Equation 2.1** to be valid, it is necessary for the step of the solvation pathway where Y replaces the co-ordinated solvent S to be fast.[53]

2.3.2.3 The interchange process

In this process, the incorporation of the entering group into the co-ordination sphere and the detachment of the leaving group from the co-ordination sphere of the metal ion, occur simultaneously, causing no change in the overall number of ligands bonded to the metal ion. Therefore, the intermediate or transition state, [Y---ML_n----X], involved in this process is not the formal three or five co-ordinated species, but rather a hybrid species as illustrated by the following equation:

$$ML_nX \longrightarrow [Y\text{----}ML_n\text{-----}X] \longrightarrow ML_nY$$

The properties of this intermediate will vary from reaction to reaction, sometimes to induce a more dissociative mechanism character into the reaction, and in other cases to induce a more associative mechanism character. Thus, the interchange mechanism resembles both S_N1 and S_N2 types of reactions simultaneously. The interchange process is therefore sometimes subdivided into two types, namely, *an associative interchange* and *a dissociative interchange mechanism.*

2.3.3 Activation Parameters

The measurement of reaction rates and rate constants, as a kinetic approach to elucidate the mechanism of chemical reactions, is conducted as a function of many chemical and physical variables. The magnitude and sign of the activation parameters, ΔH^*, ΔS^*, ΔG^* and ΔV^*, obtained for a reaction often dictate the mechanism of that particular reaction. The theory of absolute reaction rates postulates that molecules before undergoing reaction must form an activated complex in equilibrium with the reactants, and that the rate of any reaction is given by the rate of decomposition of the complex to form the reaction products. For the reaction:

$$A + B \overset{K_c^*}{\rightleftharpoons} [A{\cdot}B]^* \xrightarrow{k} \text{products}$$

The rate constant, k, of any reaction is given by the expression:

$$k = \frac{RT}{Nh} K_c^* \qquad (4)$$

where K_c^* is an equilibrium constant, R is the gas constant, h Planck's constant, N Avogadro's number and T the absolute temperature. The free energy of activation, ΔG^*, can then be defined thermodynamically as:

$$\begin{aligned} \Delta G^* &= -RT \ln K_c^* \\ &= \Delta H^* - T\Delta S^* \end{aligned} \qquad (5)$$

where ΔH^* = enthalpy of activation and ΔS^* = entropy of activation. By introducing (5) into (4), we obtain for k:

$$\ln k = \ln\left(\frac{RT}{Nh}\right) + \frac{\Delta S^*}{R} - \frac{\Delta H^*}{RT} \qquad (6)$$

Consequently, when k and ΔH^* of a reaction are known at a given temperature, ΔS^* can be calculated. The volume of activation[54] can be considered as consisting of two components, an intrinsic part ΔV^*_{intr}, and the solvation part, ΔV^*_{solv}.

$$\Delta V^* = \Delta V^*_{intr} + \Delta V^*_{solv} \qquad (7)$$

ΔV^*_{intr} reflects the volume changes due to the variations in bond lengths and angles during the formation of the transition state, while ΔV^*_{solv} arises from the changes in solvation during this process. ΔV^* for a dissociative mechanism are approximately zero due to positive values of ΔV^*_{intr} from bond cleavage and negative values of ΔV^*_{solv} from an increase in electrostriction associated with the development of two ions in the transition state.[55] On the other hand, an associative mechanism will mainly involve a negative contribution from ΔV^*_{intr} due to bond formation and only a minor contribution from ΔV^*_{solv} since uncharged species are involved. Hence, large negative ΔS^* and ΔV^* values point mainly to an associative mechanism, whereas a small negative ΔS^* and ΔV^* values are most likely an indication of a dissociative interchange process.

Considering the reactions[56] of pyridine with *trans*-$[Pt(py)_2(NO_2)Cl]$ and *trans*-$[Pt(PEt_3)_2Cl_2]$ in methanol, the low ΔH^* values and large negative value of ΔS^* and ΔV^* were clear evidence for an associative mechanism. ΔV^* values were observed to be the same, within experimental error, at different [py] for the reaction between *trans*-$[Pt(py)_2(NO_2)Cl]$ and pyridine, and were independent to temperature within the range 10-25°C.

Table 2.4: Volumes of activation for the substitution reaction: *trans*-$[Pt(py)_2(NO_2)Cl]$ + py → *trans*-$[Pt(py)_3(NO_2)]$ + Cl^-, at different temperatures and different concentrations of pyridine[56]

[py]/ mol dm^{-3}	T/ °C	ΔV^*/ cm^3 mol^{-1}
0.30	10	-11.6 ± 0.3
0.05	25	-12.2 ± 0.6
0.10	25	-11.6 ± 0.6
0.02	40	-12.0 ± 0.5
0.03	40	-13.1 ± 0.6

Also ΔS^* was found not to be sensitive to the nature of the solvent, therefore indicating that solvation effects do not play a major role in these reactions.[57]

ΔH^* is not known to be very useful in the interpretation of a reaction mechanism, although it can sometimes assist in mechanism identification. For example, a molecular model showed that the

formation of a trigonal-bipyramidal structure in the substitution reactions of *cis*- and *trans*-[$Pt(PEt_3)_2(2,4,6\text{-}Me_3Ph)Br$], offers a large steric crowding at the Pt(II) centre for the *cis* isomer compared to the *trans* isomer.[58] The decrease in the reactivity caused by steric hindrance for the *cis* isomer correlates with the increase in ΔH^* and suggests an associative mechanism.

2.3.4 Factors influencing substitution reactions rates[59]

The factors that may determine the rate of substitution reactions of square planar complexes include the type and nature of all the ligands (entering, remaining and leaving), the central metal atom and the solvent utilised.

2.3.4.1 The effect of the entering ligand

As expected for an associative mechanism, the entering ligand has a large influence on the reaction rate. This mostly depends on the nucleophilicity of that incoming ligand. The nucleophilicity is a measure of the readiness of an entering ligand to attack the positive metal centre of a complex, or its readiness to supply the electrons needed for the reaction to proceed. Thus, the rate of substitution is determined by the incoming ligand's ability to induce bond making and breaking processes. A stronger nucleophile will attack the metal centre of a complex more readily than a weaker one and would hence form a more stable bond with the central metal. Consequently, the reaction rate will increase. Nucleophilicity is, therefore, a kinetic term and differs significantly from the term "basicity" which is thermodynamic in nature and is defined by the pK_a of the conjugate acid of the Lewis base (a nucleophile). Belluco[60] and co-workers confirmed this by the determination of the rate constants for the substitution of Cl by a large variety of ligands from *trans*-[$Pt(py)_2(Cl)_2$]. **Table 2.5** summarises the rate constants of the substitution of Cl in *trans*-[$Pt(py)_2(Cl)_2$] with a number of nucleophiles in CH_3OH. These rate constants have been fitted to the Swain-Scott equation,[61] given by:

$$\log k_2 = s n_{Pt} + \log k_s$$

with s = discrimination constant (measures the sensitivity of the substrate) and n_{Pt} = nucleophilic reactivity constant. The term s and k_s depend only on the Pt complex and not on the entering ligand. The rate of the reaction can be predicted if s and n are known. The second-order rate constant, k_2,

for the reactions in CH_3OH of nucleophile Y with *trans*-$[Pt(py)_2(Cl)_2]$ chosen as the standard substrate according to the reaction

$$\textit{trans}\text{-}[Pt(py)_2(Cl)_2] + Y \xrightarrow{k_2} \textit{trans}\text{-}[Pt(py)_2(Cl)Y] + Cl^-$$

are compared with the rate constant for solvolysis, k_s, for the same substrate. $k_s = k_2$ for CH_3OH, therefore, $k_s = 0.01\ s^{-1}$.

Table 2.5: Second order rate constants, k_2, of the reactions between *trans*-$[Pt(py)_2(Cl)_2]$ and a number of nucleophiles in CH_3OH. *Cl is a radioactive labelled Cl ion

Nucleophile	$10^3\ k_2$/ $dm^3\ mol^{-1}\ s^{-1}$	n_{Pt}	pK_a
CH_3OH	1×10^{-5}	0.0	-1.7
CH_3O^-	Very slow	<2.4	15.7
$*Cl^-$	0.45	3.04	-5.7
NH_3	0.47	3.07	9.25
C_5H_5N	0.55	3.19	5.23
Br^-	3.7	3.7	-7.7
$(CH_3)_2S$	21.9	21.9	-5.3
I^-	107	5.46	-10.7
$AsPh_3$	2320	6.89	-
CN^-	4000	7.14	9.3
PPh_3	249000	8.93	2.73

It can be seen in **Table 2.5** that there is no correlation between nucleophile pK_a values and n_{Pt}. It is important to note that, in a nucleophilic substitution reaction involving square planar complexes, the nucleophilicity of the halide ions decrease in the order: $I^- > Br^- > Cl^- >> F^-$. In contrast, the nucleophilicity of the group VA bases PPh_3, $AsPh_3$, NPh_3 etc., which are, with the exception of the amines, excellent nucleophiles towards Pt(II), decrease in the order: phosphine > arsine > stibine.

Basicity of the incoming ligand has a rather small effect on the rate of associative square planar substitution reactions. **Table 2.6** summarises the second order rate constants, k_2, for the substitution of the β-diketonato ligand in [Rh(acac)(cod)],[62] [Ir(acac)(cod)][63] and [Rh(fca)(cod)][64] with derivatives of 1,10-phenanthroline and 2,2′-dipyridyl.

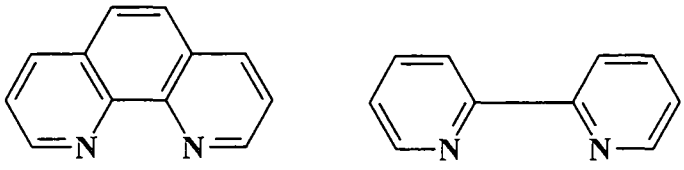

(a) (b)

Scheme 2.6: Structures of (a) 1,10-phenanthroline and (b) 2,2′-dipyridyl

Over the pK_a range of 3.57 to 6.31 for 1,10-phenanthroline derivatives, the slowest reaction rate was 12.4 and the fastest rate was 29.0 $dm^3\ mol^{-1}\ s^{-1}$ in the case of the [Rh(acac)(cod)] reactions. The rates were between 1.38 and 32.3 $dm^3\ mol^{-1}\ s^{-1}$ in the case of the [Ir(acac)(cod)] reactions and between 5.46 and 17.8 $dm^3\ mol^{-1}\ s^{-1}$ in the case of [Rh(fca)(cod)] reactions. The much faster reaction of 2,2′-dipyridyl compared to reactions of derivatives of phenanthroline was attributed to the fact that 2,2′-dipyridyl is much less rigid than phenanthroline. Large negative ΔS* values for these reactions (**Table 2.6**) indicate an associative mechanism.[65]

Table 2.6: Rate constants (k_2/$dm^3\ mol^{-1}\ s^{-1}$) for the substitution of the β-diketonato in [Rh(acac)(cod)], [Ir(acac)(cod)] and [Rh(fca)(cod)] complexes with derivatives of 1,10-phenanthroline and 2,2′-dipyridyl

Incoming ligand	pK_a [a]	[Rh(acac)(cod)] [b]			[Ir(acac)(cod)] [c]			[Rh(fca)(cod)] [b]		
		k_2	ΔH*/ kJ mol^{-1}	ΔS*/ J K^{-1} mol^{-1}	k_2	ΔH*/ kJ mol^{-1}	ΔS*/ J K^{-1} mol^{-1}	k_2	ΔH*/ kJ mol^{-1}	ΔS*/ J K^{-1} mol^{-1}
5-nitro-phenanthroline	3.57	12.4	30.8	-121	1.38	27.4	-150	5.46	25	-146
1,10-phenanthroline	4.96	29.0	32.6	-108	13.6	29.5	-125	17.8	29	-123
5,6-dimethyl-phenanthroline	5.20	19.9	38.7	-90	32.3	30.7	-113	13.7	23	-143
4,7-dimethyl-phenanthroline	5.97	18.8	36.7	-97	21.9	36.5	-97	13.2	22	-149
3,4,7,8-tetramethyl-phenanthroline	6.31	19.6	40.7	-84	22.1	28.7	-122	15.7	27	-128
2,2′-dipyridyl	4.30	124	26.8	-115	116	28.2	-109	118	31.2	-100

a) pK_a values of conjugate acid in water from ref. 66
b) in methanol at 25°C
c) in acetone at 25°C

2.3.4.2 Influence of ligands *trans* to the leaving group

(a) Monodentate ligands

The ***trans*-effect**[67] is a kinetic property relating to the influence a fixed ligand may have on the rate of substitution of a ligand trans to it. The ***trans*-influence**, however, has nothing to do with kinetics. The ***trans*-influence** is a thermodynamic property related to the influence a fixed ligand may have on the crystallographic bond length between a central metal ion and the ligand trans to the fixed ligand.

As an example of a kinetic *trans*-effect, the following reaction is considered:[68]

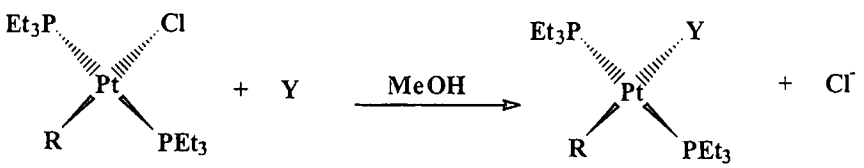

$R = Cl^-, CH_3^-$ and $C_6H_5^-$

When Y is Br^-, N_3^-, NO_2^-, or pyridine (all relatively weak nucleophiles), the *trans*-effect is in the following order of R (rate constant, k_2 in $mol^{-1}\ dm^3\ s^{-1}$) for the substitution of Cl^- by N_3^- is

$$CH_3^- (7) > C_6H_5^- (0.8) > Cl^- (0.02)$$

However, when a better nucleophile, I^- is used, the *trans*-effect order becomes (rate constant values in $mol^{-1}\ dm^3\ s^{-1}$, are given in brackets)

$$CH_3^- (40) > Cl^- (23.6) > C_6H_5^- (6.0)$$

It is concluded from the above set of data that, *trans*-effect depends on the nature of the entering group.

The thermodynamic *trans*-influence of a wide range of ligands has been measured with techniques[69] such as X-ray crystallography and infra-red, NMR, nuclear quadruple resonance, photoelectron and Mössbauer spectroscopy.[70] More precise techniques such as X-ray crystallography have led to more accurate information on the variation in bond lengths of Rh—P bonds *trans* to a variety of ligands. **Table 2.7** summarises the Rh-P bond lengths for the complexes given in **Figure 2.10** and the electronegativities of selected donor atoms. The Rh—P bond lengths *trans* to donor atoms, O, N and S, increase on going from complex **1** to **3** in **Figure 2.10**. This means that S has a larger *trans*-

influence than N, while O has the smallest. It is also concluded that the electronegativity is inversely proportional to *trans*-influence.

Table 2.7: Rh-P bond lengths for the complexes [Rh(acac)(CO)(PPh$_3$)], [Rh(dmavk)(CO)(PPh$_3$)] and [Rh(sacac)(CO)(PPh$_3$)] and the electronegativities of the donor atoms

Complex	Electronegativity of donor atom[59]	Rh-P bond lengths/ Å
[Rh(acac)(CO)(PPh$_3$)]	3.5 for O	2.244(2)
[Rh(dmavk)(CO)(PPh$_3$)]	3.1 for N	2.275(2)
[Rh(sacac)(CO)(PPh$_3$)]	2.4 for S	2.300(3)

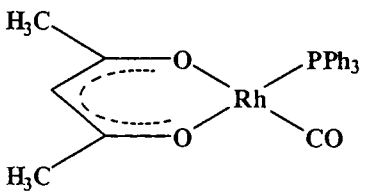

1

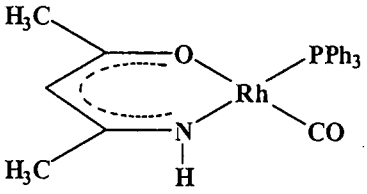

2

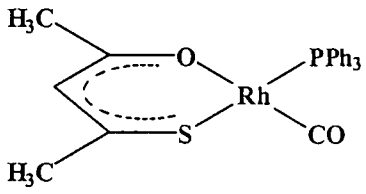

3

Figure 2.10: Structures of [Rh(acac)(CO)(PPh$_3$)] (1), [71] [Rh(dmavk)(CO)(PPh$_3$)] (2) [72] and [Rh(sacac)(CO)(PPh$_3$)] (3), [73] with dmavk = dimethyl-β-aminovinylketonato and sacac = thioacetylacetonato

Extensive studies on platinum complexes showed that, the structural *trans*-influence of a variety of groups decrease in the order:

(largest *trans*-influence) σ-R ~ H^- ≥ carbenes ~ PR_3 ≥ AsR_3 > CO ~ RNC ~

C=C ~ Cl ≈ NH_3 (smallest *trans*-influence)

It should be noted that, some groups with a high *trans*-influence also have a large *trans*-effect, while others, especially olefins, have a high *trans*-effect, but a small *trans*-influence. The reason behind this is the fact that *trans*-effect is related to the nature of the transition state, and *trans*-influence to the ground state. The effectiveness of ligands such as olefins in labilizing *trans* ligands can also be explained by the polarisation theory and the π-bonding effect.

Grinberg[74] proposed that the thermodynamic *trans*-influence was purely electrostatic by nature. This is known as his polarisation theory. According to this theory, the residual charge on the central metal atom allows the metal atom to induce a dipole on the *trans*-directing ligand (L). In turn, the ligand L then induces a dipole back on the central metal atom. The region nearest to the leaving

group (X) becomes partially negatively charged. Then, the bond strength between metal and the leaving group, becomes weakened due to a repulsive effect between the partial negative charge on the metal and on the adjacent leaving group as shown in **Figure 2.11**. This allows the entering ligand to move, attack or migrate towards the weakly bound ligand (X) and away from the strongly bound ligand (L).

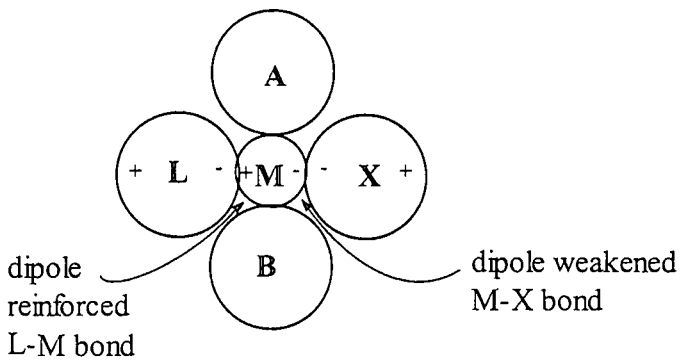

Figure 2.11: Dipole formation in a complex according to the polarisation theory of Grinberg explains the thermodynamic *trans*-influence.

The second theory that attempts to explain the *trans*-influence is the π-bonding effect,[75] which is based on the competition between *trans*-ligand, L and the leaving ligand X for the same *d*-orbital, d_{xz}, as shown in **Figure 2.12**. On the formation of the trigonal bipyramid, in substitution reactions of the square planar complexes, the orbitals d_{xy}, d_{xz}, d_{yz} and $d_{x^2-y^2}$ are on the right symmetries for π interaction.

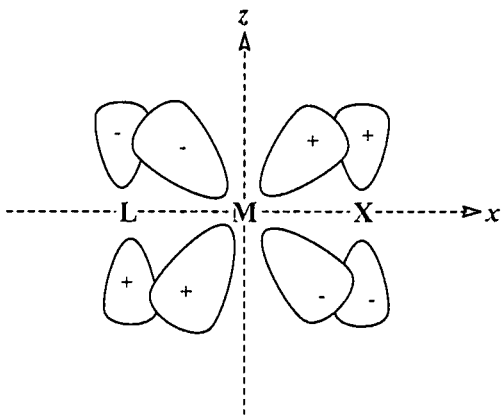

Figure 2.12: π Interaction of the *trans* d_{xz} orbitals illustrating the *trans* effect

It is significant that all these orbitals are shared in π interaction with the ligands in the trigonal plane. The ligand system consists of the *trans* group, L, the entering group, Y, and the leaving

group, X. Thus the trigonal-bipyramidal transitional state is greatly stabilised, if the *trans* group possesses empty, reasonably stable, π symmetry orbitals. The interaction of empty ligand π orbitals with the filled $d(\pi^*)$ orbitals of the metal delocalizes electronic charge to the *trans* ligand, thereby, lowering the energy of the system. Due to the π-bonding character of ligand, L, the electron density in the filled d_{xz} orbital of the metal M, is largely shifted towards L and therefore away from X. In this case the M-X bond is not weakened, but the reduction of the electron density in the vicinity of X facilitates an easy approach of the incoming ligand in that direction, leading to the displacement of X. However, should ligand L have little or no tendency to π-bond, then the electron density in the d_{xz} orbital of the metal is not disturbed. It then remains more or less distributed about ligands L and X. In other words, the *trans* ligand L helps to accommodate the excess electronic charge added to the central atom by the entering ligand. A conclusion reached from the π-bonding theory is that the fast substitutions found in square planar complexes containing at least one ligand of high *trans* effect, should follow an associative mechanism.

(b) Bidentate ligands

(i) The trans-influence

Bonati and Wilkinson[71] first prepared complexes of the type [Rh(L,L'-BID)$(CO)_2$] (L,L'-BID = mono anionic bidentate ligand with donor atoms L and L'). They showed that triphenylphosphine (PPh_3), arsine ($AsPh_3$) and olefins could replace one carbonyl group according to **Scheme 2.7**.

Scheme 2.7: Only the CO group *trans* to the donor group with the largest *trans*-influence is substituted by the PPh_3 ligand in complexes of the type [Rh(L,L'-BID)$(CO)_2$]. L has a larger *trans*-influence than L' in the above example. α = bite angle.

This made it possible to study the relative thermodynamic *trans*-influence of the bonding atoms L and L' in bidentate ligands, because the carbonyl group *trans* to the donor atom with the largest *trans*-influence will be substituted by the PPh_3 ligand. For [Rh(L,L'-BID)$(CO)_2$] complexes with symmetrical L,L'-BID ligands such as 2,4-pentanedionato[26] (acac), deprotonated di-

acetylbenzylmethane[76] (bzaa), and tropolone[77] (trop), the two carbonyl groups are chemically equivalent and substitution of any one of the two with PPh_3, will yield the same isomer (**Figure 2.13**).

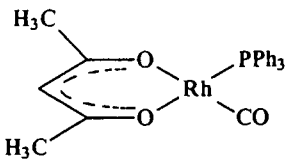

4

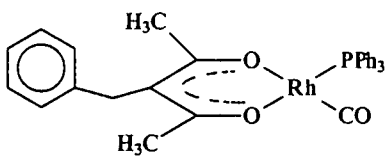

5

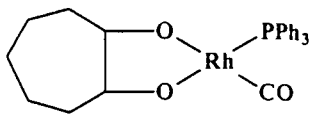

6

Figure 2.13: Structures of [Rh(acac)(CO)(PPh_3)], (4), [Rh(bzaa)(CO)(PPh_3)], (5) and [Rh(trop)(CO)(PPh_3)], (6)

In the case where the L,L′-BID ligand is unsymmetrical, the resulting [Rh(L,L′-BID)(CO)(PPh_3)] complex has been used to study the relative *trans*-influence of the donor atom, using the Rh-P bond distance as an indication of the relative *trans*-influence of the donor atom *trans* to the PPh_3. There are two categories in this case, the first one being L = L′ = O and the second one is whereby L and L′ atoms are different (can be N and O, S and O or S and N).

For the first category (L = L′ = O), examples ([Rh(tfaa)$(CO)_2$][77] and [Rh(cupf)$(CO)_2$][78]) are shown in **Figure 2.14**. Different substituents (CF_3, CH_3 or Ph) exert different electronic influences on the two CO groups. These substituents influence the effective strength of the *trans*-influence of each O atom. Larger group electronegativities for substituents (χ_{CF3} = 3.01) lower the relative *trans*-influence of the adjacent O-atoms, while lower group electronegativities (χ_{CH3} = 2.34) increase the relative *trans*-influence power of the adjacent O-atom.

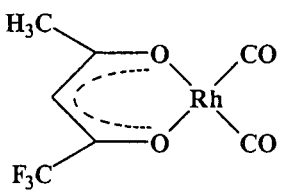

[Rh(tfaa)$(CO)_2$]

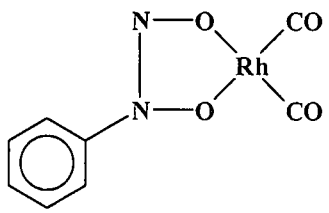

[Rh(cupf)$(CO)_2$]

Figure 2.14: Examples of unsymmetrical mono anionic bidentate ligands L,L′-BID with L = L′ = O co-ordinated to rhodium

The carbonyl ligand *trans* to the oxygen atom with the largest *trans*-influence (smallest electronegativity) is normally substituted by PPh_3. An example of this is shown in **Scheme 2.8**. This

indicates that the oxygen atom nearest to the more electron-withdrawing group of the chelate ring, such as CF_3, has the smallest *trans*-influence.

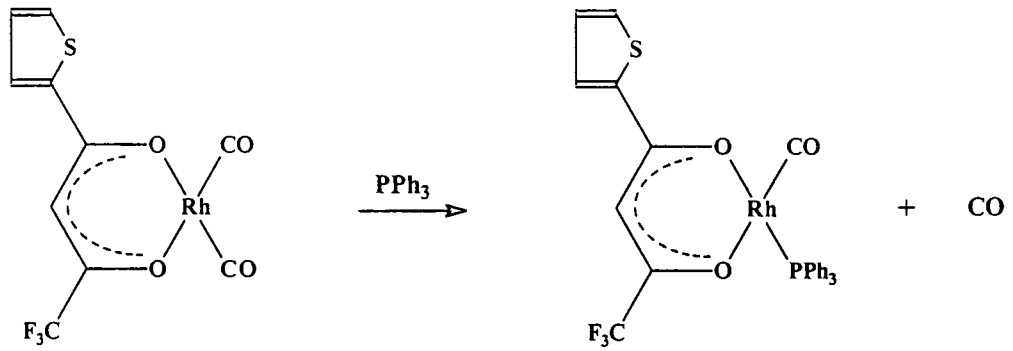

Scheme 2.8: Reaction of $[Rh(tta)(CO)_2]$ with PPh_3 to give $[Rh(tta)(CO)(PPh_3)]$ [79] tta = thenoyltrifluoroacetonato

In the reaction between $[Rh(fctfa)(CO)_2]$ and PPh_3 according to **Scheme 2.9**, it was previously reported that steric effects dominate the thermodynamic *trans*-influence.[80] It was argued that **isomer 2** should be the dominant isomer based on electronic considerations (*trans*-influence) according to the polarisation theory put forward by Grinberg.[74]

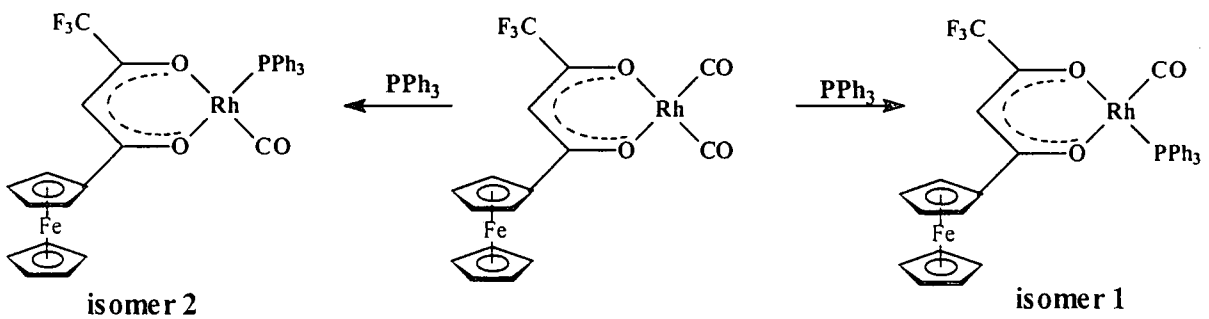

Scheme 2.9: Reaction between $[Rh(fctfa)(CO)_2]$ and PPh_3 to give two isomers of the complex $[Rh(fctfa)(CO)(PPh_3)]$.

From a recent study,[81] it was revealed that both isomers are observed by ^1H NMR and there is a fast equilibrium between these isomers. The isomer with most favourable crystallisation energy will crystallise. This isomer is not necessary the one that should dominate in solution according to polarisation theory.

(ii) The *trans*-effect

The kinetic *trans*-effect of bidentate ligands was observed in of the following substitution reaction:

$$[Rh(\beta\text{-diketonato})(CO)_2] + cod \rightarrow [Rh(\beta\text{-diketonato})(cod)] + 2CO$$

for β-diketonato = ba, dbm, tfaa, tfba and hfaa.[82]

Table 2.8: The sum of the group electronegativities of the β-diketonato side groups and second order rate constants, k_2 for the substitution reactions of cod in [Rh(β-diketonato)$(CO)_2$] complex to illustrate the *trans*-effect of various β-diketonato ligands $R^1COCHCOR^2$

β-diketonato	R^1	R^2	$\chi_{R1} + \chi_{R2}$	k_2 /dm^3 mol^{-1} s^{-1}
ba	CH_3	C_6H_5	4.55	0.10
dbm	C_6H_5	C_6H_5	4.42	0.36
tfaa	CH_3	CF_3	5.35	2.30
tfba	C_6H_5	CF_3	5.22	4.10
hfaa	CF_3	CF_3	6.02	200

The rate of substitution was found to be dependent on the terminal substituents (CH_3 (χ_{CH3} = 2.34), Ph (χ_{Ph} = 2.21) and CF_3 (χ_{CF3} = 3.01)) on the β-diketonato ligand in the following order

$$(\text{smallest } k_2)\ ba < dbm << tfaa < tfba << hfaa\ (\text{largest } k_2)$$

The influence that the terminal side groups of the β-diketonato ligands have on kinetic *trans*-effect, therefore, increase with increase in group electronegativities of individual side groups. Hence, the observed *trans*-effect of terminal side groups on β-diketones is in the order $CH_3 \approx Ph < CF_3$, with CF_3 having the largest influence. It is of interest to note that the group electronegativities of the CH_3 and the Ph group are almost equal. This implies that either of the CO groups in [Rh(PhCOCHCOCH$_3$)$(CO)_2$] may be substituted by PPh_3. This actually was observed by Preston et al.[83] in a crystallographic study. Both isomers were observed within the same crystal with a ratio 1:1 as illustrated in **Scheme 2.10**.

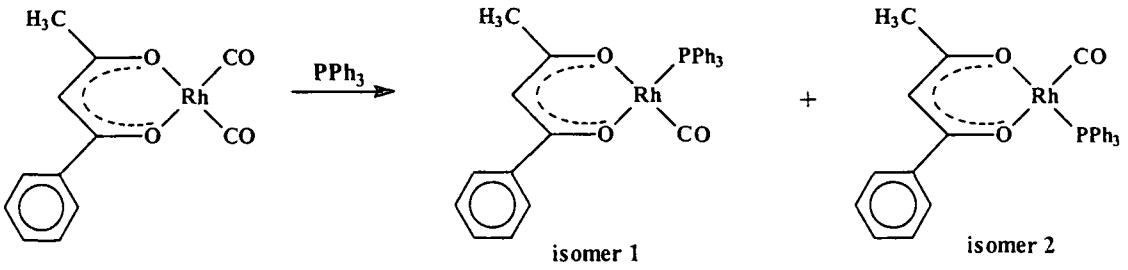

Scheme 2.10: Reaction of [Rh(ba)(CO)$_2$] with PPh$_3$ giving two isomers of [Rh(ba)(CO)(PPh$_3$)] that existed simultaneously in the solid state in the same single crystal.

In conclusion then, for bidentate ligands, the thermodynamic *trans*-influence determines the specific isomer that will be formed during substitution reactions, while, the kinetic *trans*-effect determines how fast these complexes will react in substitution reactions.

2.3.4.3 Influence of ligands *cis* to the leaving group

The kinetic ***cis*-effect** is the effect of a co-ordinated ligand upon the rate of substitution of ligands adjacent to that ligand. It is similar to the *trans*-effect, but when quantified, it is found to be a smaller effect than the *trans*-effect.[59] The similarity stems from the direct communication between *cis*-ligands *via* the metal p_y and $d_{x^2-y^2}$ orbitals. In cases where a relatively poor nucleophile acts as the entering group, the relative ability of ligands to act as *trans* labilizers is the same as their ability to act as *cis* labilizers. For example,[84] compare the *trans*-effect in **Scheme 2.11** (A) with trans ligand = X *versus* the *cis*-effect in **Scheme 2.11** (B) with cis ligand = Y of substitution reactions.

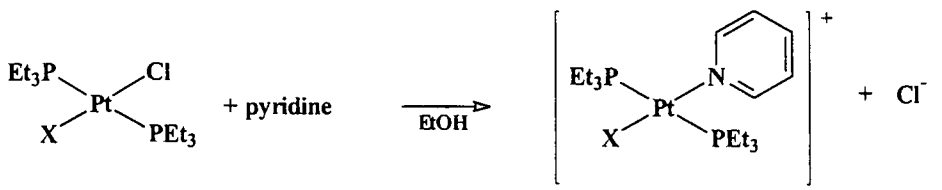

(A) (largest *trans*-effect) X = H^- (>10000) > CH_3^- (170) > $C_6H_5^-$ (40) > Cl^- (1) (smallest *trans*-effect)

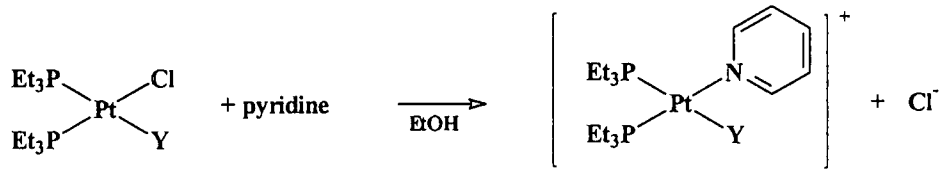

(B) (largest *cis*-effect) Y = CH_3^- (3.6) > $C_6H_5^-$ (2.3) > Cl^- (1) (smallest *cis*-effect)

Scheme 2.11: (A) Illustrates the *trans*-effect by measuring the kinetic substitution rate. X = ligand exerting the *trans*-effect. Rate constants, expressed as the ratio k(X)/k(Cl), are given in brackets after each X. (B) Illustrates the *cis*-effect by measuring the kinetic substitution rate. Y = ligand exerting the *cis*-effect. Rate constants, expressed as the ratio k(Y)/k(Cl), are given in brackets after each Y.

Molecular orbital calculations show that ligands that weaken bonds *trans* to themselves also weaken bonds *cis* to themselves, but not by as large an amount.[85] Bond breaking in the transition state becomes somewhat easier for good *cis*-directors, and the reaction rate increases, but not quite as much as would have been in the case if the *cis* ligand was in the *trans* position.

2.3.4.4 Influence of the leaving group

The effect of the leaving group is often related to the strength of the M-X bond (metal-ligand bond, where X = the leaving ligand). A stronger M-X bond makes it more difficult for X to be substituted by another ligand, resulting into a decrease in the substitution rate, whereas the opposite applies to the weaker M-X bond. The ligands *trans* and *cis* to the leaving group play vital roles in determining the M-X bond strength. The groups with a pronounced ability to *trans*-labilize are the least easily replaced ones. An extensive study of relative leaving group rates has been made, for the following reaction:[86]

$$Pt(dien)X^+ + pyridine \rightarrow Pt(dien)(py)^{2+} + X$$

The rate effects of the various leaving groups, X, were determined. The order of increasing ease of substitution was found to be:

(slowest to replace) $CN^- < NO_2^- < SCN^- < N_3^- << I^-, Br^- < Cl^- < H_2O < NO_3^-$ (easiest to replace)

The members of the above series differ in rate constants by as much as 10^5 from the slowest (CN^-) to the fastest (NO_3^-) substituted ligand.

In addition, the second order rate constant, k_2, of a substitution reaction of a square planar complex increases with the decrease in basicity (pK_a values) of the leaving group. By way of example, a linear free energy relationship exists for the substitution reaction

$$[M(\beta\text{-diketonato})(cod)] + 1,10\text{-phenanthroline} \rightarrow [M(phen)(cod)]^+ + \beta\text{-diketonato}$$

with M = Rh[16] or Ir.[63] Ligands with smaller pK_a values have larger substitution rate constants. Results are summarised in **Table 2.9** and are applicable to the above reaction.

Table 2.9: Rate constants at 25°C and the activation parameters for the reaction between [M(β-diketonato)(cod)] and phen, with M = Rh and Ir.

β-diketonato	pK_a/	[Rh(β-diketonato)(cod)][(a)]			[Ir(β-diketonato)(cod)][(b)]		
		k_2/ $dm^3\ mol^{-3}\ s^{-1}$	ΔH^*/ $kJ\ mol^{-1}$	ΔS^*/ $J\ K^{-1}\ mol^{-1}$	k_2/ $dm^3\ mol^{-3}\ s^{-1}$	ΔH^*/ $kJ\ mol^{-1}$	ΔS^*/ $J\ K^{-1}\ mol^{-1}$
acac	8.95	29.0	32.6	-108	13.6	29.5	-125
ba	8.70	51.2	31.6	-106	85.8	31.5	-102
dbm	9.35	61.4	27.3	-119	413	26.3	-106
tfaa	6.30	1330	30.5	-83	17100	24.0	-83
tfba	6.30	2420	26.2	-93	25100	23.1	-81
hfaa	4.35	276000	23.2	-63	3000000	-	-

(a) in methanol at 25°C
(b) in acetone at 25°C

This particular type of reaction was also the subject of this study. During this study we introduced the influence a second metal centre in the form of a ferrocenyl group may have on this type of substitution reaction, as well as the influence of bulkier R groups, particularly H, CH_3, CH_2CH_3, $CH(CH_3)_2$ and $C(CH_3)_3$.

2.3.4.5 Influence of the central metal atom

The effect of a central metal atom on the rate of substitution is determined by the ease with which the metal enhances the replacement of the ligand attached to it, by another ligand, and such a metal needs to be able to form a five co-ordinate complex, if the reaction proceeds via the associative mechanism. The easier a metal can form a five co-ordinate complex (intermediate) in a square planar substitution reaction, the more stable is the transition state in an associative mechanism, and hence substitution is enhanced. For the substitution reaction[84]

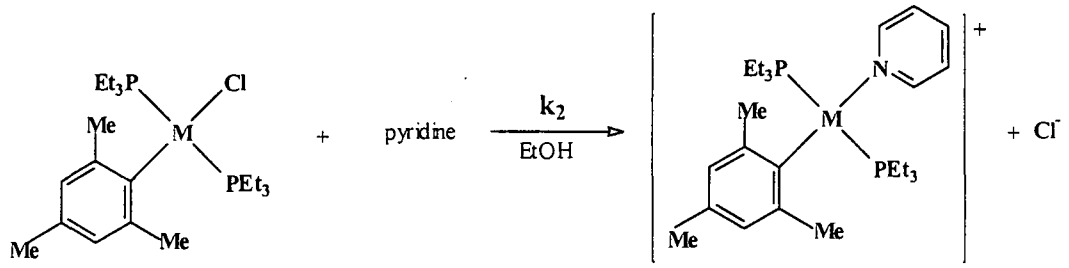

Scheme 2.12: Substitution reaction of Cl with pyridine from complex $[M(Cl)(mesityl)(PEt_3)_2]$. (M = Ni, Pd and Pt)

second order rate constants, k_2, are equal to 33 $dm^3\ mol^{-1}\ s^{-1}$ for M = Ni, 0.58 $dm^3\ mol^{-1}\ s^{-1}$ for M = Pd and 6,7 x 10^{-6} $dm^3\ mol^{-1}\ s^{-1}$ for M = Pt. This result is consistent with the higher electron density of the third transition Pt atom not favouring an associative mechanism. The large difference in k_2 for these complexes is due to the fact that the mesityl blocks the positions above and below the plane making the smaller Ni(II) complex much more capable of stabilising labile five co-ordinate transition states than the bulky, electron dense Pt(II) complex.[84] The relative rate of substitution decreases in going from top to bottom in a given group of transition metals as well as in going from right to left in a given row of the transition metals.

2.3.4.6 Influence of the solvent

The solvent has been found to play a crucial role in substitution reactions of square planar complexes. Solvation of the ground and activated states influences the energetics of the activation process. The solvent's role lies mainly on the solvolysis steps of the reaction as seen in **Scheme 2.5**, page 23. The nucleophilicity and polarity of the solvent play a major role in the influence exerted by the solvent. For a solvent to act as a nucleophile it must have an ability to donate electrons and to supply them to the metal centre, therefore, co-ordinating strongly to the metal. The order observed[87] for some solvents (with large k_s values) is as follows:

$(CH_3)_2SO > CH_3NO_2, H_2O > ROH$

Bonding of these solvents to the metal causes a weakening of any existing metal-ligand bond, thus enhancing the nucleophilic attack of the incoming ligand. The nucleophilicity, therefore, dictates the co-ordination power of the solvent and k_s. Solvents that are poor co-ordinators such as C_6H_6 and CCl_4, have little or no influence on the reaction rate as $0 \approx k_s << k_2$ in the reaction sequence shown in **Scheme 2.5**.[87]

2.3.4.7 The steric effects of the ligands

This refers to the influence of different bulky ligands co-ordinated to the same metal centre. It has been observed that increasing sizes of reacting complexes and ligands lower the rate of reaction. In sterically crowded complexes, bulky ligands shield the metal centre, thereby blocking the approach of the incoming ligand. The rate constants for the hydrolysis of *cis*-$[Pt(Cl)L(PEt_3)_2]$[88] (replacement of Cl^- by H_2O) decreases as more bulkier ligands are used as follows:

L = pyridine, $k = 8 \times 10^{-1}\ s^{-1}$

L = 2-methylpyridine, $k = 2.0 \times 10^{-4}\ s^{-1}$

L = 2,6-dimethylpyridine, $k = 1.0 \times 10^{-6}\ s^{-1}$

The *ortho*-CH_3 groups of the aryl ligands block positions above and below the plane of the complex as illustrated in **Figure 2.15** (a), therefore increasing the hindering effect. It was also observed that if L is *trans* to Cl^- the effect is smaller than when they were *cis* to each other. This is explained by the CH_3 groups being further from leaving group, Cl, as shown in **Figure 2.15** (b).

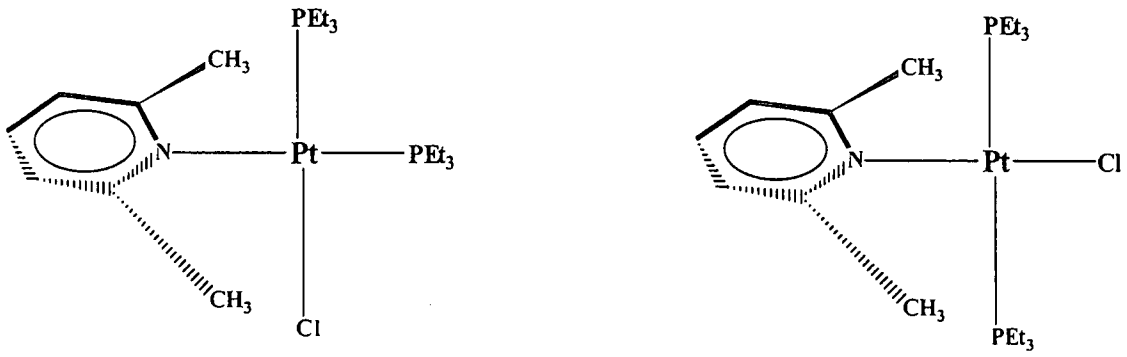

(a) *cis* isomer (b) *trans* isomer

Figure 2.15: [Pt(2,6-dimethylpyridine)(Cl)$(PEt_3)_2$] complexes ((a) *cis* isomer, (b) *trans* isomer) illustrating that *ortho*-CH_3 groups of 2,6-dimethylpyridine may sterically hinder nucleophilic attack of an entering group from both above and below the plane of the molecule in *cis* and *trans* isomers. However, *cis* isomer is sterically more crowded in the Cl position than the *trans* isomer and hence, Cl displacement is slower in the *cis* isomer.

2.4 Cyclic voltammetry

2.4.1 Introduction

Cyclic voltammetry (CV) was first reported in 1938 and described theoretically in 1948 by Randles and Sevcik.[89] It is one of the most frequently used techniques for examining the electrochemical properties of a chemical substance or material. Organic chemists[90, 91] have applied the technique to the study of biosynthetic reaction pathways and to study electrochemically generated free radicals. CV has also been used to evaluate the effects of ligands on the oxidation/reduction potential of the central metal ion in complexes and multinuclear clusters in inorganic chemistry.[92] The effectiveness of CV results stems from its capability for rapidly observing the redox behaviour of a compound over a wide potential range. Both thermodynamic and kinetic information is available in a single experiment. Thus both reduction potential and heterogeneous electron transfer rates can be measured and also the rate and nature of a chemical reaction coupled to the electron transfer step can be studied. It is also useful in the selection of the proper oxidising agent, which can be used to convert the metal complex in an intermediate oxidation state.

2.4.2 The Basic CV Experiment[93]

Cyclic voltammetry consists of cycling the potential of an electrode, which is immersed in an unstirred solution, and measuring of the resulting current. The potential of this working electrode is controlled *versus* a reference electrode such as a saturated calomel electrode (SCE) or a silver/silver chloride electrode (Ag/AgCl). The controlling potential that is applied across these two electrodes can be considered an excitation signal. The excitation signal for a CV is a linear potential scan with a triangular waveform, from an initial value, E_i, to a predetermined limit $E_{\lambda 1}$, (known as the switching potential) where the direction of the scan is reversed (see **Figure 2.16**). The scan can be stopped anywhere or it can do cycles between $E_{\lambda 1}$ and some other preselected value, $E_{\lambda 2}$.

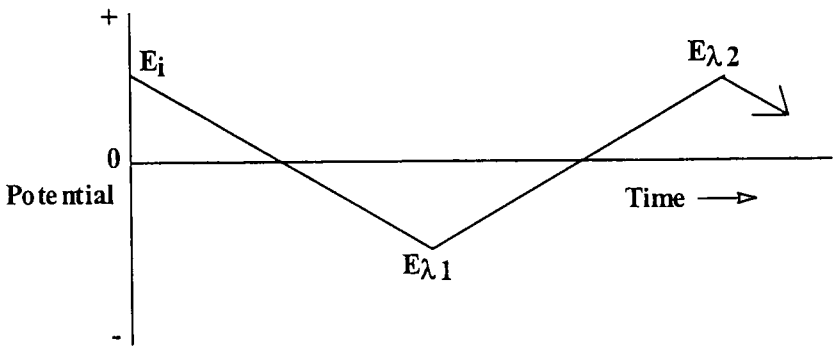

Figure 2.16: A typical potential-time excitation signal for cyclic voltammetry, $E_{\lambda 1}$ and $E_{\lambda 2}$ are the switching potentials. E_i is the initial potential.

The current response is plotted as a function of the applied potential. Often there is very little difference between the first cycle and successive scans. However, the changes that do appear on repetitive cycles are important keys to unlocking information about reaction mechanisms.

2.4.3 Important parameters of cyclic voltammetry

The important parameters of cyclic voltammetry include the magnitudes of the anodic peak current (i_{pa}), and cathodic peak current (i_{pc}), the anodic peak potential (E_{pa}) and cathodic peak potential, (E_{pc}) as shown in **Figure 2.17**.

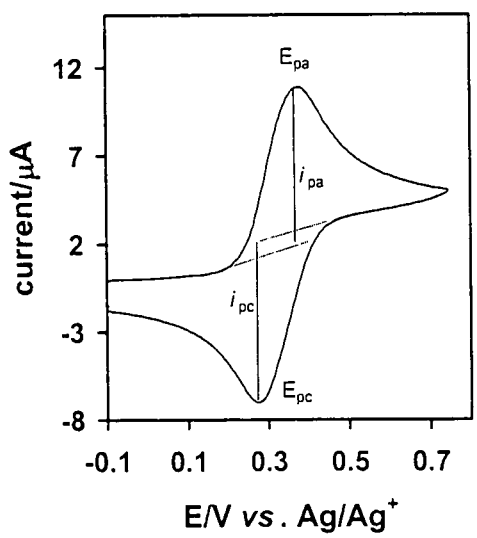

Figure 2.17: Cyclic voltammetry of a 2.00 mmol dm^{-3} Hbfcm ($FcCOCH_2COPh$) measured in 0.1 mol dm^{-3} $TBAPF_6/CH_3CN$ on a Pt working electrode at 25°C. Scan initiated at –0.097 V in a positive direction at scan rate 0.1 V s^{-1}.

One method of measuring i_p involves extrapolation of a baseline current as illustrated in **Figure 2.17**. The establishment of a correct baseline is essential for the accurate measurements of the peak currents.

A redox couple may or may not be electrochemically reversible. By electrochemical reversibility, it is meant that the rate of electron transfer between the electrode and substrate is fast enough to maintain the concentration of the oxidised and reduced forms in equilibrium with each other at the electrode surface. It is common practice to report the average of the forward and return peak potentials, the formal reduction potential, $E^{o\prime}$, for the electrochemically reversible redox couple as given by the following equation:

$$E^{o\prime} = \frac{E_{pa} + E_{pc}}{2} \qquad \textbf{Equation 2.2}$$

Electrochemical reversible couples imply that $\Delta E_p = E_{pa} - E_{pc} \approx 59$ mV at 25°C for $1e^-$ transfer process. The number of electrons transferred in the electrode reaction (n) for a reversible couple can be determined from the separation between the peak potentials, ΔE_p from the following equation:

$$\Delta E_p = E_{pa} - E_{pc} \cong \frac{0.059V}{n} \qquad \textbf{Equation 2.3}$$

Many systems are reversible when the voltage is scanned slowly, but at higher scan rates ΔE_p becomes larger than $59/n$ mV. This implies that the rate of electron transfer between substrate and electrode are comparable to or slower than the scan rate.[94] In practice, though, a system with a potential difference, ΔE_p, up to 80 mV is still considered as an indication of a reversible couple, even though theory predicts 59 mV for $1e^-$ transfer processes.

Another characteristic of reversible systems is the dependence of the peak height on the square root of the scan rate. At 25°C the peak current, as defined by the Randles-Sevcik equation, is:

$$i_p = (2.69 \times 10^5)\, n^{3/2} A D^{1/2} \nu^{1/2} C \qquad \textbf{Equation 2.4}$$

Here i_p is the peak current (measured in amperes), A is the electrode area (cm^2), D is the diffusion coefficient ($cm^2\ s^{-1}$), ν is the scan rate ($V\ s^{-1}$) and C is the concentration of the substrate ($mol\ cm^{-3}$).

The above relationship between peak current and concentration is particularly important in analytical applications and in studies of electrode mechanisms. Also for an electrochemical reversible couple, which is not followed by any chemical reactions, the values of i_{pc} and i_{pa} should be identical. That is:

$$\frac{i_{pa}}{i_{pc}} = 1 \qquad \textbf{Equation 2. 5}$$

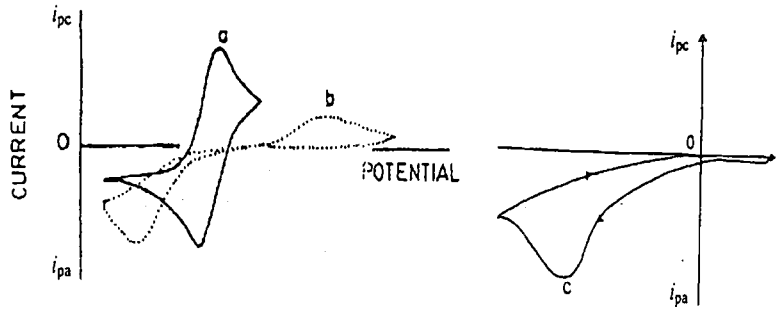

Figure 2.18: A schematic presentation of the cyclic voltammogram expected for (a) an electrochemical reversible process (b) an electrochemical quasi-reversible process ($80 < \Delta E_p < 100$ mV) and (c) an electrochemical irreversible process ($\Delta E_p > 100$ mV, often $i_{pa}/i_{pc} \neq 1$)

Systems can also be quasi-reversible or totally irreversible (see **Figure 2.18**). For quasi-reversible systems, kinetics are slow but the electron transfer process still takes place at a rate that allows $80 < \Delta E_p < 100$ mV. In such cases, scan rates should be slowed down to minimise ΔE_p. However, for quasi-reversible processes, the peak current is not proportional to $\nu^{1/2}$.

A completely irreversible system is one where only oxidation (or reduction) is possible or where the scan rate of the experiment cannot be made so slow that $\Delta E_p < 100$.[95] This can inter alia be caused by very slow electron exchange of redox species with the working electrode. In such a case **Equations 2.2**, **2.3**, **2.4** and **2.5** are not applicable.

2.4.4 Solvents and supporting electrolytes in electrochemistry

All electrochemical phenomena occur in a suitable medium, which generally consists of a solvent containing a supporting electrolyte. Considerations must be given as to how the chemical and the electrochemical properties of the electrode reaction in question may be affected by the solvent system.

The major requirement of a solvent is that the species under investigation must be soluble and stable in it.[96] The material under investigation must be soluble to the extent of at least 1 x 10^{-4} mol dm^{-3} and the concentration of the electrolyte must be at least 10x that of the material under investigation. An ideal electrochemical solvent should possess an electrochemical and chemical inertness over a wide potential range, it should be a good solvent for both electrolyte and substrate and it should preferably be unable to solvate the substrate. The solvents that are often used, are dipolar aprotic solvents. These solvents have large dielectric constant (≥ 10) and low proton availability. Acetonitrile, CH_3CN, is commonly used in anodic studies but is moderately nucleophilic. CH_3CN has a dielectric constant of 37 and is an excellent solvent for polar organic compounds and inorganic salts and is stable after purification. If a strictly non co-ordinating solvent is required, dichloromethane, CH_2Cl_2, is often employed. The electrochemical studies reported in this study were performed with CH_3CN as the solvent.

A supporting electrolyte is used to increase conductivity in the majority of electroanalytical and electrosynthetic experiments. Most of the current is carried by ions of the supporting electrolyte. Tetrabutylammonium hexafluorophosphate, TBAHFP/$TBAPF_6$, is widely used as a supporting electrolyte and it is also soluble in CH_3CN. A solution of TBAHFP/$TBAPF_6$ in acetonitrile exhibits a very wide accessible potential range with positive and negative decomposition potentials, 3.4 V and –2.9 V (*vs.* SCE) respectively.[97]

2.4.5 Cyclic voltammetry of ferrocene-containing β-diketones

The fifth aim (Chapter 1) of this study was to determine the formal reduction potentials of the iron core in the ferrocenyl fragment of the β-diketones as well as of the Rh^I centre in our new [Rh(β-diketonato)(cod)] complexes. Results of a cyclic voltammetry study of previously studied ferrocene containing β-diketones of the type $FcCOCH_2COR$ are important within the context of this study. CV results[20] of five different ferrocene-containing β-diketones 1-ferrocenyl-4,4,4-trifluorobutane-1,3-dione (Hfctfa, R = CF_3), 1-ferrocenyl-4,4,4-trichlorobutane-1,3-dione (Hfctca, R = CCl_3), 1-ferrocenylbutane-1,3-dione (Hfca, R = CH_3), 1-ferrocenyl-3-phenylpropane-1,3-dione (Hbfcm, R = Ph) and 1,3-diferrocenylpropane-1,3-dione (Hdfcm, R = Fc) are listed in **Table 2.10** and displayed in **Figure 2.19**. The difference in peak anodic, E_{pa}, and peak cathodic, E_{pc}, potentials, ΔE_p, for all the β-diketones indicates reasonable electrochemical reversibility at scan rates of 50 mV s^{-1}. All formal reduction potentials, $E^{0\prime}$, values remained constant between scan rates of 50 and 200 mV s^{-1}. The ratio i_{pc}/i_{pa} was in all cases close to unity, implying that the electrochemical oxidation of the

iron (II) nucleus of the ferrocenyl group is not followed by a chemical induced reduction of the iron (III) nucleus of the ferrocenium group by the hydroxyl group of the enol form of the β-diketone.

Table 2.10: Peak anodic potentials, E_{pa} (*vs.* Fc/Fc^+); difference in peak anodic and peak cathodic potentials, ΔE_p; formal reduction potentials, $E^{o\prime}$; peak anodic current, i_{pa}; and peak anodic/cathodic current ratios, i_{pa}/i_{pc}, for 2.0 mmol. dm^{-3} solutions of β-diketones of the type $FcCOCH_2COR$, measured in 0.1 mol. dm^{-3} $TBAPF_6/CH_3CN$ on a Pt electrode at 25°C at a scan rate of 50 mV s^{-1}. Data from reference 20

β-diketone	E_{pa} /V	ΔE_p /mV	$E^{o\prime}$ /V	$i_{pa}/\mu A$	i_{pa}/i_{pc}
Hdfcm-first ferrocenyl group	0.220	66	0.187	10.00	1.00
Hbfcm	0.267	73	0.230	11.58	0.97
Hfca	0.279	86	0.240	12.46	0.99
Hdfcm-second ferrocenyl group	0.333	72	0.297	12.14	1.02
Hfctca	0.332	78	0.293	12.08	0.98
Hfctfa	0.354	74	0.317	10.53	0.96

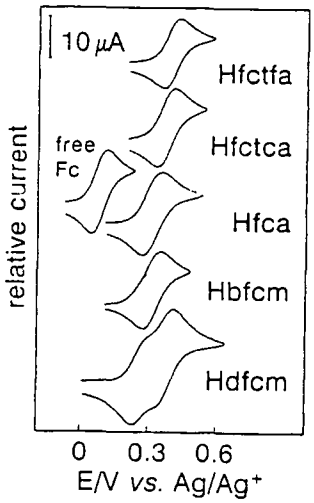

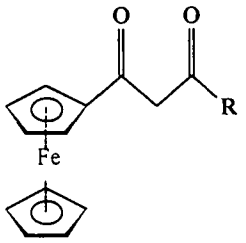

R = CF_3; Hfctfa
R = CCl_3; Hfctca
R = CH_3; Hfca
R = Ph; Hbfcm
R = Fc; Hdfcm

Figure 2.19: Cyclic voltammograms of 2 mmol dm^{-3} solutions of ferrocene and β-diketones measured in 0.1 M $TBAPF_6/CH_3CN$ at a scan rate of 50 mV s^{-1} on a Pt working electrode at 25.0(1) °C *versus* Ag/Ag^+

The spread of the formal reduction potential, measured *vs.* Fc/Fc^+, of the ferrocenyl groups of the β-diketones in **Table 2.10** is large: from 0.187 V for Hdfcm to 0.317 V for Hfctfa. This large spread in $E^{o\prime}$ is the result of good communication between the ferrocenyl group and the R substituents on the β-diketones via the backbone of the pseudo-aromatic β-diketone core. Formal reduction potentials of the ferrocenyl group on the β-diketones were found to be directly proportional to the

group electronegativities of the other substituent (R) on the β-diketone. This result implied that there is good communication due to electron delocalization between the ferrocenyl group and the R group on the β-diketone.

As seen in **Table 2.10** and in **Figure 2.19,** Hdfcm shows two formal reduction potentials $E^{o\prime}$ = 0.187 and 0.297 *vs.* Fc/Fc^+. This is in contrast to ^1H NMR measurements that could not differentiate between the two ferrocenyl groups. This observation was explained by the fact that the two ferrocenyl groups are not oxidised simultaneously at the surface of the electrode. Firstly, one ferrocenyl group is oxidised according to the reaction

$$FcCOCH_2COFc \rightarrow FcCOCH_2COFc^+ + e^- \qquad E^{o\prime} = 0.187 \text{ V } vs. \text{ } Fc/Fc^+$$

The group electronegativity of a Fc^+ group (χ_{Fc+} = 2.82) is, however, larger than that of Fc group (χ_{Fc} = 1.87), causing the Fc^+ group to be much more electron withdrawing. The second Fc group that still has to be oxidised in $FcCOCH2COFc^+$ is now, by conjugation, experiencing stronger electron withdrawing properties of the Fc^+ group making it much more difficult to oxidise according to the reaction

$$FcCOCH_2COFc^+ \rightarrow Fc^+COCH_2COFc^+ + e^- \qquad E^{o\prime} = 0.297 \text{ V } vs. \text{ } Fc/Fc^+$$

2.4.6 Cyclic voltammetry of Rhodium(I) complexes

Square planar rhodium complexes, being co-ordinatively unsaturated, can undergo oxidative addition reactions with various organic and inorganic molecules.[98] These reactions have been studied in order to gain more understanding of the electronic and steric factors influencing the oxidative reactions. The relation between electrochemical oxidation (oxidation potential by means of cyclic voltammetry) and the pK_a values of various β-diketone co-ordinated onto the rhodium is expected to be independent of steric parameters, where in contrast chemical oxidation (oxidation by means of, for example, CH_3I) is influenced by steric parameters. Electrochemical investigations can therefore offer numerous ways to explore the steric hindrance effect on rhodium complexes.

Redox results[99] of the rhodium core of four [Rh^I(β-diketonato)(CO)(PPh_3)] complexes, in which the free β-diketones has different electronegativities and steric hindrances, are presented in **Table 2.11**.

Table 2.11: Oxidation and reduction peak potentials *vs.* Fc/Fc^+ of the various [Rh(β-diketone)(CO)(PPh_3)] complexes and their respective free β-diketone pK_a values[99]

Free β-diketones	pK_a[17]	Complex	E_{pa}/ V	E_{pc}/ V
Dibenzoylmethane (Hdbm)	9.4	[Rh(dbm)(CO)(PPh_3)]	0.308	-0.76
Benzoylacetone (Hba)	8.7	[Rh(ba)(CO)(PPh_3)]	0.336	-0.80
Benzoyltrifluoroacteone (Hbtfa)	6.3	[Rh(btfa)(CO)(PPh_3)]	0.448	-0.64
Trifluoroacetone (Htfaa)	6.3	[Rh(tfaa)(CO)(PPh_3)]	0.491	-0.66

The larger the pK_a values of the free β-diketones (cited in **Table 2.11**) the less positive the oxidation potential and the more negative the reduction potential. This indicates easier oxidation of Rh(I) to Rh(III), and more difficult reduction of the Rh(III) to Rh(I) when the metal is co-ordinated to more basic β-diketones. For these complexes ΔE_p is larger than 1 V, indicating definite electrochemical irreversibility.

As expected, the steric effects from different terminal β-diketonato substituents did not have an influence during electrochemical oxidation. This was shown by the same E_{pc}, within experimental error, of the [Rh(btfa)(CO)(PPh_3)] and [Rh(tfaa)(CO)(PPh_3)].

2.5 Cytotoxic studies

2.5.1 Introduction

Potentially good chemotherapeutic drugs often find limited clinical use due to the many negative medical and physical side-effects they show. For cisplatin, [$Pt(NH_3)_2Cl_2$], the most successful metal-containing chemotherapeutic drug to date, these include *inter alia* high toxicity to the kidneys and bone marrow,[100] loss of appetite (anorexia),[101] development of drug resistance after continued drug dosage,[102] a high rate of excretion from the body,[103] low aqueous solubility and perhaps, most important of all, inability to distinguish between healthy and cancerous cells.[104] To combat these negative aspects surrounding cisplatin and other chemotherapeutic drugs, new antineoplastic materials are continuously being synthesised and evaluated. New methods of delivering an active drug to a cancerous growth are being developed[105] and combination therapy has been investigated in the hope of finding synergistic effects.[106]

2.5.2 Ferrocene derivatives on chemotherapy

A new field of potential application of both β-diketone complexes of rhodium(I) and derivatives of ferrocene has evolved in recent years with reports that some of these compounds show antineoplastic activity. It has been shown that certain ferrocenium salts[107] have more favourable 50% lethal dosage values than cisplatin.[108] Kanzawa and co-workers[109] showed that ferrocenylacetic acid induced good to excellent cure rates against human adenocarcinoma, squamous cell carcinoma and large cell carcinoma of the lung in *in vitro* human tumour clonogenic assays. Recently, Osella and co-workers[110] determined the mechanism of action of the ferrocenyl moiety in chemotherapy, which is based on electron transfer. The Fe^{II}-containing ferrocenyl group needs first to be activated by oxidation to a Fe^{III}-containing ferricenium species by redox-active enzymes in a particular body compartment. The ferricenium species then interact with water and oxygen to generate a hydroxyl radical ($OH^{\cdot}$). The hydroxyl radical then cleaves the DNA strands, which results in cell death. Electrochemical and biological studies performed in this laboratory,[111] indicated that only ferrocenyl derivatives with formal reduction potential less positive than ca. 0.216 V *vs.* SCE or 0.134 V *vs.* Ag/Ag^{+} are active in cytotoxicity experiments. Ferrocenyl oxidation by redox enzymes in the cell becomes thermodynamically impossible in compounds with much more positive formal reduction potentials and the ferrocenyl derivatives become for all practical purposes, inactive.

New ferrocene-containing compounds of the type $FcCOCH_2COR$ (with R = H, CH_3, CCl_3, CF_3, Ph, and Fc) and their rhodium complexes of the type [Rh(FcCOCHCOR)(cod)] have been investigated for their cytotoxic properties. IC_{50}-values (mean drug concentration expressed in μmol dm^{-3} causing 50% cell death) of HeLa cancer cell line and PHA-stimulated cells[112] are summarised in **Table 2.12** and illustrated for the rhodium complexes in **Figure 2.20**. It was found that IC_{50} value was dependent on the R substituent for both β-diketones and rhodium complexes. CF_3-containing compounds were observed to be having the lowest IC_{50} values, therefore having the highest cytotoxicity.

Table 2.12: IC_{50} values of the indicated ferrocene-containing β-diketones and their rhodium complexes against HeLa cancer cells and PHA-stimulated human lymphocytes. PHA = Phytohaemaglutin stimulated human mononuclear lymphocytes.

β-diketones	IC_{50} /μmol dm^{-3}		Rhodium complexes	IC_{50} /μmol dm^{-3}	
	HeLa	PHA-stimulated lymphocyte		HeLa	PHA-stimulated lymphocyte
$FcCOCH_2COH$	73.4	-	[Rh(FcCOCHCOH)(cod)]	62.4	-
$FcCOCH_2COCH_3$	66.6	-	[Rh(FcCOCHCOCH$_3$)(cod)]	64.4	-
$FcCOCH_2COFc$	54.4	>100	[Rh(FcCOCHCOFc)(cod)]	18.4	42.2
$FcCOCH_2COPh$	54.2	>100	[Rh(FcCOCHCOPh)(cod)]	28.3	97.2
$FcCOCH_2COCCl_3$	37.7	67.5	[Rh(FcCOCHCOCCl$_3$)(cod)]	7.9	4.7
$FcCOCH_2COCF_3$	6.8	83.1	[Rh(FcCOCHCOCF$_3$)(cod)]	12.5	41.6

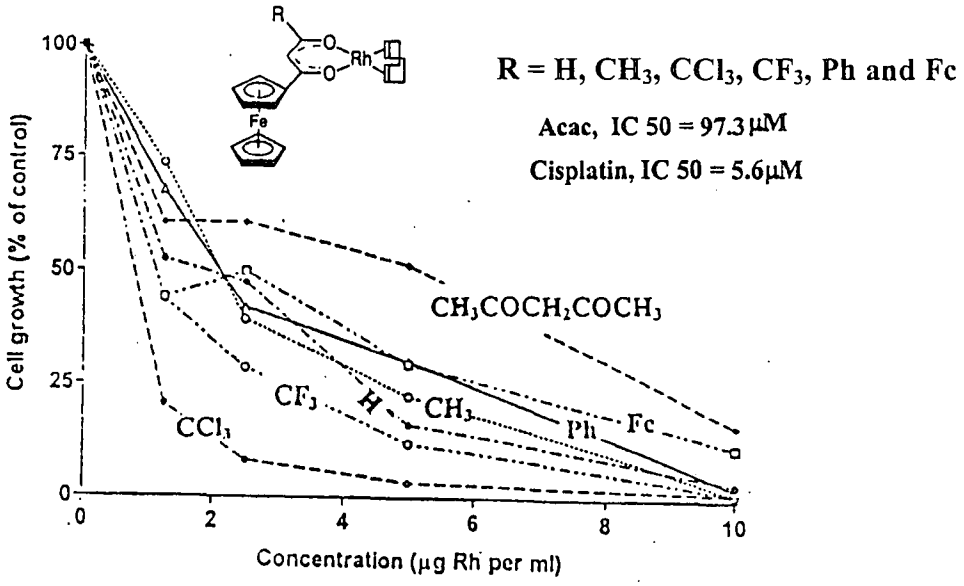

Figure 2.20: Percentage cell survival of HeLa cancer cell lines relative to the control experiment *vs.* concentration (μg Rh cm^{-3}) for the rhodium complexes of the type [Rh(FcCOCHCOR)(cod)] (with R indicated on the graph) and [Rh($CH_3COCHCOCH_3$)(cod)].

Most of the complexes of **Table 2.12** were more effective at killing cancer cells as compared to healthy cells as determined by PHA-stimulated human lymphocytes. The only exception is that of [Rh(FcCOCHCOCCl$_3$)(cod)]. The β-diketone $FcCOCH_2COCF_3$ was 83.1/6.8 ≈ 14 times more effective in killing cancer cells than healthy lymphocytes. Rhodium complexes showed much more cytotoxic activity than the free β-diketones. The rhodium complexes also behave as radiosensitizers

under hypoxic conditions, while the free β-diketones do not. The benefit of this is especially important in treatment of advanced cancers. When cancer gets advanced, it begins to function in an oxygen-starved environment, known as hypoxic conditions. Normally, drugs as well as radiation therapy then, become less effective. Any drug that can be activated under such conditions or that can enhance radiation therapy effectiveness under such conditions obviously is very appealing in cancer therapy. It was found that the rhodium-containing drugs become radiosensitizers under hypoxic conditions.[113] In particular, a dose modifying factor of 3 for [Rh(FcCOCHCOCF$_3$)(cod)] (i.e. radiation becomes 3x more effective in cancer treatment in the presence of [Rh(FcCOCHCOCF$_3$)(cod)] than in its absence) was found. This complex also exhibited an oxygen enhancement ratio of 2.4 (i.e. radiation effectiveness remains unchanged even if the oxygen supply falls 2.4 times from normal).

No detailed information on the mechanism of action of rhodium complexes in chemotherapy is, however, currently available. From a chemical point of view it is reasonable to assume that either a substitution reaction involving Rh-containing drug and DNA, or an oxidative addition reaction where Rh^{I} gets oxidised to Rh^{II} or Rh^{III}, is involved. For the purpose of this study substitution kinetics of [Rh(FcCOCHCOR)(cod)] complexes were studied as a function of different R groups. Attention has also been focussed to determine the effect that the size of an alkyl group, R, has on cytotoxic activity. The R groups that were focussed on in this study are: R = H, CH_3, CH_2CH_3, $CH(CH_3)_2$ and $C(CH_3)_3$.

2.6 References

[1] Hauser, C.R., Swamer, F.W. and Adams, J.T., *Organic Reactions,* John Wiley and Sons, New York, **8**, chapter 3, p59, 1954.

[2] Walker, H.G. Jr., Sanderson, J.J. and Hauser, C.R., *J. Am. Chem. Soc.,* **75**, 4109 (1953)

[3] Adams, J.T. and Hauser, C.R., *J. Am. Chem. Soc.,* **66**, 1220 (1944).

[4] Swamer, F.W. and Hauser, C.R., *J. Am. Chem. Soc.,* **68**, 2647 (1946).

[5] Cullen, W.R., Rettig, S.J. and Wickenheiser, E.B., *J. Mol. Catal.,* **66,** 251 (1991)

[6] Moon, S. and Kwon, Y., *Magn. Reson. Chem.,* **39,** 89 (2001).

[7] Gero, A., *J. Org. Chem.*, **19,** 469 (1954).

[8] Semerano, G. and Chisini, A., *Gazz. Chim. Ital.*, **66,** 504 (1936).

[9] Conant, J.B. and Thompson Jr, A.F., *J. Am. Chem, Soc.*, **54,** 4039 (1932).

[10] Wheland, G.W., *Advanced Organic Chemistry,* (3rd edition), John Wiley and Sons, New York, 1960.

[11] Irving, R.J. and Riberio da Silva, M.A.V., *J. Chem. Soc. Dalton*, 798 (1975).

[12] Bratoz, S., Hadzi, D. and Rossmy, G., *Trans. Faraday Soc.*, **52,** 464 (1956).

[13] Jarrett, H.S., Sadler, M.S. and Shoolery, J.N., *J. Chem. Phys.*, **21,** 2092 (1953).

[14] Reeves, L.W., *Canad. J. Chem.* **35,** 1351 (1957).

[15] Du Plessis, W.C., Vosloo, T.G. and Swarts, J.C., *J. Chem. Soc., Dalton Trans.,* 2507 (1998).

[16] Leipoldt, J.G. and Grobler, E.C., *Transition Met. Chem. (Weinheim, Ger.)*, **11,** 110 (1986).

[17] Stary, J., *The Solvent Extraction of Metal Chelates,* Pergamon Press LTD Oxford, England, p 196, 1964.

[18] Park, J.D., Brown, H.A. and Lachen, J.R., *J. Am. Chem. Soc.*, **75,** 4753 (1953).

[19] Klose, G., Thomas, P., Uhlemann, E. and Marki, J., *Tetrahedron*, **22,** 2695 (1966).

[20] Du Plessis, W.C., Erasmus, J.J.C., Lamprecht, G.J., Conradie, J., Cameron, T.S., Aquino, M.A.S. and Swarts, J.C., *Can. J. Chem.,* **77,** 378 (1999).

[21] Bell, W., Glidewell, C., Crayston, J.A., Mazid, M.A. and Hursthouse, M.B., *J. Organomet. Chem.,* **434,** 115 (1992).

[22] Du Plessis, W.C., Davis, W.L., Cronje, S.J. and Swarts, J.C., *Inorg. Chim. Acta,* **314,** 97 (2001).

[23] Yogev, A. and Mazur, Y., *J. Org. Chem.,* **36,** 2162 (1967).

[24] Gibson, D., *Coord. Chem. Rev.,* **4,** 225 (1969).

[25] Sidgwick, N.J., *The Chemical Elements and their Compounds,* Claredon Press, Oxford, **1,** p 641, 1950.

[26] Leipoldt, J.G., Basson, S.S., Bok, L.D.C. and Gerber, T.I.A., *Inorg. Chim. Acta.,* **26,** L35 (1978).

[27] Juranic, N., *J. Chem. Soc. Dalton Trans.*, 79 (1988).

[28] Morgan, G.T. and Drew, H.D.K., *J. Chem. Soc.,* **117,** 1456 (1920).

[29] Bonati, F. and Minghetti, G., *J. Organomet. Chem.,* **22,** 5 (1970).

[30] Gibson, D., Johnson, B.F.G. and Lewis, J., *J. Chem. Soc.*, **(A),** 367 (1970).

[31] Morgan, G.T. and Drew, H.D.K., *J. Chem. Soc.*, **121,** 926 (1922).

[32] Nyholm, R.S., *Proc. Chem. Soc.*, 273 (1961).

[33] Matsumoto, T., Periana, R.A., Taube, D.J. and Yoshida, H., *J. Mol. Catal. A: Chem.*, **180,** 1 (2002).

[34] Allen, G., Lewis, J., Long, R.F. and Oldham, C., *Nature,* **202,** 590 (1964).

[35] Shibata, S., *Bull. Chem. Soc. Japan,* **30,** 753 (1957).

[36] Mehrotra, R.C., Bohra, R. and Gaur, D.P., *Metal β-Diketonates and Allied Derivatives,* Academic Press, London, New York, San Francisco, p58, 1978.

[37] Richardson, M.F. and Sievers, R.E., *Inorg. Chem.*, **10,** 498 (1971).

[38] Pope, W.G., Steinbach, J.R. and Wagner, W.F., *J. Inorg. Nucl. Chem.*, **20,** 304 (1961).

[39] Springer Jr, C.S., Meek, D.W. and Sievers, R.E., *Inorg Chem.*, **6,** 1105 (1967).

[40] Eisentraut, K.J. and Sievers, R.E., *J. Inorg. Nucl. Chem.*, **29,** 1931 (1967).

[41] Collman, J.P., Moss, R.A.,Maltz, H. and Heindel, C.C., *J. Am. Chem. Soc.*, **83,** 531 (1961).

[42] Singh, P.R. and Sahai, R., *Austral. J. Chem.*, **20,** 649 (1967).

[43] Collman, J.P. and Yamada, M., *J. Org. Chem.*, **28,** 3017 (1963).

[44] Singh, P.R. and Sahai, R., *Inorg. Chim. Acta.*, **2,** 102 (1968).

[45] Singh, P.R. and Sahai, R., *Indian J. Chem.*, **8,** 178 (1970).

[46] Collman, J.P., Marshall, R.L., Young III, W.L. and Goldby, S.D., *Inorg. Chem.*, **1,** 704 (1962).

[47] Kluiber, R.W., *J. Am. Chem. Soc.*, **83,** 3030 (1961).

[48] Collman, J.P., Moss, R.A., Goldby, S.D. and Trhanovsky, W.S., *Chem. and Ind.*, 1213 (1960).

[49] Collman, J.P., Marshall, R.L., Young III, W.L. and Sears Jr, C.T., *J. Org. Chem.*, **28,** 1449 (1963).

[50] Cross, R.J., *Chem. Soc. Rev.*, **14,** 197 (1985).

[51] Mathey, F. and Sevin, A., *Molecular Chemistry of the Transition Elements*, John Wiley & Sons, Chichester, p28-50, 1996.

[52] Wilkins, R.G., *Kinetics and Mechanism of Reactions of Transition Metal Complexes,* 2nd thoroughly revised edition, VCH, Weinheim, p103, 232 – 242, 1991.

[53] Cross, R.J., *Adv. In Inorg. Chem.*, **34,** 219 (1989).

[54] Stranks, D.R., *Pure Appl. Chem.*, **38,** 303 (1974).

[55] Whalley, E., *J. Chem. Phys.*, **38,** 1400 (1963).

[56] Kotowski, M., Palmer, D.A. and Kelm, H,. *Inorg. Chem.*, **18,** 2555 (1979).

[57] Van Eldik, R., Studies in Inorganic Chemistry 7, Inorganic High Pressure Chemistry, Kinetics and Mechanism, Elsevier Science Publishers B.V., Amsterdam, 1986.

[58] Van Eldik, R., Palmer, D.A. and Kelm, H., *Inorg. Chem.*, **18,** 572 (1979).

[59] Purcell, K.F. and Kotz, J.C., *Inorganic Chemistry,* W.B. Saunders Company, Philadelphia, p 59, 700-708 1977.

[60] Belluco, U., Cattalini, L., Pearson, R.G. and Turco, A., *J. Amer. Chem. Soc.*, **87,** 241 (1965).

[61] Swain, C.G. and Scott, C.B., *J. Am. Chem. Soc.*, **75,** 141 (1953).

[62] Leipoldt, J.G., Lamprecht, G.J. and Steynberg, E.C., *J. Organomet. Chem.*,**402,** 259 (1991).

[63] Leipoldt, J.G., Basson, S.S., van Zyl, G.J. and Steyn, G.J.J., *J. Organomet. Chem.*, **418,** 241 (1991).

[64] Vosloo, T.G. and Swarts, J.C., *Trans. Met. Chem.*, **27,** 411 (2002).

[65] Leipoldt, G.J., Steynberg, E.C. and Van Eldik, R., *Inorg Chem.*, **26,** 3069 (1987).

[66] Robb, W. and Nicholson, C.G., *S. Afr. J. Chem.*, **31,** 1 (1978).

[67] Werner, A., *Z.anorg. Chem.*, **3,** 267 (1893).

[68] Belluco, U., Graziana, M. and Rigo, P., *Inorg. Chem.*, **5,** 1123 (1966).

[69] Appleton, T.G., Clark, H.C. and Manzer, L.E., *Coord. Chem. Rev.*, **10,** 335 (1973).

[70] Bancroft, G.M. and Butler, K.D., *J. Amer. Chem. Soc.*, **96,** 7203 (1974).

[71] Bonati, F. and Wilkinson, G., *J. Chem. Soc.*, 3156 (1964).

[72] Damoense, L.J., Purcell, W., Roodt, A. and Leipoldt, J.G., *Rhodium Ex.*, **5,** 10 (1994).

[73] Botha, L.J., Basson, S.S. and Leipoldt, J.G., *Inorg. Chim. Acta.*, **126,** 25 (1987).

[74] Grinberg, A.A., *Acta Physiochim.*, USSR, **3,** 573 (1935).

[75] Emsely, J. and Hall D., *The Chemistry of Phosphorous,* Harper & Row Publishers, London p 199, 1976.

[76] Roodt, A., Leipoldt, J.G., Swarts, J.C. and Steyn, G.J.J., *Acta Cryst.*, **C48,** 547 (1992).

[77] Leipoldt, J.G., Bok, L.D.C., Basson, S.S. and Meyer, H., *Inorg. Chim. Acta,* **42,** 105 (1980).

[78] Basson, S.S., Leipoldt, G.J., Roodt, A. and Venter, J.A., *Inorg. Chim. Acta,* **118,** L45 (1986).

[79] Leipoldt, J.G., Bok, L.D.C., van Vollenhoven, J.S. and Pieterse, A.I., *J. Inorg. Nucl. Chem.*, **40,** 61 (1978).

[80] Lamprecht, G.J., Swarts, J.C., Conradie, J. and Leipoldt, J.G., *Acta Crystallogr.*, Sect. C **49,** 82 (1993).

[81] Conradie, J., Lamprecht, G.J., Otto, S. and Swarts, J.C., *Inorg. Chim. Acta,* **328,** 191 (2002).

[82] Leipoldt, J.G., Basson, S.S., Schelbusch, J.J.J. and Grobler, E.C., *Inorg. Chim. Acta* ,**62,** 113 (1982).

[83] Purcell, W., Basson, S.S., Leipoldt, J.G., Roodt, A. and Preston, H., *Inorg. Chim. Acta,* **234,** 153 (1995).

[84] Basolo, F., Chatt, J., Gray, H.B., Pearson, R.G. and Shaw, B.L., *J. Chem. Soc.* 2207 (1961).

[85] Zumdahl, S.S. and Dargo, R.S., *J. Am. Chem. Soc.*, **90,** 6669 (1968).

[86] Basolo, F., Chatt, J., Gray, H.B. and Pearson, R.G., *J. Amer. Chem. Soc.*, **82,** 4200 (1960).

[87] Pearson, R.G., Gray, H.B. and Basolo, F., *J. Am. Chem. Soc.*, **82,** 787 (1960).

[88] Shriver, D.F, Atkins, P. and Langford, C.H., *Inorganic Chemistry,* 2nd ed., Freeman, New York, p467, 1994.

[89] Christensen, P.A. and Hammet, A., *Techniques and Mechanism in Electrochemistry,* Blackie Academic & Professional, Chapter 2, 1994.

[90] Bobbitt, J.M., and Wills, J.P., *J. Org. Chem.*, **45,** 1978 (1980).

[91] Nelsen, S.F., Kessel, C.R., Brien, D.J. and Weinhold, F., *J. Org. Chem.*, **45,** 2116 (1980).

[92] Powers, M.J. and Meyer, T.J., *J. Amer. Chem. Soc.*, **102,** 1289 (1980).

[93] Kissinger, P.T. and Heineman, W.R., *J. Chem. Ed.*, **60(9),** 702 (1983).

[94] Bard, A.J. and Faulkner, L.R., *Electrochemical Methods: Fundamentals and Applications,* Wiley, New York, chapter 6, 1980.

[95] Christensen, P.A. and Hammet, A., *Techniques an Mechanism in Electrochemistry,* Blackie Academic & Professional, London p.55-67, 170-175, 1994.

[96] Van Benschoten, J.J., Lewis, J.Y., Heineman, W.R., Roston, D.A. and Kissinger, P.T., *J. Chem. Ed.*, **60(9),** 772 (1983).

[97] Kissinger, P.T. and Heineman, W.R., *Laboratory Techniques in Electroanalytical Chemistry,* Dekker, New York Chapter 13, 1984.

[98] Collman, J.P., *Acc. Chem. Res,*. **1,** 136 (1968).

[99] Lamprecht, D. and Lamprecht, G.J., *Inorg. Chim. Acta,* **309,** 72 (2000).

[100] Rozencweig, M., Van Hoff, D.D., Slavik, M. and Chrislom, J., *Ann. Intern. Med.*, **86,** 803 (1977).

[101] Burchenal, J.H., Kalaher, K., O'Toole, T. and Chrisholm, J., *Cancer Res.*, **37,** 3455 (1977).

[102] Wolf, W. And Manaka, R.C., *J. Clin. Hemotol. Oncol.*, **7,** 79 (1977).

[103] Drobonik, J. And Horacek, P., *Chem-Biol. Interact. I,* **7,** 223 (1973).

[104] Duncan, R. And Kopecek, J., *Adv. Polym. Sci.*, **57,** 51 (1984).

[105] Swarts, J.C. Neuse, E.W., Perlwitz, A.G., Stephanou, A.S. and Lamprecht, G.J., *Angew. Makromol. Chem.*, **207,** 123 (1993).

[106] Gale, G.R., Atkins, L.M. and Meischen, S.J., *Cancer Treat. Rep.*, **61,** 445 (1977).

[107] Köpf-Maier, P., Köpf, H. And Neuse, E.W., *J. Cancer Res. Clin. Oncol.*, **108,** 336 (1984).

[108] Ward, J.M., Grabin, M.E., Berlin, E. and Young, D.M., *Cancer Res.*, **37,** 1238 (1977).

[109] Neuse, E.W. and Kanzawa, F., *Appl. Organomet. Chem.*, **4,** 19 (1990).

[110] Osella, D., Ferrali, M., Zanello, P., Laschi, F., Fontani, M., Nervi, C. and Cavigiolio, G., *Inorg. Chim. Acta,* **306,** 42 (2000).

[111] Swarts, J.C., Swarts, D.M., Maree, D.M., Neuse, E.W., La Madeleine, C. and Van Lier, J., *Anticancer Research,* **21,** 2033 (2001).

[112] Swarts, J.C., unpublished results, with permission.

[113] Falzone, N., Slabbert, J.P., Swarts, J.C. and Van Rensburg, C.E.J., *Anti-cancer drug design,* In press (2002).

CHAPTER 3

RESULTS AND DISCUSSION

3.1 Introduction

The synthesis and characterisation of new ferrocene containing β-diketones of the type [$FcCOCH_2COR$], with R = H, CH_2CH_3, $CH(CH_3)_2$ and $C(CH_3)_3$ are described in this chapter. Characterisation of these β-diketones includes techniques such as ^1H NMR, cyclic voltammetry and keto-enol equilibrium studies as well as kinetics of conversion from enol to keto isomer. A discussion of the complexation reactions of these β-diketones with $[Rh_2Cl_2(cod)_2]$ to give [Rh(FcCOCHCOR)(cod)] complexes is also presented. Substitution kinetics of the β-diketonato ligand with 1,10-phenanthroline and the cyclic voltammetry of these [Rh(FcCOCHCOR)(cod)] complexes are also described. The influence of group electronegativities of R groups in the β-diketonato ligand on the rhodium centre is quantified, using parameters such as ferrocenyl formal reduction potentials, second order rate constants for the substitution of $(FcCOCHCOR)^-$ with 1,10-phenanthroline in [Rh(FcCOCHCOR)(cod)] and β-diketone pK_a values. Some cytotoxic properties of these compounds on cancer cells are presented in the final section of this chapter.

3.2 Synthesis and identification of compounds

3.2.1 Synthesis of ferrocene containing β-diketones

As shown in **Scheme 3.1**, page 59, acetylferrocene (**2**) was prepared (in 81% yield) by treating ferrocene (**1**) with acetic anhydride in the presence of phosphoric acid. It was important to maintain an internal reaction temperature between 100 and 105°C to maximise yields. After abstraction of the methine proton of acetylferrocene with a strong base like lithium diisopropylamide, LiDIPA, the lithium salt of acetylferrocene underwent a Claisen condensation reaction with a range of monocarboxylic esters to afford the β-keto-aldehyde, 2-ferrocenoyl-etan-1-al (ferrocenoylacetaldehyde, Hfch (**3**)) and β-diketones, 1-ferrocenylbutane-1,3-dione (ferrocenoylacetone, Hfca (**4**)), 1-ferrocenylpentane-1,3-dione (ferrocenoylpropan-2-one, Hfcp (**5**)), 1-ferrocenyl-4-methylpentane-1,3-dione (ferrocenoyl-3,3-dimethylacetone, Hfcdma (**6**)) and 1-ferrocenyl-4,4-dimethylpentane-1,3-dione (ferrocenyl-3,3,3-trimethylacetone, Hfctma (**7**)). It was observed that the more hydrogen atoms of the CH_3 group of $FcCOCH_2COCH_3$ are substituted with a methyl group, the lesser the yields became. Hfca (R = CH_3) was isolated in yields of about 38%,

Hfcp (R = CH_2CH_3) was isolated in 24% yields, Hfcdma (R = $CH(CH_3)_2$) in 21% yields and Hfctma (R = $C(CH_3)_3$) in 17% yields. The β-keto-aldehyde, $FcCOCH_2COH$, was obtained by reacting acetylferrocene with methyl methanoate in 32% yield. Hfcp (**5**) was very sluggish to form crystals and was recrystallized with hexane and ether and stored in the freezer for about 2 weeks. The other β-diketones crystallised within 7 days. A self-aldol condensation product of acetylferrocene, 1,3-diferrocenylbut-2-en-1-one (1-ferrocenoyl-2-ferrocenylpropene (**8**)), was obtained in all syntheses as a by-product. The highest yields (40%) of the by-product (**8**) was obtained during Hfctma synthesis. Flash column chromatography was used to purify all the β-diketones, but the keto-aldehyde (**3**) fixated on a silica gel column, and then decomposed to a black product. Hfch was, therefore, purified mainly by crystallisation.

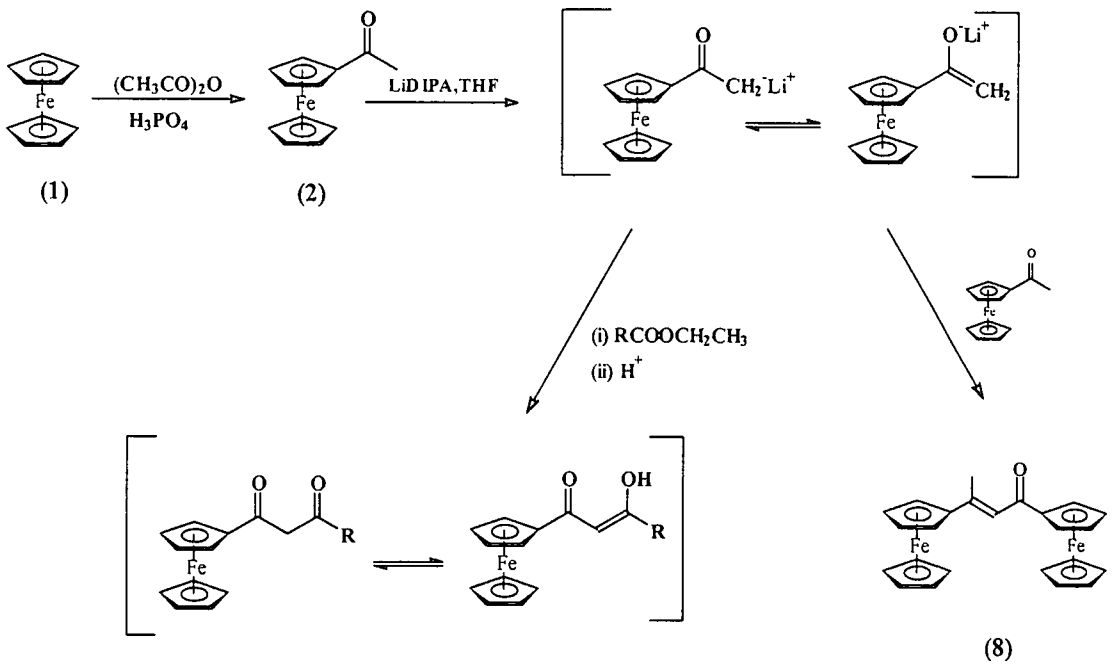

(3) R = H, Hfch
(4) R = CH_3, Hfca
(5) R = CH_2CH_3, Hfcp
(6) R = $CH(CH_3)_2$, Hfcdma
(7) R = $C(CH_3)_3$, Hfctma

Scheme 3.1: Claisen condensation of acetylferrocene (2) with an appropriate ester gives the β-diketones Hfch (3), Hfca (4), Hfcp (5), Hfcdma (6) and Hfctma (7). Self-aldol condensation of acetylferrocene led to the side product (8).

β-Diketones exist in solution (and in the vapour phase[1]) as mixtures of keto and enol tautomers in equilibrium with each other (**Scheme 3.1**). This equilibrium was studied for β-diketones **3-7** and will be discussed in section **3.3**.

3.2.2 Synthesis of ferrocene-containing β-diketonato rhodium(I) complexes

The rhodium dimer (**9**) was obtained by standard methods[2] in yields up to 73%. The method involved refluxing of $RhCl_3 \cdot 3H_2O$ and cyclooctadiene in the presence of ethanol for $2^1/_2$ hours at 78°C, to give $[Rh_2Cl_2(cod)_2]$ as a yellow powder. Complexation of the β-diketones **3-7** with $[Rh_2Cl_2(cod)_2]$ (**9**) in DMF at room temperature **(Scheme 3.2)**, leads to the formation of Rh(I) complexes of the type [Rh^I(β-diketonato)(cod)] with yields of 75% for [Rh(fch)(cod)], **10**, 80% for [Rh(fca)(cod)], **11**, 85% for [Rh(fcp)(cod)], **12**, 90% for [Rh(fcdma)(cod)], **13** and 88% for [Rh(fctma)(cod)], **14**.

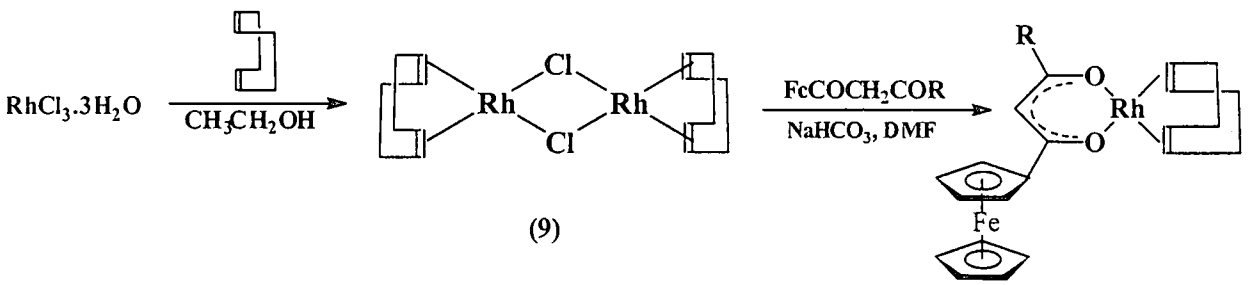

(9)

(10) R = H
(11) R = CH_3
(12) R = CH_2CH_3
(13) R = $CH(CH_3)_2$
(14) R = $C(CH_3)_3$

Scheme 3.2: Reaction for the complexation of ferrocene-containing β-diketones with $[Rh_2Cl_2(cod)_2]$ (9) at room temperature in the presence of $NaHCO_3$ to give [Rh(fch)(cod)] (10), [Rh(fca)(cod)] (11), [Rh(fcp)(cod)] (12), [Rh(fcdma)(cod)] (13) and [Rh(fctma)(cod)] (14).

The base, $NaHCO_3$, added in stoichiometric amounts to the ferrocene-containing ligand, was used to extract the methine proton from the β-diketone to form a β-diketonato anion. The β-diketonato anion is the actual complexing ligand in **Scheme 3.2**. It has been found[3] that β-diketones with pK_a values > 7 react more slowly than those with lower pK_a values. Although complexes **11, 13** and **14**

were easy to crystallise. [Rh(fcp)(cod)], (**12**), did not form crystals. It was a thick waxy substance. Attempts to crystallise **12** from acetone and water led to its decomposition. The rhodium complex with keto-aldehyde, (**10**), was purified by recrystallisation as it could not be eluted from a silica gel column. Complexes **11-14** could be purified with silica gel column chromatography.

3.3 Keto-enol equilibrium in β-diketones

3.3.1 The observed solution phase equilibrium constant, K_c

All β-diketones exist in principle as a mixture of keto and enol forms as shown in **Scheme 3.3**. Although two enol isomers for the β-diketones, $FcCOCH_2COR$ are possible, in solution it was found that at equilibrium enol isomer **A** does not contribute much to the overall mixture.

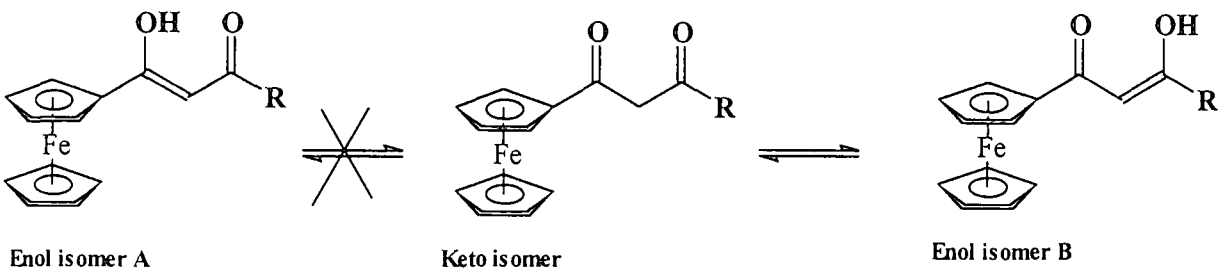

Scheme 3.3: Keto-enol equilibrium for ferrocene-containing β-diketones

The dominant isomers found in the overall mixture of each compound are the keto isomer and enol isomer **B**. The reason why enol isomer **B** dominates over enol isomer **A** will be explained later (section **3.4.3**). The apparent absence of enol isomer **A** allows writing of the simple equilibrium:

$$Fc\text{-}CO\text{-}CH_2\text{-}CO\text{-}R \overset{K_C}{\rightleftharpoons} Fc\text{-}CO\text{-}CH{=}C(OH)\text{-}R$$

Reaction 3.1

with $$K_c = \frac{[Fc\text{–}CO\text{–}CH{=}C(OH)\text{–}R]}{[Fc\text{–}CO\text{–}CH_2\text{–}CO\text{–}R]}$$

$$= \frac{\%\ \text{enol isomer}}{\%\ \text{keto isomer}}$$

$$= \frac{100 - \% \text{ keto isomer}}{\% \text{ keto isomer}} \qquad \textbf{Equation 3.1}$$

In this study, K_c values for β-diketones, in $CDCl_3$ solutions, were obtained from ^1H NMR spectroscopy at 19°C. **Figure 3.1** shows the equilibrium ^1H NMR spectrum of Hfcdma, **6**. From this spectrum, utilising the integral values of protons of the keto and enol isomers, the equilibrium constant, K_c, can be calculated. Integration of the spectrum was done in such a way that the methine proton of the enol isomer, $FcCOC\underline{H}=C(OH)CH(CH_3)_2$, was assigned an integral value of one.

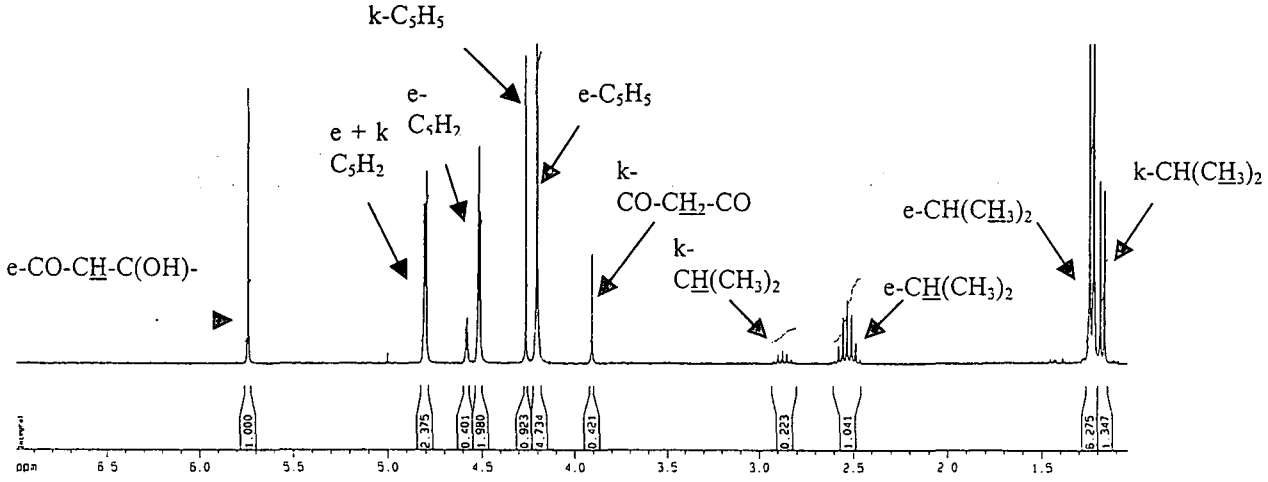

Figure 3.1: The ^1H NMR spectrum of Hfcdma, 6, at equilibrium: Fc-CO-CH_2-CO-$CH(CH_3)_2$ ⇋ Fc-CO-CH=C(OH)-$CH(CH_3)_2$, at 19°C. The spectrum was obtained after enough time elapsed to ensure that the sample was at equilibrium. The prefix 'e' implies a signal of the enol isomer, while the prefix 'k' implies a signal of the keto isomer. Fc = $C_5H_5FeC_5H_4$

Utilising the $CH(C\underline{H}_3)_2$ signal of $FcCOCH_2COCH(CH_3)_2$ in **Figure 3.1**, the % keto isomer in Hfcdma, **6**, is

$$\% \text{ keto isomer} = (I \text{ of keto signal}) / \{(I \text{ of keto signal}) + (I \text{ of enol signal})\} \times 100$$
$$= 1.347 / (1.347 + 6.275) \times 100$$
$$= 17.7\%$$

Utilising the $C\underline{H}(CH_3)_2$ signal, the % keto isomer is 17.6%. From the C_5H_5 signal, the % keto signal is 16.3%, while from the C_5H_2 signal it is 16.8%. From the methine proton signals, $FcCOC\underline{H}=C(OH)CH(CH_3)_2$ and $FcCOC\underline{H}_2COCH(CH_3)_2$, the % keto isomer is calculated to be 17.4%. The average % keto isomer is therefore 17.2%. Substitution of this value in **Equation 3.1** gives:

$$K_c = \frac{100 - \%\ \text{keto isomer}}{\%\ \text{keto isomer}}$$

$$= \frac{(100 - 17.17)\%}{17.17\%}$$

$$= 4.82$$

for the equilibrium

$$\text{Fc-CO-CH}_2\text{-CO-CH(CH}_3)_2 \underset{}{\overset{K_C}{\rightleftharpoons}} \text{Fc-CO-CH=C(OH)-CH(CH}_3)_2$$

In a similar fashion, by fitting the average % keto isomer for **3**, **4**, **5** and **7** using appropriately unambiguously definable ^{1}H NMR signals, the K_c value for each β-diketone was determined. Results are summarised in **Table 3.1**.

Table 3.1: Equilibrium constant, K_c, at 19°C, the % keto isomer at equilibrium for the keto-enol equilibrium, with Gibb's free energy for β-diketones 3-7

Compounds	**% keto**	**K_c in $CDCl_3$ at 19°C**	**ΔG / kJ mol^{-1}**
Hfch, ($FcCOCH_2COH$), **3**	9.7	9.3	-5.5
Hfca, ($FcCOCH_2COCH_3$), **4**	22	3.4	-3.0
Hfcp, ($FcCOCH_2COCH_2CH_3$), **5**	29.8	2.4	-2.1
Hfcdma, ($FcCOCH_2COCH(CH_3)_2$), **6**	17.2	4.8	-3.8
Hfctma, ($FcCOCH_2COC(CH_3)_3$), **7**	12	7.3	-4.8

From the well known thermodynamic expression[4]

$$\Delta G = -RT \ln K_c$$

The Gibbs free energy, ΔG for **Reaction 3.1**, page 61, can be calculated. Results are tabulated in **Table 3.1**. A decrease in the equilibrium keto content (increase in the equilibrium enol content) gives rise to an increase in equilibrium constant, K_c. As more **H** atoms of the CH_3 group of $FcCOCH_2COCH_3$, **4**, are substituted with a methyl group, in **5**, **6** and **7**, larger K_c values are observed. This implies that the enol isomer becomes increasingly thermodynamically stable in moving from **5** to **6** to **7**. This is probably in part a consequence of the electron donating inductive

effect of alkyl groups. Tertiary alkyl groups are more electron donating than secondary and primary alkyls. There is also a correlation observed between Gibbs free energy, ΔG, and % keto isomer of β-diketones. As ΔG becomes more negative, the % keto content becomes smaller. This means that the thermodynamic driving force of the above equilibrium becomes more favourable to shift the equilibrium to the right. Increased % enol content is, therefore, observed on β-diketones with a more negative ΔG value for the equilibrium in **Reaction 3.1** page 61

3.3.2 Kinetics of keto-enol conversion

From a kinetic point of view, the equilibrium constant, K_c, can also be expressed in terms of the quotient of the rate of conversion of keto to enol isomers and the rate of conversion of enol to keto isomers, as given by the following reaction

$$\underset{\text{Keto isomer}}{\text{Fc-CO-CH}_2\text{-CO-R}} \underset{k_{-1}}{\overset{k_1}{\rightleftharpoons}} \underset{\text{Enol isomer}}{\text{Fc-CO-CH=C(OH)-R}} \qquad \textbf{Reaction 3.2}$$

In particular, $K_c = \frac{k_1}{k_{-1}}$, with k_1 = rate constant for the conversion of keto to enol isomer and k_{-1} = rate constant for the conversion of enol to keto isomer. To obtain a solution of the β-diketones **3-7** enriched in keto content, a solution of, for example, Hfcp, **5** (4 mg) in diethyl ether was extracted by aqueous NaOH. The original organic layer was discarded and $CDCl_3$ (3 cm^3) was added to the aqueous layer. Acidification with HCl allowed extraction of the β-diketone into the $CDCl_3$ layer in sufficient concentrations to obtain a ^1H NMR spectrum. The aqueous layer was discarded and the $CDCl_3$ layer was quickly washed with water and a portion of the organic layer (0.7 cm^3) was taken to record a ^1H NMR spectrum. A keto-enriched spectrum of Hfcp was obtained and is shown in **Figure 3.2** (A). In the solid state, however, after enough time has elapsed, the equilibrium in **Reaction 3.2**, is essentially driven completely to the enol side. Aged samples of β-diketones were therefore used to obtain enol-enriched spectra. **Figure 3.2** (C) shows such a spectrum for Hfcp, **5**. Slow conversion of the enol isomer to the keto isomer until the solution equilibrium position (**Figure 3.2** (B)) is reached, was monitored by recording a ^1H NMR spectrum at specific time intervals until the % keto isomer (see page 62 for its calculation) remained constant.

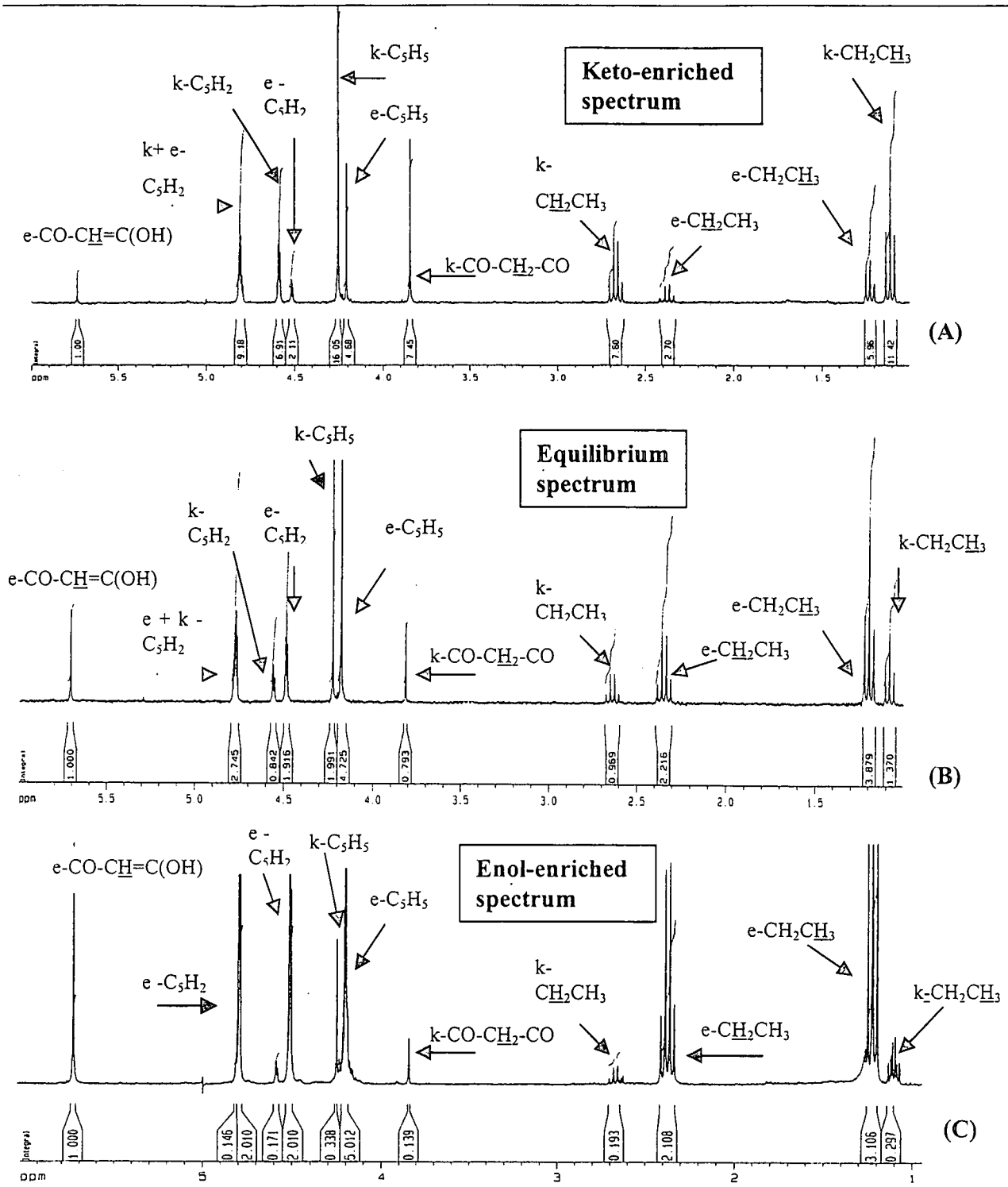

Figure 3.2: (A) A keto-enriched ^{1}H NMR spectrum of Hfcp, 5 (Fc-CO-CH_2-CO-CH_2CH_3 ⇋ Fc-CO-CH=C(OH)-CH_2CH_3). The spectrum was recorded directly after extraction of Hfcp into aqueous NaOH and recovery into $CDCl_3$ after acidification. (B) ^{1}H NMR spectrum of Hfcp in $CDCl_3$ at equilibrium. (C) ^{1}H NMR of an aged sample of Hfcp containing mostly the enol isomer. All spectra were recorded at 19°C. e = enol signal, k = keto signal.

For each time interval the % keto isomer was determined and the observed first-order rate constant, k_{obs}, was obtained from **Equation 3.2**,[5] utilising the fitting program MINSQ.[6]

$$[A]_t = [A]_i + ([A]_o - [A]_i)\exp^{[-(k_{obs})t]} \qquad \textbf{Equation 3.2}$$

with $[A]_t$ = % keto isomer at time t, $[A]_i$ = % keto isomer at infinite time, $[A]_o$ = initial % keto isomer, $k_{obs} = k_1 + k_{-1}$. Hence rate constants k_1 and k_{-1} were obtained by simultaneously solving the equations $k_{obs} = k_1 + k_{-1}$ and $K_c = \frac{k_1}{k_{-1}}$.

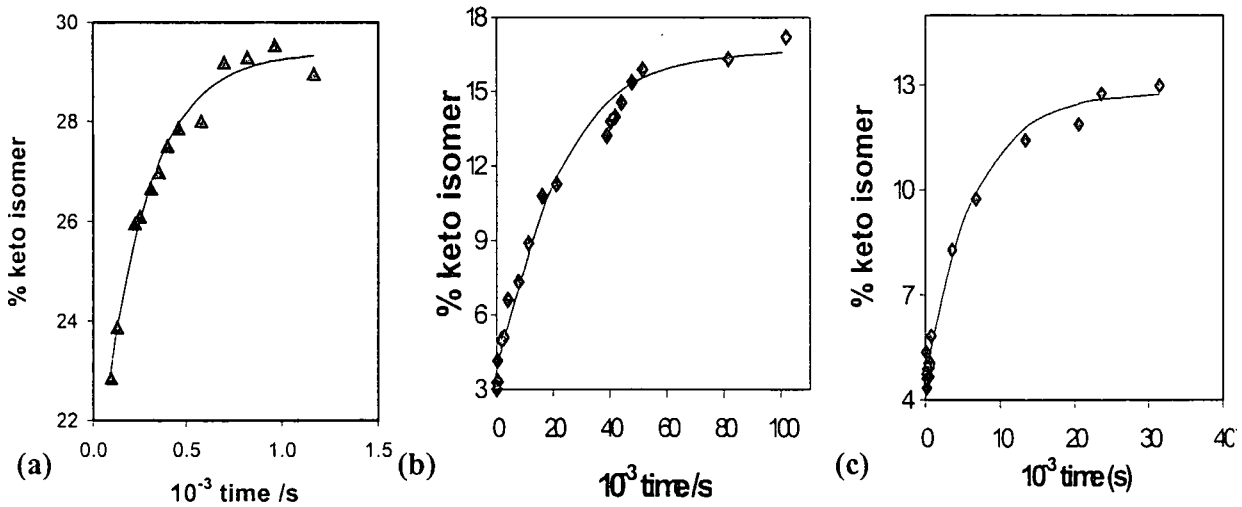

Figure 3.3: Time traces showing the conversion from enol to keto isomers of (a) Hfcp, 5, (b) Hfcdma, 6 and (c) Hfctma, 7 at 19°C in $CDCl_3$.

From the kinetic conversions of β-diketones from enol isomer to keto isomer (**Figure 3.3**), first order rate constant, k_{obs} were found to be 7.72(2) x 10^{-4} s^{-1} for Hfch, 5.7(2) x 10^{-5} s^{-1} for Hfca, 4.36(4) x 10^{-3} s^{-1} for Hfcp, 4.07(4) x 10^{-5} s^{-1} for Hfcdma and 1.57 x 10^{-4}(2) s^{-1} for Hfctma. From this data rate constants for the forward reaction, k_1 and reverse reaction, k_{-1}, in **Reaction 3.2** were easily obtained and are given in **Table 3.2**.

Table 3.2: Rate constants for the conversion of keto to enol isomer, k_1 and for the conversion of enol isomer to keto isomer, k_{-1} for β-diketones of the type $FcCOCH_2COR$.

Compound	$10^6\ k_1\ /s^{-1}$	$10^6\ k_{-1}\ /s^{-1}$
Hfch, **3**	697(4)	75(2)
Hfca, **4**	44(2)	13(2)
Hfcp, **5**	3070(10)	1300(10)
Hfcdma, **6**	34(2)	7(2)
Hfctma, **7**	138(3)	19(2)

Larger rate constants for the conversion of keto to enol isomers were observed as compared to the conversion of enol to keto isomers for all β-diketones in this study. This implies that the enol isomer is the favoured stable isomer in which β-diketones **3-7** exist in $CDCl_3$ solutions. Hfcp reached the equilibrium (within 30 minutes) much faster and had less enol content than the other β-diketones. Hfcdma took much longer times (~ 1700 minutes) to reach equilibrium.

3.4 Group electronegativities

3.4.1 Introduction

Compounds containing the carbonyl group have been the subject of many investigations and a considerable amount of experimental data has been accumulated concerning the IR stretching frequencies of the C=O bond. From these data it is possible to draw certain conclusions with regard to the effects of various substituents on the carbonyl frequency. A C=O linkage may assume a single or triple bond character according to the following equations:

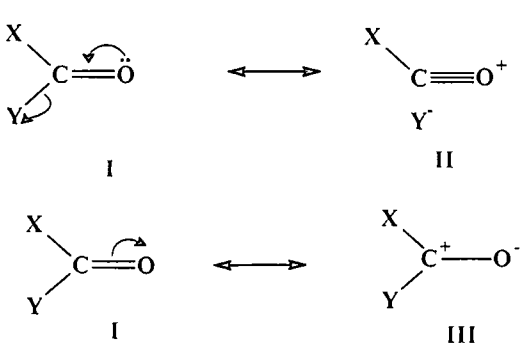

If X or Y are strongly electronegative (i.e. electron withdrawing) they will tend to pull electron density from the double bond to the C-atom by an inductive effect through the carbon atom, resulting in a greater contribution from **II** to the overall structure of the compound. This will lead to a relative increase in the IR carbonyl stretching frequency of the compound. For example,[7] an increase in IR ν(C=O) stretching frequencies from ca. 1718 cm^{-1} for CH_3COCH_3 to 1840 cm^{-1} for CH_3COF is observed. On the other hand, if X or Y is electron donating in character, the oxygen atom will gain electron density and the double bond will be weakened due to the larger contribution of canonical form **III** to the overall structure **I**. This leads to a decrease in carbonyl stretching frequency from ca. 1718 cm^{-1} for CH_3COCH_3 to 1658 cm^{-1} for CH_3COFc (Fc = ferrocenyl group), by way of example. The atom or group electronegativities χ_R, of R = F, CH_3, Fc are 4.0, 2.34 and 1.87 respectively.[8, 10] Since electronegativity of an atom or group of atoms, is a measure of its relative electron attracting or donating power, a relationship between carbonyl stretching frequency and group or atomic electronegativities of the substituents on the carbonyl compound would be expected.

3.4.2 Determination of group electronegativities from carbonyl stretching frequencies

In this study, group electronegativities, χ_R, of the R groups of the β-diketones, $FcCOCH_2COR$ were determined by using the carbonyl stretching frequencies, ν(C=O), of the ethyl ester series, $RCOOCH_2CH_3$, with R = H, CH_3, CH_2CH_3, $CH(CH_3)_2$ and $C(CH_3)_3$. A calibration curve (**Figure 3.4**) of known χ_R values against ν(C=O) for esters, with R = $CHCl_2$, CH_2Cl, CH_2Br, Cl, CCl_3, CF_3, Ph and Fc, was constructed using the data of **Table 3.3**. The experimentally determined ν(C=O) for R = H, CH_3, CH_2CH_3, $CH(CH_3)_2$ and $C(CH_3)_3$ were then fitted to this calibration curve and χ_R values were read off on the x-axis.

Table 3.3: IR stretching frequencies of ethyl esters of the type $RCOOCH_2CH_3$ and group electronegativities, χ_R, of each R group. R groups are indicated in the table.

R groups of ethyl esters	ν(C=O)/ cm^{-1}	χ_R	Reference
CF_3	1785	3.01	9
Cl	1772	2.97	10
CCl_3	1763	2.76	9
$CHCl_2$	1750	2.62	10
CH_2Cl	1747	2.48	11
CH_2Br	1738	2.44	11
CH_3	1736	2.38[(a)]	This study
CH_2CH_3	1733	2.34	This study
$CH(CH_3)_2$	1730	2.29	This study
$C(CH_3)_3$	1728	2.27	This study
Ph	1725	2.21	9
H	1717	2.11[(b)]	This study
Fc	1700	1.87	9

(a) reference 10 reports 2.34

(b) reference 9 reports 2.13 from a spectroscopic study, reference 3 reports 2.55 from an electrochemical study

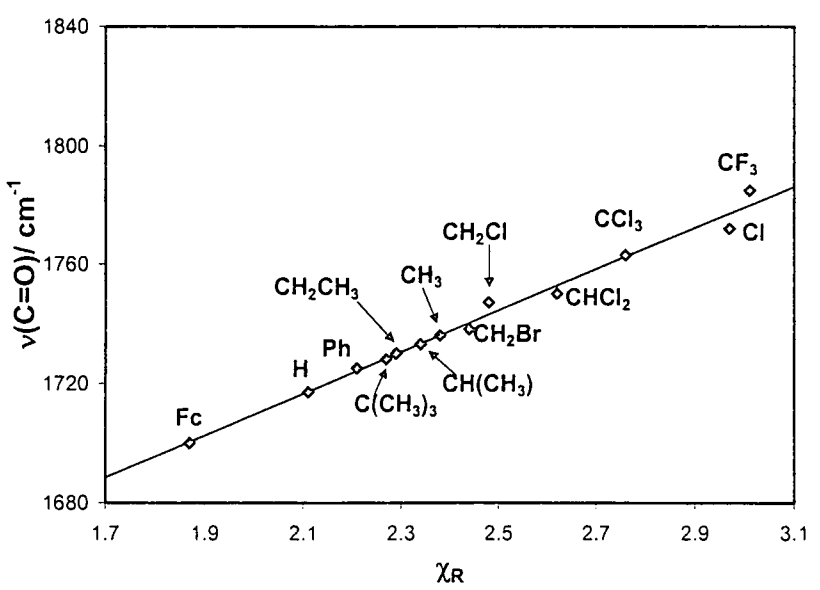

Figure 3.4: Linear relationship observed between group electronegativities, χ_R, and the carbonyl stretching frequencies of ethyl esters of the type $RCOOCH_2CH_3$.

From the graphical relationship above, group electronegativities for R substituents in this study were obtained as 2.11 for R = H, 2.38 for R = CH_3, 2.34 for R = CH_2CH_3, 2.29 for R = $CH(CH_3)_2$ and 2.27 for R = $C(CH_3)_3$. The newly obtained χ_H is mutually consistent with what Du Plessis et al[9] in spectroscopic studies found, i.e. 2.13. A tertiary alkyl group is found to be more electron donating than a secondary alkyl group, which in turn is more electron donating than a primary alkyl group. Group electronegativities, therefore decrease in the order:

(largest χ_R) $CH_3 > CH_2CH_3 > CH(CH_3)_2 > C(CH_3)_3 > H$ (smallest χ_R)

However as will be seen in later sections, the position of H, as determined by spectroscopic techniques in the above series is incorrect. The correct position of H is actually before CH_3.

3.4.3 Determination of dominant enol isomer using group electronegativities

Two driving forces that explain the dominance of the observed enol isomer in β-diketones have been postulated.[10] These forces were labelled electronic- and resonance driving forces. In the electronic driving force, the formation of the preferred enol isomer is controlled by the electronegativities of Fc and R groups in the β-diketone Fc-CO-CH_2-CO-R. When the electronegativity of R is greater than that of Fc, the carbon atom of the carbonyl group adjacent to Fc will be less positive in character than the carbon atom of the other carbonyl group. The dominant enol isomer, therefore will be Fc-C(OH)=CH-CO-R. As determined in the previous section the group electronegativities of R = H, CH_3, CH_2CH_3, $CH(CH_3)_3$ and $C(CH_3)_3$ (see **Table 3.3**) are infact larger than that of Fc (χ_{Fc} = 1.87). This implies that enolisation should be in the direction of ferrocenyl group (i.e. Fc-C(OH)=CH-CO-CH_2CH_3, enol isomer **I** in **Scheme 3.4**). This is in contrast to what was practically observed in solution utilising results from the ^{1}H NMR studies of these β-diketones as well as in the solid state from X-ray crystallographic studies for Hfctfa[9] and Hfca.[10] The observed dominant enol isomer had enolisation in the direction furthest from the ferrocenyl group (enol isomer **II** in **Scheme 3.4**, i.e. Fc-CO-CH=C(OH)-CH_2CH_3). To understand why the enol isomer **II** dominates over **I** in solution, implying that the equilibrium between **I** and **II** is shifted very far towards **II**, one should realise that enol isomer **I** may convert to anyone of its canonical forms **III**, while isomer **II** may convert to anyone of its canonical forms **IV**. To decide which canonical forms **III** or **IV** is most stable, and therefore should dominate, the existence of resonance driving force was described.[10] The resonance driving force implies that the formation of

different canonical forms of a specific isomer will lower the energy of this specific isomer enough to allow it to dominate over the existence of the other isomer. Crystallographic studies[10] of Hfca (R = CH_3) have shown that zwitterion resembling **IV** and which arises from isomer **II** dominates over canonical form **III** arising from isomer **I**. Only one structural canonical form for **IV** is shown, but like **III** it really is a mixture of several. The isomer **II** can only to dominate in solution and in solid state if, the zwitterionic canonical form **IV** dominates over **III**. Canonical form **IV** will only dominate over canonical form **III** if the conjugation between the ferrocenyl group and the α-carbonyl group is much more effective and energy lowering than conjugation between the ferrocenyl group and the γ-carbonyl group. Since R, here shown as CH_2CH_3, has no double bonds that can conjugate with its neighbouring carbonyl group, the γ-carbonyl group, it follows that canonical forms such as **IV** must dominate over canonical forms resembling **III**. Hence, resonance driving force determines which enolate is favoured and not electronic factors.

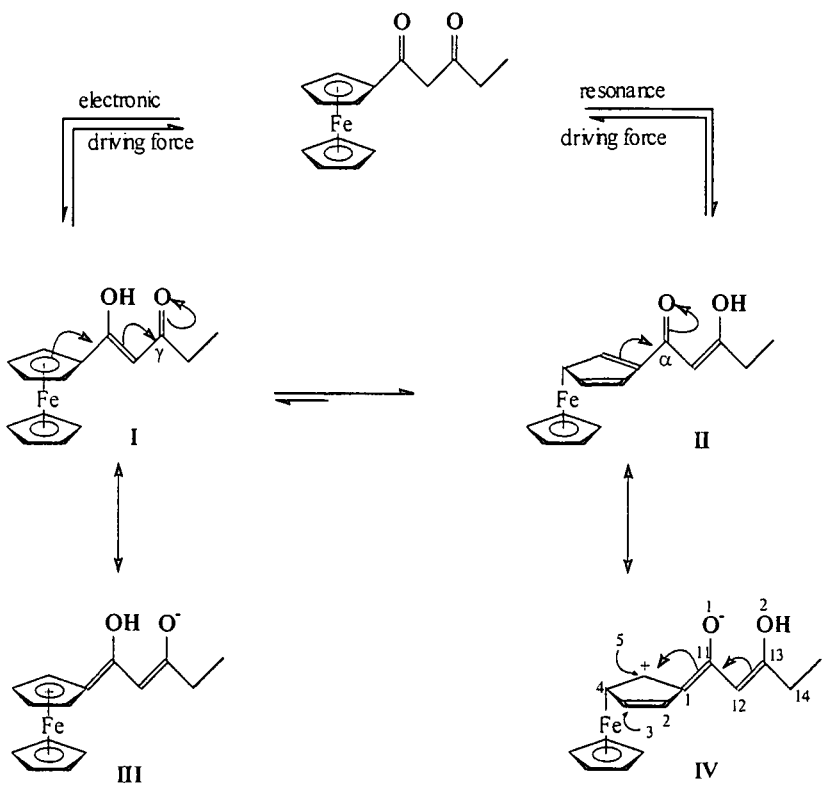

Scheme 3.4: Electronic considerations in terms of group electronegativity favour isomer I as the enol form of Hfcp. However, structure II was found to be dominant which implies that the equilibrium between I and II lies far to the right. The ferrocenyl group in II and IV is shown in just one canonical form but in both cases the iron atom can be bound to any of the five cyclopentadienyl carbon atoms as indicated in I. Likewise, the positive charge of IV is not confined to the single position shown but rather oscillates between C2 and C5 (it cannot be on C1, atom numbers are indicated next to individual atoms) to give rise to four different canonical forms as indicated in III.

3.5 pK_a' determination

3.5.1 The pK_a' values of Hfcp, Hfcdma and Hfctma

Apparent pK_a values for ferrocene-containing β-diketones refers to the following process:

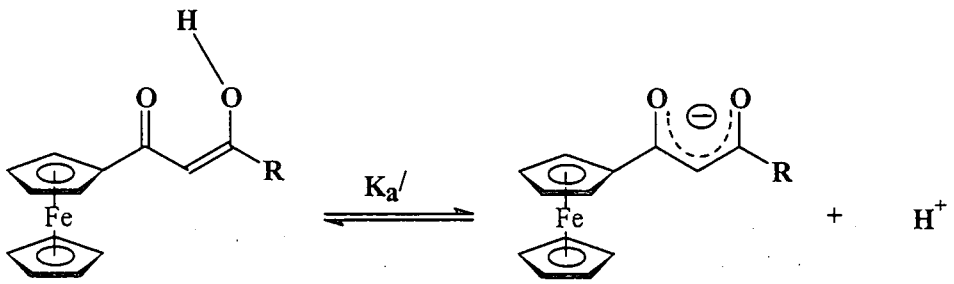

Enol form **Basic form**

Scheme 3.5: Schematic representation showing the enolic and basic forms of the β-diketones, with R = H (Hfch), CH_3 (Hfca), CH_2CH_3 (Hfcp), $CH(CH_3)_2$ (Hfcdma) and $C(CH_3)_3$ (Hfctma).

'Apparent' pK_a values were determined in this study since it was not possible to separate pK_a values for the enol and keto tautomers. The symbol pK_a' therefore, refers to 'apparent' pK_a values, which include inter alia simultaneous contribution of the keto and enol isomers to the experimentally determined pK_a' values. Since the β-diketones were not soluble in pure water, 10% acetonitrile in water was used as solvent. Martell[12] found that such mixtures have much less effect on β-diketone pK_a' determinations than do, for example, 1,4-dioxane, methanol, ethanol or propan-2-ol mixed with water. This was tested on β-diketones Hfca and Hfctfa, $FcCOCH_2COCF_3$.[10] The pK_a' of Hfca in water and water containing 10% acetonitrile were 9.96 and 10.01 respectively. For Hfctfa the pK_a' was 6.53 in water containing 10% acetonitrile, 6.9 in water containing 5% aqueous 1,4-dioxane and 7.0 in 50% aqueous acetonitrile (at 21°C and μ = 0.1 mol dm^{-3} ($NaClO_4$)).

The UV/visible spectra of the protonated (enolic) and deprotonated (basic) forms of β-diketones Hfcp, Hfcdma and Hfctma are shown in **Figure 3.5.**

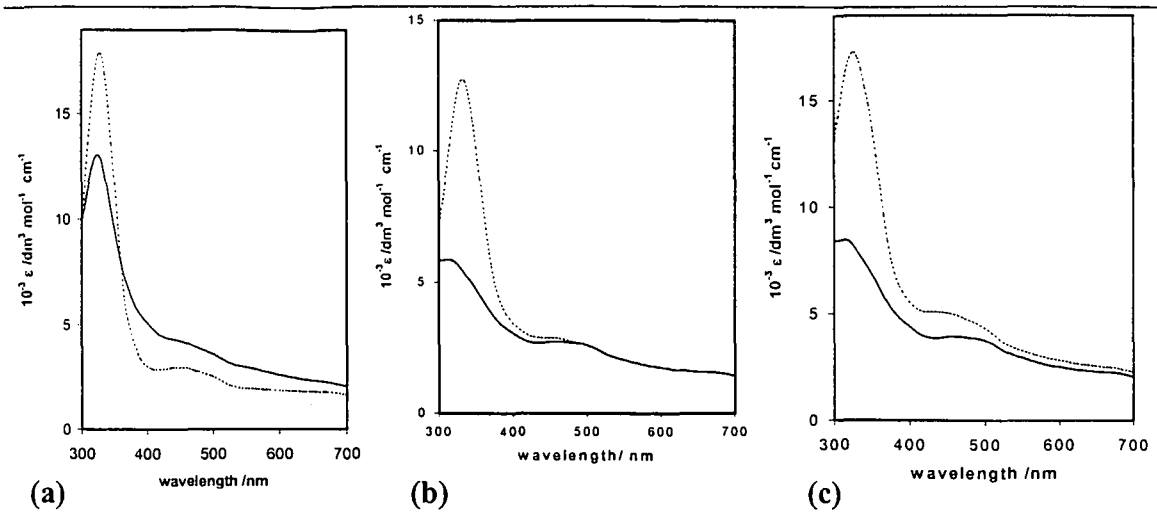

Figure 3.5: UV /Visible spectra of the β-diketone (solid line) and β-diketonate (dotted line) forms of (a) Hfcp, (b) Hfcdma and (c) Hfctma in a 10 % acetonitrile/water mixture, μ = 0.100 mol dm^{-3} ($NaClO_4$) at 25°C.

Table 3.4 gives the concentrations of the β-diketones and the keto-aldehyde, Hfch, during the pK_a' determination as well as pK_a' values as determined from the data in **Figure 3.6**.

Table 3.4: pK_a' values, UV/Vis spectroscopic data of β-diketones (Hfch, Hfca, Hfcp, Hfcdma and Hfctma) and β-diketonates (fch^-, fca^-, fcp^-, $fcdma^-$ and $fctma^-$) in water containing 10% acetonitrile at 25°C and μ = 0.100 mol dm^{-3} ($NaClO_4$). Values in brackets are extinction coefficients in dm^3 mol^{-1} cm^{-1} at λ_{max} of the protonated form.

β-diketone	β-diketone λ_{max} /nm	β-diketonate λ_{max} / nm	10^4 c[(a)] / mol dm^{-3} (ε /dm^3 mol^{-1} cm^{-1})	λ_{exp}[(b)] / nm	pK_a'
Hfch[(c)]	302	305	1.17 (15380)	320	7.04(1)
Hfca[(d)]	473	325	1.32 (24420)	325	10.01(2)
Hfcp	320	325	0.94 (11563)	325	10.57(1)
Hfcdma	315	330	1.14 (5508)	330	10.80(1)
Hfctma	320	330	0.79 (8392)	327	11.47(4)

(a) concentration of β-diketones during pK_a' determination
(b) wavelength utilised during pK_a' determination
(c) data from reference 3
(d) data from reference 10

These pK_a' values were determined by measuring UV absorbance/ pH data with titration from high to low pH and a least squares fit of the absorbance/pH data using **Equation 3.3**.

$$A_T = \frac{A_{HA}10^{-pH} + A_A 10^{-pK_a'}}{10^{-pH} + 10^{-pK_a'}}$$ **Equation 3.3**

A_T = the total absorbance; A_{HA} = the absorbance of the β-diketone in the enolic form and A_A = the absorbance of the β-diketonate (basic) form.

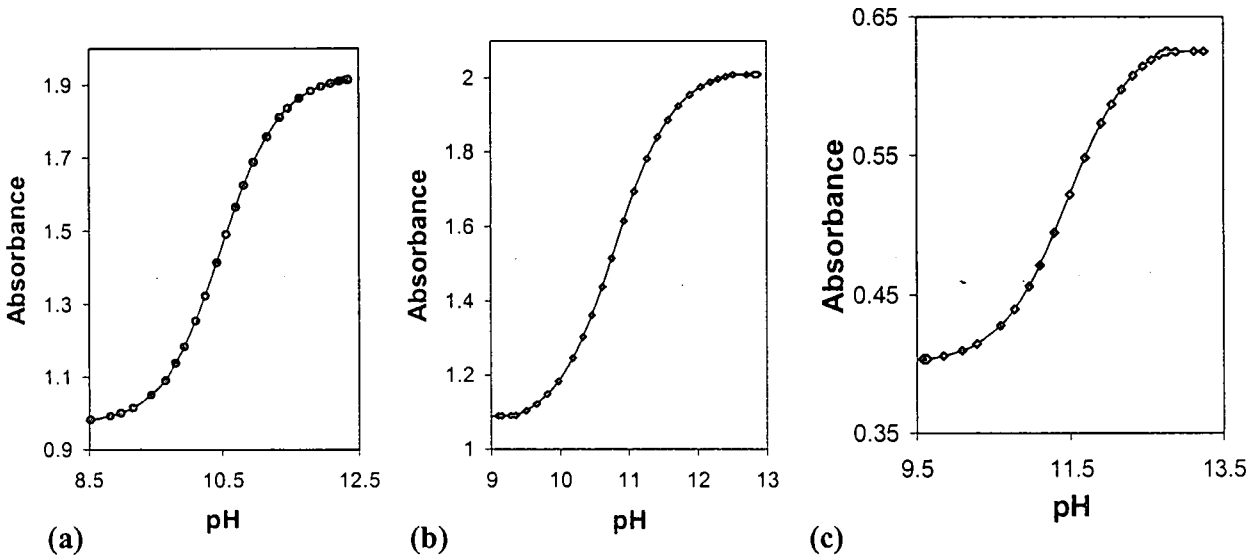

Figure 3.6: Absorbance dependence on pH for (a) Hfcp at 325 nm, (b) Hfcdma at 330 nm and (c) Hfctma at 327 nm in 10 % acetonitrile/water mixture, μ = 0.100 mol dm^{-3} ($NaClO_4$) at 25°C. The solid line presents the least squares fit to Equation 3.3.

3.5.2 β-Diketone pK_a' values in relation to other physical quantities

Three physical quantities, the number of C-atoms on the R substituent, group electronegativities of the R groups and the IR ν(C=O) stretching frequencies of the ethyl esters RCOOEt are related to pK_a'. It was observed that the β-diketone with the most methyl groups, $FcCOCH_2C(CH_3)_3$, had the largest pK_a' value, while the keto-aldehyde, $FcCOCH_2COH$, with no methyl groups, had the smallest pK_a' value. (**Figure 3.7** (a)).

The basicity of β-diketones, $FcCOCH_2COR$, also increased (i.e. higher pK_a' values) as the electronegativity of the R groups decreased. The relationship between these two quantities is illustrated in **Figure 3.7** (b). The keto-aldehyde (R = H) is the most acidic (i.e. least basic, pK_a' = 7.04(1)) and Hfctma is the most basic β-diketone of the series studied in this project. From the plot in **Figure 3.7** (b), it is obvious that $\chi_H \neq 2.11$ as obtained IR spectroscopic measurements on

$HCOOCH_2CH_3$ (section **3.4.2** page 68). Utilising pK_a'-χ_R relationship shown in **Figure 3.7** (b) a new χ_H = 2.64 was obtained, which is consistent with what was found by Conradie[3] from electrochemical studies (χ_H = 2.55).

A linear relationship is observed between ν(C=O) stretching frequencies of the ethyl esters, RCOOEt, and pK_a' values as shown in **Figure 3.7** (c) From this graph it is apparent that ν(C=O) for HCOOEt is expected at 1753 cm^{-1}, although the peak was actually observed at 1717 cm^{-1}. A possible reason for this anomalous measurement may lie in the formation of extended hydrogen-bonded networks as shown in **Figure 3.7** (d).

For Hfctma, the tertiary alkyl group donates more electron density to the carbon atom of the adjacent C-(OH) group than, for example, the primary alkyl group of Hfca, as indicated by the group electronegativities of $C(CH_3)_3$ = 2.27 and that of CH_3 = 2.38. This would have a knock-on effect in that more electron density is also distributed to the O-atom of Hfctma, and to the enol H-atom than for Hfca. As a result the enol H-atom would have lesser tendency to dissociate as a H^+ cation according to **Scheme 3.5** in Hfctma than in Hfca. This automatically also implies that the O-H bond of the enol isomer of Hfctma is stronger than the O-H bond of the enol isomer in Hfca.

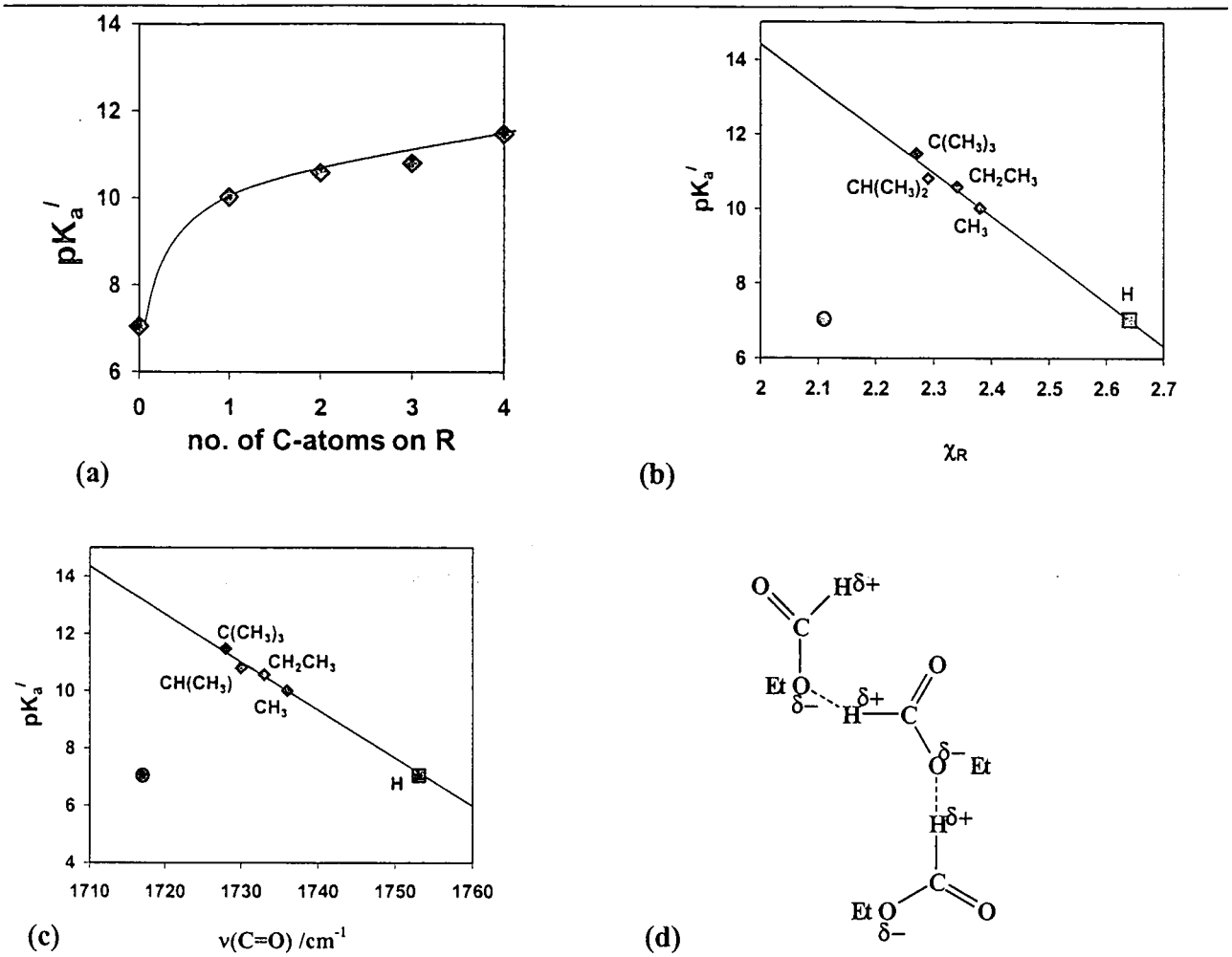

Figure 3.7: (a) Relationship between pK_a' values of β-diketones, $FcCOCH_2COR$, and the number of CH_3 groups on R. (b) Linear relationship between the pK_a' values and group electronegativities, χ_R. The point marked ● indicates $\chi_H = 2.11$ obtained from the IR studies. The newly obtained $\chi_H = 2.64$ is marked ■. (c) Linear relationship between the pK_a' values and ν(C=O) stretching frequencies of ethyl esters. The point marked ● indicates $\nu(C{=}O)_H = 1717\ cm^{-1}$ as described by reference 3 while this graphs predicts $\nu(C{=}O)_H = 1753\ cm^{-1}$. R groups are as indicated on the graphs. (d) Schematic representation illustrating hydrogen-bonded networks that can form between molecules of HCOOEt

3.6 Cyclic Voltammetry

3.6.1 Introduction

In this section the formal reduction potentials, $E^{o/}$, of the iron core in the free β-diketones, $FcCOCH_2COR$, and in [Rh(FcCOCHCOR)(cod)] complexes, are reported. All values were measured *vs.* Ag/Ag^+, some in the presence of ferrocene as an internal standard. Peak anodic oxidation potentials, E_{pa}, of the rhodium(I) nucleus in [Rh(FcCOCHCOR)(cod)] complexes as well as correlation between $E^{o/}$ or E_{pa} and parameters such as pK_a' and group electronegativities, χ_R, are presented.

3.6.2 Cyclic voltammetry of β-diketones Hfca, Hfcp, Hfcdma and Hfctma

The electrochemical reversible Fc/Fc^+ couple of β-diketones, $FcCOCH_2COR$, according to the following equation was investigated:

$$Fc \leftrightharpoons Fc^+ + e^-$$

Electrochemical reversibility of a one-electron process is characterised by the difference in peak anodic (E_{pa}) and peak cathodic potentials (E_{pc}), ΔE_p, of 59 mV theoretically. In practice, in this study, ΔE_p values up to 90 mV are taken as an indication of electrochemical reversibility. The cyclic voltammograms of the free β-diketones Hfca, Hfcp, Hfcdma and Hfctma shown in **Figure 3.8** (a) all imply an electrochemically reversible ferrocenyl based electron transfer process with ΔE_p values less than 90 mV for 50 mV s^{-1} scan rates, see **Table 3.5**, page 80. The peak current ratio, i_{pa}/i_{pc}, for all β-diketones investigated was found to approach 1 at scan rates 50-250 mV s^{-1}. This implies that the electrochemical oxidation of the Fe(II) nucleus of the ferrocenyl group is not followed by any chemical reaction (reduction, substitution or complexation) of the newly formed ferrocenium group.[13] The $E^{o/}$ values remained constant between scan rate 50 to 250 mV s^{-1} (**Table 3.5**)

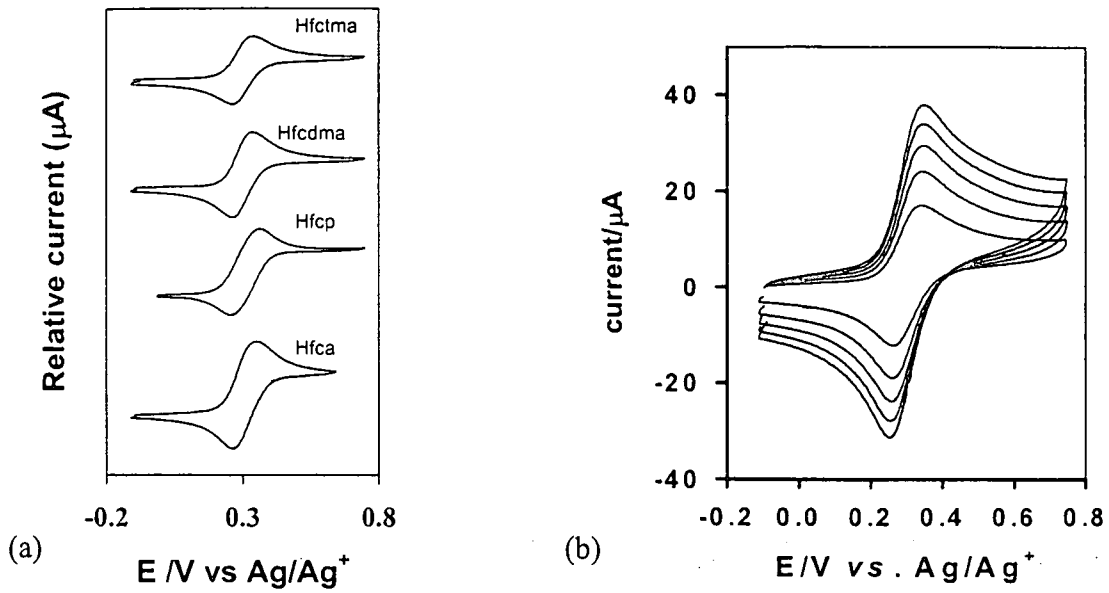

Figure 3.8: (a) Cyclic voltammograms of 1.0 mmol dm^{-3} $FcCOCH_2COR$ solutions of Hfca (4, R = CH_3), Hfcp (5, R = CH_2CH_3), Hfcdma (6, R = $CH(CH_3)_2$) and Hfctma (7, R = $C(CH_3)_3$) measured in 0.1 mol dm^{-3} $TBAPF_6/CH_3CN$ at scan rate of 100 mV s^{-1} on a glassy carbon working electrode at 25.0(1)°C *versus* Ag/Ag^+. (b) Cyclic voltammograms of 1 mmol dm^{-3} solution of Hfcdma measured in 0.1 mol dm^{-3} $TBAPF_6/CH_3CN$ at scan rates 50, 100, 150, 200 and 250 mV s^{-1} on a glassy carbon working electrode at 25.0(1) °C *versus* Ag/Ag^+.

The electrochemistry of ferrocene itself was found to be reversible (ΔE_p = 62 mV, i_{pa} / i_{pc} = 1.00 at a scan rate of 50 mV s^{-1}) with $E^{o\prime}$ = 0.077 mV *versus* Ag/Ag^+ in acetonitrile. The same electrochemical results for ferrocene and Hfcdma were obtained when ferrocene was added as internal standard to the Hfcdma solution as illustrated in **Figure 3.9** (a). However, due to the difficulty to accurately measure i_{pa} of β-diketones in the presence of free Fc, experiments were conducted in the absence of free ferrocene and potentials are referenced to the Ag/Ag^+ reference electrode.

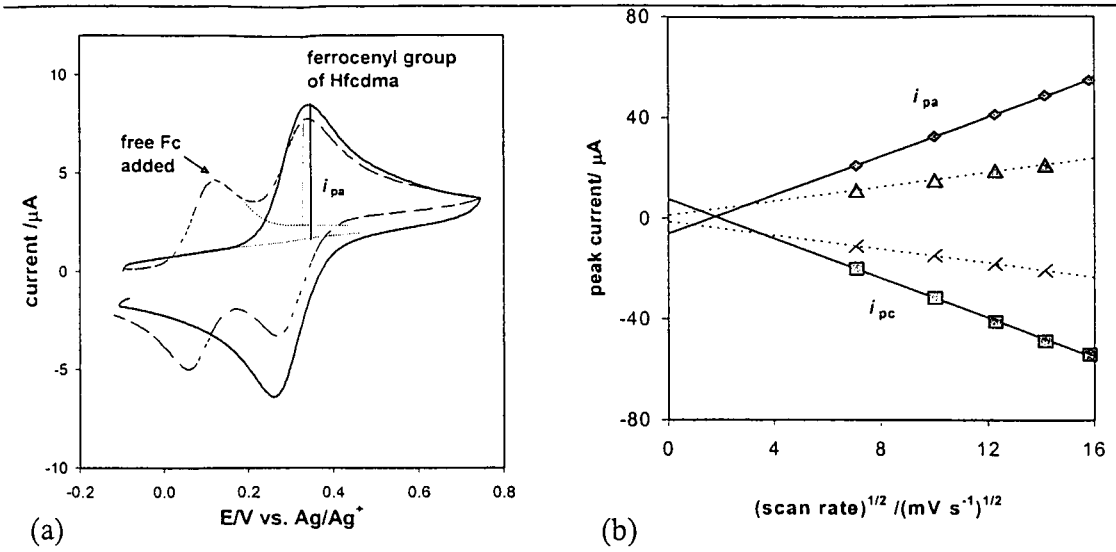

Figure 3.9: (a) CV of Hfcdma in the absence of ferrocene (—) and in the presence of ferrocene (- - -) added as an internal standard at scan rate of 100 mV s^{-1}. $E^{o\prime}$ = 0.075 mV and ΔE_p = 82.1 mV for free added ferrocene. (b) A graph of anodic and cathodic peak currents *vs.* (scan rate)$^{1/2}$ is linear for both Hfch (------) and Hfcdma (—) with y-intercepts i_{pa} = 1.17 and i_{pc} = -1.20 for Hfch and i_{pa} = -6.05 and i_{pc} = 7.70 for Hfcdma. Y-intercepts for other β-diketones were found to be i_{pa} = 2.26 and i_{pc} = -1.86 for Hfca; i_{pa} = -9.76 and i_{pc} = 9.32 for Hfcp and i_{pa} = -6.95 and i_{pc} = 10.15 for Hfctma.

The Randles-Sevcik equation is given by:

$$i_p = (2.69 \times 10^5)n^{3/2}AD^{1/2}C\nu^{1/2}$$

where n is the amount of electrons transferred, A is the electrode area (cm^2), D is the diffusion coefficient (cm^2 s^{-1}), C is the concentration of the substance (mol cm^{-3}) and ν is the scan rate (V s^{-1}). The peak current, i_p should be directly proportional to the square root of the scan rate, $\nu^{1/2}$, and the graph should have a zero intercept if the electrochemical response is an electrochemical reversible process that is only diffusion controlled. For all the β-diketones in study a linear relationship between i_p and $\nu^{1/2}$ was observed (see **Figure 3.9** (b)). It is clear that the y-intercepts of $FcCOCH_2COR$ with R = H are smaller than those of the other ligands with R = CH_3, CH_2CH_3, $CH(CH_3)_2$ and $C(CH_3)_3$ (as mentioned in **Figure 3.9** (b)). This is consistent with the smaller size of $FcCOCH_2COH$ experiencing much less resistance to diffusion. It follows that the electrochemistry of all the alkyl-containing β-diketones is less ideal than that of $FcCOCH_2COH$ in that the plots in **Figure 3.9** (b) show electron transfer that is not 100% diffusion controlled (because of definite non-

zero y-intercepts). Other factors such as slow electron exchange at the surface of the electrode may play a marginal role in explaining the non-zero y-intercepts of **Figure 3.9** (b) as well.

Table 3.5: Electrochemical data of 1.0 mmol dm^{-3} solutions of β-diketones of the type $FcCOCH_2COR$, measured in 0.1 mol dm^{-3} $TBAPF_6/CH_3CN$ on a glassy carbon electrode at 25.0(1) °C *versus* Ag/Ag^+.

ν /mV s^{-1}	E_{pa} / V	ΔE_p /mV	$E^{o/}$ / V	i_{pa} / μA	i_{pa}/i_{pc}	E_{pa} / V	ΔE_p / mV	$E^{o/}$ / V	i_{pa} / μA	i_{pa}/i_{pc}
Hfca, $FcCOCH_2COCH_3$						**Hfcp, $FcCOCH_2COCH_2CH_3$**				
50	0.352	89	0.308	25.52	1.01	0.371	87	0.310	18.00	1.00
100	0.354	92	0.308	36.54	1.01	0.371	90	0.309	29.82	1.01
150	0.357	101	0.308	43.75	1.03	0.373	93	0.309	39.21	1.02
200	0.358	102	0.307	49.80	1.02	0.375	100	0.308	46.00	1.02
250	0.362	108	0.308	55.10	1.00	0.379	102	0.309	52.58	1.01
Hfcdma, $FcCOCH_2COCH(CH_3)_2$						**Hfctma, $FcCOCH_2COC(CH_3)_3$**				
50	0.341	78	0.302	21.05	1.05	0.344	80	0.304	20.00	1.05
100	0.345	86	0.302	32.55	1.03	0.348	86	0.305	31.22	1.05
150	0.346	89	0.302	41.06	1.00	0.352	96	0.304	40.88	1.03
200	0.347	94	0.300	48.62	1.00	0.354	100	0.304	47.52	1.00
250	0.349	98	0.300	54.58	1.01	0.354	98	0.305	53.24	0.99
Hfch, Fc-CO-CH_2-CO-H[(a)]										
50	0.384	82	0.342	11.26	1.02					
100	0.388	88	0.344	15.21	1.02					
150	0.388	89	0.344	18.79	1.03					
200	0.389	94	0.342	21.18	1.02					

(a) Results from reference 3

The formal reduction potential, $E^{o/}$, for the β-diketones of this study with R = primary, secondary or tertiary alkyl groups (**Table 3.5**) show no significant difference from one β-diketone to the other. This indicates that the potential at which the ferrocenyl group on $FcCOCH_2COR$ is oxidised, for all practical purposes was independent of the R group for these β-diketones if R = CH_3, CH_2CH_3, $CH(CH_3)_2$ and $C(CH_3)_3$. This is somewhat suprising in view of the IR and pK_a' results described in previous sections. However, when R is not an alkyl group but a proton, i.e. $FcCOCH_2COH$, $E^{o/}$ becomes more positive by almost ca. 40 mV.

The increase in the number of C-atoms on the R substituent in moving from primary to tertiary alkyl groups has very little influence on the formal reduction potential of the ferrocenyl group inter alia due to the lack of conjugation between the ferrocenyl group and the alkyl R groups in $FcCOCH_2COR$ (see **Figure 3.10** (a)) and also because any electronic effects induced by electron donating alkyl substituents may be so small that they cannot be detected by cyclic voltammetry. A linear relationship is observed between substituent group electronegativities and reduction potentials of the ferrocenyl group (see **Figure 3.10** (b)). The larger $E^{o\prime}$ value when R = H implies a larger atom electronegativity for H on the Gordy scale than for compounds with alkyl R groups. This result implies that $\chi_H = 2.64$ is a much more valid value than $\chi_H = 2.11$ from spectroscopic measurements and also consistent with determinations of utilising pK_a'- χ_R relationship in section **3.5.2**, page 74.

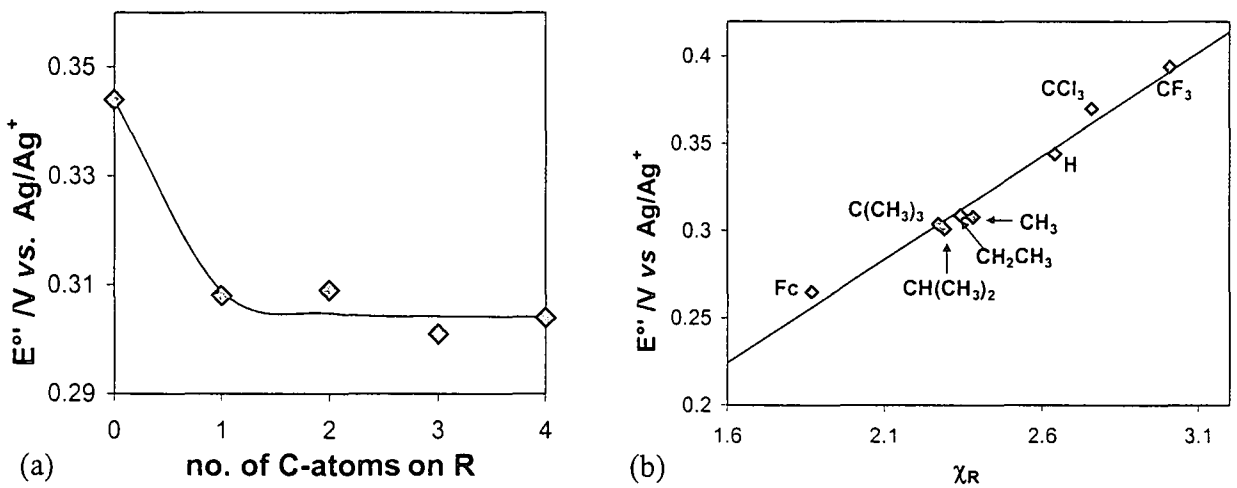

Figure 3.10: (a) Relationship between the formal reduction potential, $E^{o\prime}$, and the number of C-atoms on R substituent. (b) Linear relationship between formal reduction potential, $E^{o\prime}$, and group electronegativity, χ_R, of R groups in $FcCOCH_2COR$, with R = CF_3 ($E^{o\prime}$ = 0.394 V, χ = 3.01) CCl_3 ($E^{o\prime}$ = 0.370 V, χ = 2.76), Fc ($E^{o\prime}$ = 0.265 V, χ = 1.87), H, CH_3, CH_2CH_3, $CH(CH_3)_2$ and $C(CH_3)_3$. Fc = ferrocenyl group. The group electronegativity of H, χ_H = 2.64, fitted in this series. This χ_H value is also consistent with the value Conradie,[3] reported i.e. χ_H = 2.55.

Table 3.6 summarises the χ_R, $E^{o\prime}$ and pK_a' values of β-diketones obtained during this study.

E° and K_a are thermodynamic quantities linked by the following equation:[14]

$$E^\circ = (RT/nF)\ln(K_a)$$
$$= -RT/2.303\ nF\ pK_a$$
$$= -0.011\ pK_a \qquad \text{at } 25^\circ C$$

Therefore a graph of $E^{o/}$ *vs.* $pK_a^{/}$ should be linear (by using $E^{o/}$ instead of E^{o} and $pK_a^{/}$ instead of pK_a, the slope (=-0.011) may be affected but not its linearity). The dependence of the reduction potentials, $E^{o/}$, on the $pK_a^{/}$ of $FcCOCH_2COR$ is demonstrated in **Figure 3.11**. From our results the slope was found to be -0.012, which agrees very well with what theory predicts.

Table 3.6: Group electronegativities, χ_R, formal reduction potentials, $E^{o/}$ *vs.* Ag/Ag^+ of the ferrocenyl group and $pK_a^{/}$ values of $FcCOCH_2COR$, for the indicated R groups

R	χ_R	$E^{o/}$ /V *vs.* Ag/Ag^+	$pK_a^{/}$
H	2.64	0.344[(a)]	7.04(1)[(a)]
CH_3	2.38	0.308	10.01(2)
CH_2CH_3	2.34	0.309	10.57(1)
$CH(CH_3)_2$	2.29	0.301	10.80(1)
$C(CH_3)_3$	2.27	0.304	11.47(4)

(a) results from reference 3

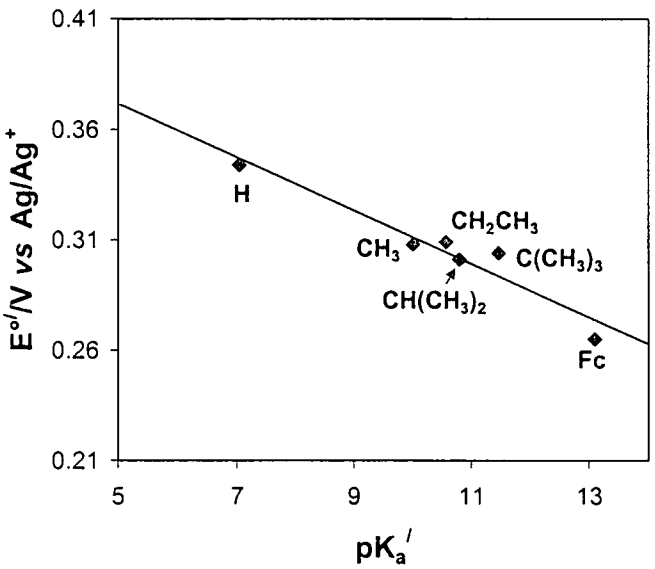

Figure 3.11: Linear relationship between the formal reduction potentials, $E^{o/}$, of the ferrocenyl group and the $pK_a^{/}$ of $FcCOCH_2COR$. The slope of the graph was obtained as -0.012. $pK_a^{/}$ value for Fc = 13.1.

3.6.3 Cyclic voltammetry of [Rh(β-diketonato)(cod)] complexes

The cyclic voltammograms of the ferrocene-containing rhodium complexes, [Rh(β-diketonato)(cod)], (β-diketonato = fca, fcp, fcdma and fctma) are shown in **Figure 3.12** (b). They all exhibit an electrochemically irreversible anodic peak, which corresponds to the oxidation of rhodium(I), **Equation 3.4**, as well as an electrochemically reversible Fc/ Fc^+ couple according to **Equation 3.5**.

$$Rh^I \rightarrow Rh^{III} + 2e^- \qquad \textbf{Equation 3.4}$$

$$Fc \leftrightharpoons Fc^+ + e^- \qquad \textbf{Equation 3.5}$$

The overall reaction sequence observed is

$$Rh^I Fc \rightarrow Rh^{III} Fc \leftrightharpoons Rh^{III} Fc^+ \qquad \textbf{Equation 3.6}$$

The cyclic voltammograms of [Rh(fcdma)(cod)] displayed in **Figure 3.12** (a) represents the general trend observed for all [Rh(β-diketonato)(cod)] complexes at different scan rates. The ratio, i_{pa}/i_{pc} for the ferrocenyl group was found to be close to unity for all the rhodium complexes. ΔE_p of the ferrocenyl group was observed to be less than 76 mV at slow scan rates (50 mV s^{-1}) for all the [Rh(FcCOCHCOR)(cod)] complexes (**Table 3.7**), which implied excellent electrochemical reversibility for the Fc/Fc^+ couple.

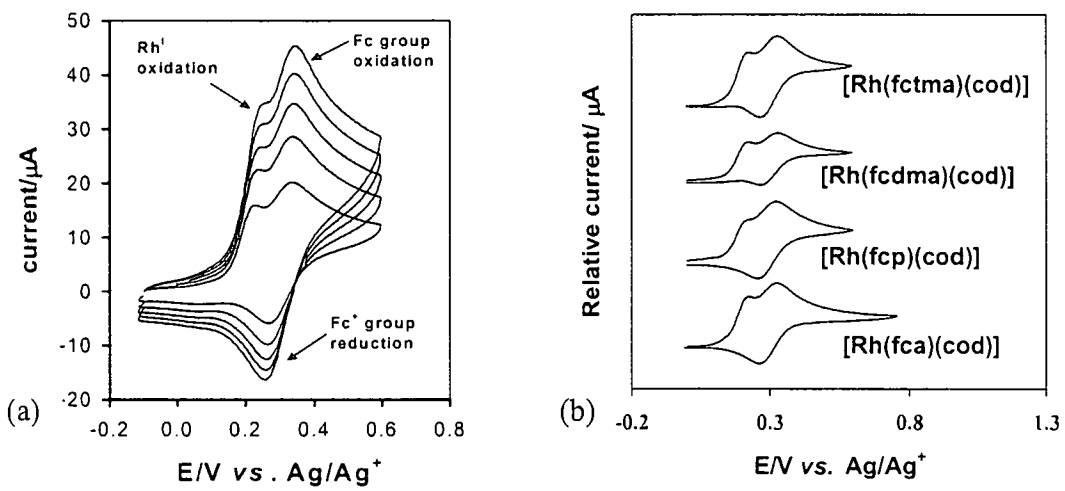

Figure 3.12: (a) Cyclic voltammograms of a 1 mmol dm^{-3} solution of [Rh(fcdma)(cod)] measured in 0.1 mol dm^{-3} $TBAPF_6/CH_3CN$ at scan rates of 50, 100, 150, 200 and 250 mV s^{-1} on a glassy carbon working electrode at 25.0(1) °C *versus* Ag/Ag^+. (b) Cyclic voltammograms of 1 mmol dm^{-3} solutions of different [Rh(FcCOCHCOR)(cod)] complexes at scan rate 100 mV s^{-1} under the same conditions as in (a).

The anodic peak current of the ferrocenyl group, i_{pa} (Fc) (peak 2 in **Figure 3.13**), could not be measured directly from the CV of [Rh(FcCOCHCOR)(cod)] due to the overlapping of the oxidation

peak of the ferrocenyl group (peak 2 in **Figure 3.13**), with the oxidation peak of rhodium(I) (peak 1 in **Figure 3.13**). To construct an accurate decay curve for peak 1, the following techniques and arguments were employed. Since the Fc group and Rh nucleus are part of the same molecule in each [Rh(FcCOCHCOR)(cod)] complex, the diffusion rate of the Rh^{III} Fc species (see **Equation 3.6**) and the Rh^{III} Fc^{+} species should be approximately the same even though Rh^{I} oxidation represents a 2 electron and Fc a 1 electron process.

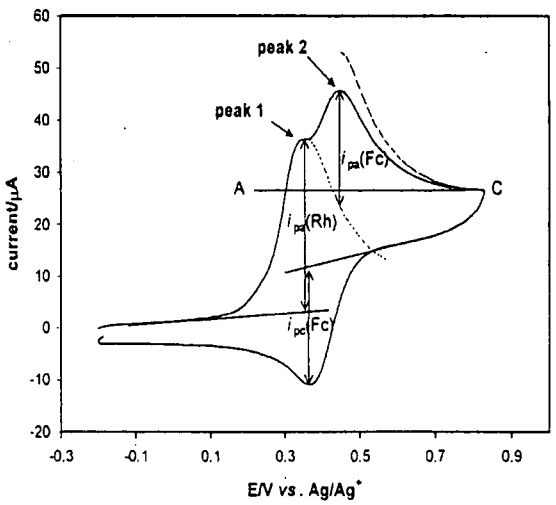

Figure 3.13: Construction of the decay current of Rh(I) oxidation (peak 1) may be achieved by multiplying the decaying current of Fc oxidation (peak 2) with ratio i_{pa}(Rh)/i_{pc}(Fc). The artificially obtained line is shown as -----. This line is then translatorily shifted without distortion to coincide exactly with the E_{pa} value of the Rh(I) oxidation peak and is indicated by ..... The anodic peak current i_{pa}(Fc) of the ferrocenyl group can then be measured as the current between peak 2 and the newly obtained anodic decay current for Rh(I) oxidation.

The decay current of rhodium(I) oxidation to form Rh^{III} Fc during the generation of peak 1 can therefore be constructed by multiplying the decaying current of Fc oxidation during the formation of peak 2 from the basis line AC with ratio i_{pa}(Rh)/i_{pc}(Fc) to allow for the 2 electron flow during Rh(I) oxidation as compared to the 1 electron flow during Fc oxidation. The artificially obtained line is shown as ---- in **Figure 3.13**. This line may then be translatorily shifted without distortion to coincide exactly with the E_{pa} value of the Rh(I) oxidation peak and is indicated by the dotted line, (...), in **Figure 3.13**. The anodic peak current of the ferrocenyl group can then be measured as the perpendicular current between the maximum of peak 2 and the newly obtained anodic decay current for Rh(I) oxidation, as illustrated in **Figure 3.13**.

Table 3.7: Electrochemical data of 1.0 mmol dm^{-3} solutions of [Rh(FcCOCHCOR)(cod)] complexes measured in 0.1 mol dm^{-3} $TBAPF_6/CH_3CN$ on a glassy carbon working electrode at 25.0(1) °C *versus* Ag/Ag^+.

v/	Rhodium		Ferrocenyl group					Rhodium		Ferrocenyl group				
mV s^{-1}	E_{pa} /V	i_{pa} /μA	E_{pa} /V	ΔE_p /mV	$E^{o/}$ /V	$-i_{pc}$ /μA	i_{pa}/i_{pc}	E_{pa} /V	i_{pa} /μA	E_{pa} /V	ΔE_p /mV	$E^{o/}$ /V	$-i_{pc}$ /μA	i_{pa}/i_{pc}
	[Rh(FcCOCHCOCH$_3$)(cod)], 11							[Rh(FcCOCHCOCH$_2$CH$_3$)(cod)], 12						
50	0.248	26.1	0.336	74	0.299	12.8	0.98	0.252	22.4	0.339	74	0.302	12.2	0.98
100	0.246	37.0	0.338	74	0.301	17.8	1.02	0.248	32.6	0.339	79	0.300	19.8	1.01
150	0.250	45.5	0.340	76	0.302	25.8	0.98	0.251	39.5	0.336	72	0.300	25.3	0.99
200	0.248	52.9	0.342	83	0.301	33.2	1.02	0.251	46.7	0.340	80	0.300	29.1	0.98
250	0.250	56.1	0.344	87	0.301	41.0	0.99	0.252	51.5	0.342	84	0.300	33.4	0.99
	[Rh(FcCOCHCOCH(CH$_3$)$_2$)(cod)], 13							[Rh(FcCOCHCOC(CH$_3$)$_3$)(cod)], 14						
50	0.246	20.8	0.336	71	0.301	12.9	0.98	0.247	18.9	0.334	76	0.296	11.0	0.95
100	0.244	30.8	0.338	78	0.299	18.5	1.02	0.248	25.9	0.336	75	0.299	17.6	0.97
150	0.251	36.4	0.335	72	0.299	24.0	1.01	0.253	31.8	0.336	76	0.298	23.2	0.98
200	0.252	42.6	0.338	75	0.301	29.5	0.99	0.250	35.5	0.342	88	0.298	28.4	0.98
250	0.254	47.5	0.338	73	0.302	35.0	0.99	0.251	40.1	0.345	90	0.300	32.9	0.97
	[Rh(FcCOCHCOH)(cod)][(a)], 10													
50	0.263	31.5	0.380	79	0.341	22.0	0.98							
100	0.273	49.3	0.380	83	0.338	33.4	0.97							
150	0.281	61.8	0.384	91	0.338	40.1	0.97							
200	0.294	73.1	0.387	97	0.338	46.8	0.99							

(a) results from reference 3

CV results of [Rh(FcCOCHCOR)(cod)] complexes, with R = H, CH_3, CH_2CH_3, $CH(CH_3)_2$ and $C(CH_3)_3$, indicated that Rh(I) (**Figure 3.12** (b)) is oxidised at potentials not too far from the potential range in which the ferrocenyl fragment is active. At scan rate of 50 mV s^{-1}, $\Delta E_{pa} = E_{pa}(Fc) - E_{pa}(Rh)$ = 117 mV for the β-keto aldehyde while for the β-diketones (R = CH_3, CH_2CH_3, $CH(CH_3)_2$ and $C(CH_3)_3$) this value was between 87 and 90 mV. The Rh^I nucleus (E_{pa} = 0.263 V) of [Rh(fch)(cod)] was oxidised at a potential of 11 - 17 mV more positive than for the alkyl-substituted complexes (E_{pa}'s = 0.246 – 0.252 V) . This is consistent with H being more electronegative (χ_H = 2.64) than alkyl groups with $2.27 < \chi_{alkyl} < 2.38$. The larger $E^{o/}$ value for the ferrocenyl group of the β-keto aldehyde may also be traced to the larger χ_H value compared to that of alkyl groups.

Although previous studies[3] have showed a weak Rh^{III} reduction wave at ca. -0.44 V for [Rh(FcCOCHCOR)(cod)] with R = H and CH_3 (see **Figure 3.14**), no Rh^{III} reduction could be uniquely detected for the new complexes with R = CH_2CH_3, $CH(CH_3)_3$ and $C(CH_3)_3$ of this study (see **Figure 3.15**).

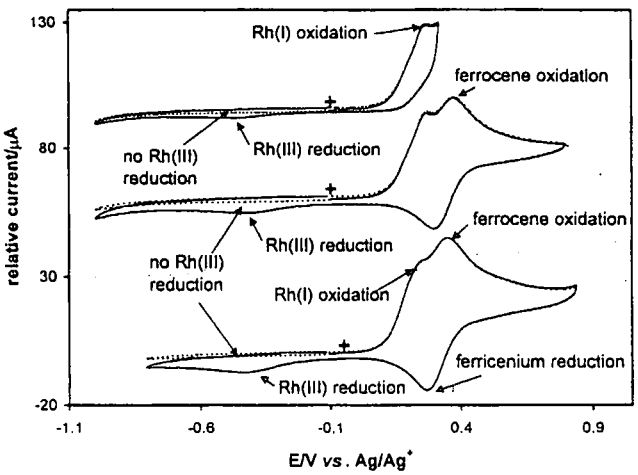

Figure 3.14: Cyclic voltammogram of 1.2 mmol dm^{-3} [Rh(fca)(cod)] (bottom) and 1.1 mmol dm^{-3} [Rh(fch)(cod)] (middle and top) measured in 0.1 mol dm^{-3} $TBAPF_6/CH_3CN$ at scan rate of 100 mV s^{-1} on a glassy carbon working electrode at 25.0(1) °C *versus* Ag/Ag^+. Scans initiated at + in the positive scan direction for the solid lines and in the negative scan direction for the dashed lines. The scans shown above are from reference 3.

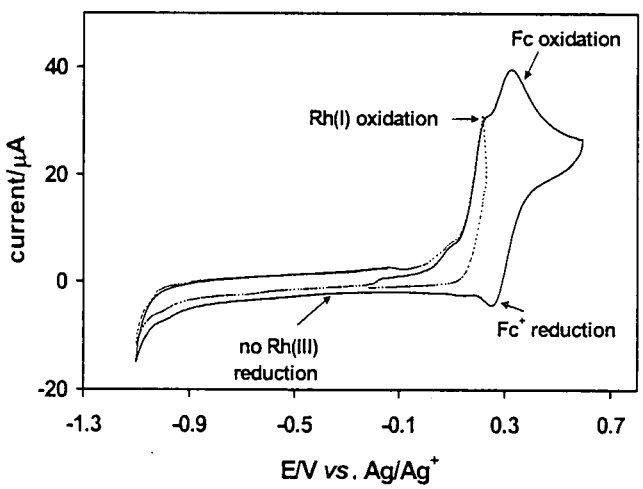

Figure 3.15: Cyclic voltammogram of 1 mmol dm^{-3} solution of [Rh(fcp)(cod)] measured in 0.1 mol dm^{-3} $TBAPF_6/CH_3CN$ at a scan rate of 100 mV s^{-1} on a glassy carbon working electrode at 25.0(1) °C *versus* Ag/Ag^+. Solid line is the scan in the positive direction reversed at 0.65 V and the dotted line is the scan in the positive direction reversed at 0.2 V.

The rhodium anodic peak potentials, E_{pa}(Rh) and the formal reduction potential of the ferrocenyl group, $E^{o/}$(Fc), in these [Rh(FcCOCHCOR)(cod)] complexes as well as various physical quantities are summarised in **Table 3.8**. The relationship between E_{pa}(Rh) or $E^{o/}$(Fc) and the $pK_a^{/}$ of the free uncoordinated $FcCOCH_2COR$ is shown in **Figure 3.16** (a).

Table 3.8: Electrochemical and chemical data for [Rh(FcCOCHCOR)(cod)] complexes. Oxidation peak potentials are reported *versus* Ag/Ag^+. $pK_a^{/}$ values are for free uncoordinated β-diketones.

Complex	R	χ_R	E_{pa}(Rh)/ V	$E^{o/}$(Fc)/ V	$pK_a^{/}$
[Rh(fch)(cod)][(a)]	H	2.64	0.273	0.338	7.04(1)
[Rh(fca)(cod)]	CH_3	2.38	0.246	0.301	10.01(2)
[Rh(fcp)(cod)]	CH_2CH_3	2.34	0.248	0.300	10.57(1)
[Rh(fcdma)(cod)]	$CH(CH_3)_2$	2.29	0.244	0.299	10.80(1)
[Rh(fctma)(cod)]	$C(CH_3)_3$	2.27	0.248	0.299	11.47(1)

(a) results from reference 3

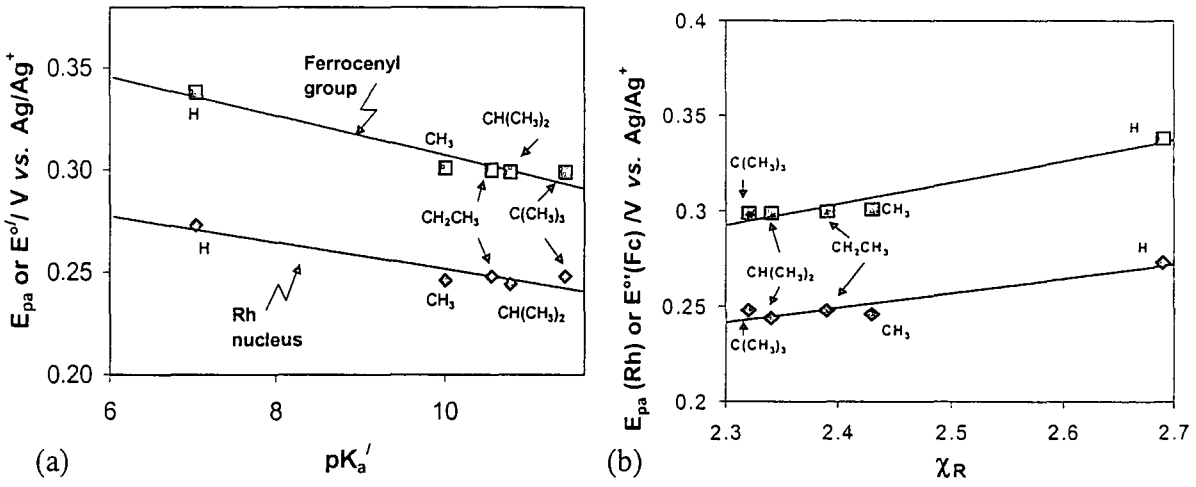

Figure 3.16: (a) Linear relationship between E_{pa} of Rh or $E^{o/}$ of the Fc group in [Rh(FcCOCHCOR)(cod)] and the $pK_a^{/}$ of the free uncoordinated $FcCOCH_2COR$. (b) Linear relationship between: (i) E_{pa} of Rh in [Rh(FcCOCHCOR)(cod)] (-◈-) and the group electronegativities, χ_R. (ii) $E^{o/}$ of Fc in [Rh(FcCOCHCOR)(cod)] (-⊡-) and the group electronegativities, χ_R.

The relationship between E_{pa} (Rh) and the group electronegativities, χ_R, indicates that the Rh(I) core becomes increasingly difficult to oxidise as the R groups of the co-ordinated β-diketonato

ligand, becomes more electronegative. However, this trend is not clearly observable for R groups ranging from CH_3 to $C(CH_3)_3$. The group electronegativities (in brackets) of these substituents are of comparable values CH_3 (2.38) ≈ CH_2CH_3 (2.34) ≈ $CH(CH_3)_2$ (2.29) ≈ $C(CH_3)_3$ (2.27). Therefore the E_{pa} and $E^{o/}$ values of [Rh(FcCOCHCOR)(cod)] (**Table 3.8**) are expected to vary only *slightly*. The fact that they are *almost* constant indicates that a further factor than merely $pK_a^{/}$ or χ_R influences the observed E_{pa} and $E^{o/}$ values. The discussion on page 97 will show that this factor probably relates to slow kinetics of heterogeneous electron transfer between electrode and compound as a result of the increase in bulkiness of R groups in moving from H to $C(CH_3)_3$.

3.7 Substitution reactions

This section concerns the kinetics of substitution of β-diketonato ligands, $(FcCOCHCOR)^-$, from [Rh(FcCOCHCOR)(cod)] with 1,10-phenanthroline (phen), to give $[Rh(phen)(cod)]^+$.

3.7.1 The Beer Lambert Law

The UV spectra of [Rh(fcp)(cod)] and the product of the substitution reaction between [Rh(fcp)(cod)] and 1,10-phenanthroline (phen), *viz.* $[Rh(phen)(cod)]^+$, in methanol at 25°C are given in **Figure 3.17** (a). Linear relationships between the absorbance, A, and concentration, c, of [Rh(FcCOCHCOR)(cod)] with R = CH_2CH_3, $CH(CH_3)_2$ and $C(CH_3)_3$, at $\lambda_{experimental}$ (**Figure 3.17** (b)) confirm the validity of the Beer Lambert law ($A = \varepsilon cl$, with ε = extinction coefficient and l = path length = 1 cm) for each one of these complexes. The extinction coefficient for each complex at the experimental wavelength where substitution was monitored is given in **Table 3.9**.

Table 3.9: Molar extinction coefficients, ε, at the indicated wavelengths, λ, for [Rh(β-diketonato)(cod)] complexes

Complex	λ_{exp}/ nm	ε/ dm^3 mol^{-1} cm^{-1}
[Rh(fch)(cod)],[(a)] **10**	525	661
[Rh(fca)(cod)],[(b)] **11**	472	2390
[Rh(fcp)(cod)][(c)], **12**	480	384
[Rh(fcdma)(cod)][(c)], **13**	460	427
[Rh(fctma)(cod)][(c)], **14**	480	418

(a) results from reference 3
(b) results from reference 16
(c) this study

Since complexes **12-14** each obey the Beer-Lambert law at the indicated wavelengths, the kinetics of substitution of β-diketonato ligands from the complexes [Rh(β-diketonato)(cod)] with 1,10-phenanthroline could be studied utilising UV/Vis spectroscopy.

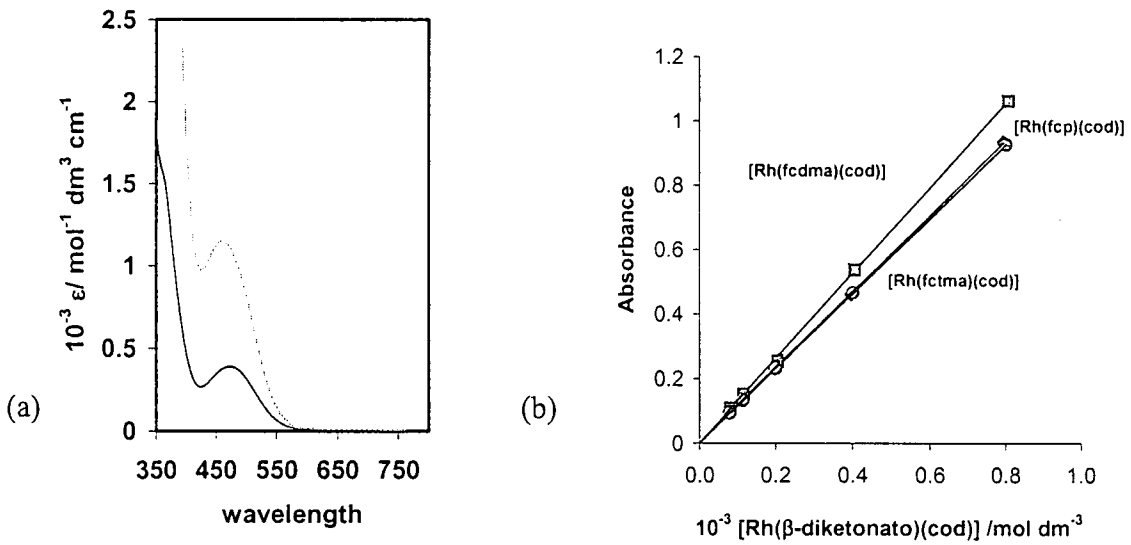

Figure 3.17: (a) UV spectra of [Rh(fcp)(cod)] (_____) and $[Rh(phen)(cod)]^+$ (.....) in methanol at 25°C. (b) The linear relationship between absorbance and concentration of [Rh(β-diketonato)(cod)] complexes at λ = 480 nm for [Rh(fcp)(cod)] (-◇-), λ = 460 nm for [Rh(fcdma)(cod)] (-▣-) and λ = 480 nm for [Rh(fctma)(cod)] (-③-) confirms the validity of the Beer Lambert law.

3.7.3 Substitution kinetics of [Rh(β-diketonato)(cod)] with 1,10-phenanthroline

The substitution reaction between rhodium complexes of the type [Rh(FcCOCHCOR)(cod)] and phen to form $[Rh(phen)(cod)]^+$ is illustrated in **Scheme 3.6**. The general rate law applicable to this substitution reaction is given by **Equation 3.7**.

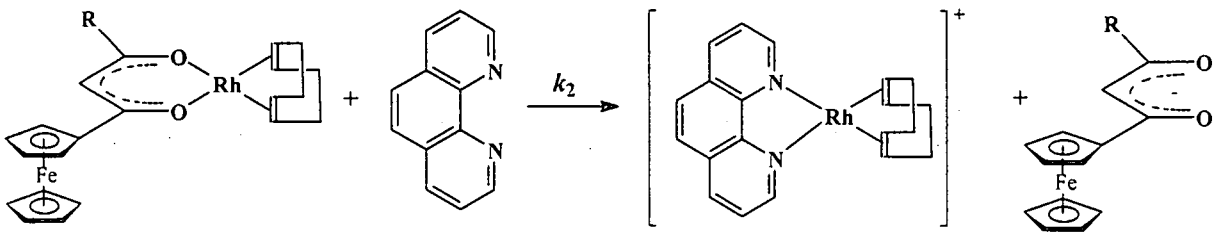

Scheme 3.6: Schematic representation for the substitution of $(FcCOCHCOR)^-$ ligand from [Rh(FcCOCHCOR)(cod)] complex with 1,10-phenanthroline to liberate $[Rh(phen)(cod)]^+$ and $(FcCOCHCOR)^-$. R = H, CH_3, CH_2CH_3, $CH(CH_3)_3$ and $C(CH_3)_3$

$$\text{Rate} = \{k_s + k_2\,[\text{phen}]\}[\text{Rh(FcCOCHCOR)(cod)}]$$

$$= k_{obs}\,[\text{Rh(FcCOCHCOR)(cod)}] \qquad \textbf{Equation 3.7}$$

with the pseudo-first-order rate constant, $k_{obs} = k_s + k_2[\text{phen}]$. k_2 is the second-order rate constant for the substitution process and k_s is the rate constant associated with solvent taking part in the reaction. This substitution reaction may occur via a dissociative (**Equation 3.8**) or an associative mechanism (**Equation 3.9**, NN = 1,10-phenanthroline).

$$\left.\begin{array}{l}[Rh(FcC^{K}OCHC^{K}OR)(cod)] \rightleftharpoons [Rh(cod)]^+ + (FcCOCHCOR)^- \text{ or} \\ [Rh(FcCOCHC^{K}OR)(cod)] \xrightarrow{NN} [Rh(^{K}N^{K}N)(cod)]^+\end{array}\right\} \quad \textbf{Equation 3.8}$$

$$\left.\begin{array}{l}[Rh(FcC^{K}OCHC^{K}OR)(cod)] \overset{NN}{\rightleftharpoons} [Rh(FcC^{K}OCHC^{K}OR)(cod)(^{K}NN)] \rightleftharpoons \\ [Rh(FcC^{K}OCHCOR)(cod)(^{K}N^{K}N)] \rightarrow [Rh(^{K}N^{K}N)(cod)]^+ + (FcCOCHCOR)^-\end{array}\right\} \quad \textbf{Equation 3.9}$$

In both reactions the notation ^{K}O or ^{K}N indicates that the specified O-atom or N-atom is co-ordinated via a co-ordination bond to the rhodium nucleus. The expected transition state for a dissociative mechanism may either be the cationic 12-electron $[Rh(cod)]^+$ species or the neutral 14-

electron [Rh(FcCOCHC $^{\kappa}$OR)(cod)] species in which the β-diketonato ligand (FcCOCHCOR)$^-$ reverted from being a bidentate ligand to a monodentate ligand after one Rh-$^{\kappa}$O bond has broken. In the associative mechanism, a neutral five-co-ordinated 18-electron intermediate species [Rh(FcC$^{\kappa}$OCHC $^{\kappa}$OR)(cod)($^{\kappa}$NN)], in which only one N atom of phen is co-ordinated to the Rh nucleus, is expected to form first. As 12-electron or 14-electron Rh species are extremely unlikely, **Equation 3.9**, which demonstrates the associative path, is the most possible mechanism of substitution. To prove this expectation, results of a temperature dependent kinetic study are presented on page 93. The large negative entropies of activation that were found are conclusive proof that the substitution process under investigation in this study proceeds via an associative mechanism as shown in **Equation 3.9**. Proof of associative mechanism may also be obtained by determining activation volumes from a pressure dependent kinetic study, but this method was considered outside the scope of this study.

The reaction rate constants for the reaction in **Scheme 3.6** with R = H (see reference 3), CH_3 (see reference 16), CH_2CH_3, $CH(CH_3)_2$ and $C(CH_3)_3$ (this study) were obtained by following the formation of $[Rh(phen)(cod)]^+$ at wavelengths indicated in (page 89) for each complex. An excess of 10-400 fold 1,10-phenanthroline over [Rh(FcCOCHCOR)(cod)] concentrations was used for all experiments in order to achieve pseudo-first order reaction conditions. For each kinetic run, absorbance-time data was collected and the observed pseudo-first-order rate constants, k_{obs}, were determined from a linear fit of data to **Equation 3.10**[15]

$$\ln (A_o/A_t) = k_{obs}\, t \qquad \textbf{Equation 3.10}$$

A_o indicates initial absorbance and A_t absorbance at time t. The pseudo-first-order rate constants determined experimentally were converted to second-order rate constants, k_2, by determining the slopes of the linear plots of k_{obs} against concentration of the incoming phen ligand (**Equation 3.11**)

$$k_{obs} = k_s + k_2\,[phen] \qquad \textbf{Equation 3.11}$$

where k_s is the rate constant of the solvent path.

A graph of k_{obs} against phen concentration was linear in all cases as shown in **Figure 3.18** (a). All complexes showed a zero intercept (i.e. $k_s \approx 0$), thereby confirming that the solvent path did not make an observable contribution to the reaction. This was in fact expected since the displacement of

bidentate ligands such as $(FcCOCHCOR)^-$ with monodentate solvent molecule (MeOH in this study) would be much more difficult, and hence slower, than the displacement of a bidentate β-diketonato ligand with the bidentate phenanthroline ligand.

Activation parameters were obtained from a fit of k_2 and temperature data to the Eyring equation[15] (**Equation 3.12**). All mathematical fits were carried out using the fitting program MINSQ.[6]

$$\ln (k_2/T) = -\Delta H^* /(RT) + \Delta S^* /R + \ln (k_b/h) \qquad \textbf{Equation 3.12}$$

The Eyring plots of ln (k_2/T) *versus* 1/T for the substitution reactions for these complexes, over a temperature range of 10 - 35°C, are given in **Figure 3.18** (b). A summary of the second-order rate constant, k_2, as well as the entropy of activation, ΔS^*, activation enthalpy, ΔH^* and the activation free energy ΔG^*, which were determined from the temperature study, is given in **Table 3.10**. The activation free energy was obtained from the following equation:

$$\Delta G^* = \Delta H^* - T\Delta S^*$$

Results in **Table 3.10** show that the entropy driving force becomes more dominant in complexes with bulkier R groups [e.g. $C(CH_3)_3$], while the enthalpy driving force is more important in complexes with smaller R substituents, here R = H, at 25°C. It is also important to note that the sign of ΔG^* is positive and not negative. This must be so because ΔG^* is the free energy of **activation**, not the free **reaction** energy.

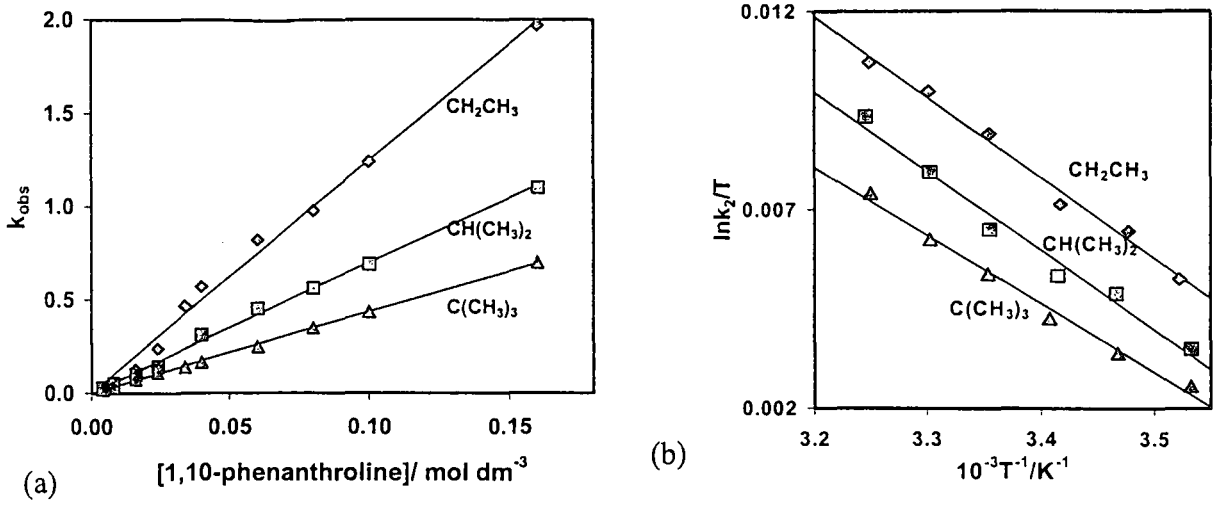

Figure 3.18: (a) Graphs of pseudo-first-order rate constant, k_{obs}, *versus* [phen] at 25°C for the [Rh(FcCOCHCOR)(cod)] complexes passing through the origin implying $k_s \approx 0$. (b) Eyring plots of $\ln(k_2/T)$ *versus* 1/T at various temperatures (10 - 35°C) for the [Rh(FcCOCHCOR)(cod)] complexes. R substituents are indicated on the graphs.

Table 3.10: Second-order rate constants, k_2, activation enthalpy, ΔH*, entropy of activation, ΔS* and Gibbs activation free energy, ΔG*, for the substitution reaction of $(FcCOCHCOR)^-$ with 1,10-phenanthroline in [Rh(FcCOCHCOR)(cod)] complexes at 25°C. pK_a' values of the free uncoordinated $FcCOCH_2COR$ ligand, group electronegativities, χ_R of the R groups and Rh-O bond lengths are also tabulated. R substituents are indicated in the table.

R	k_2 / $dm^3\ mol^{-1}\ s^{-1}$	ΔH* / kJ mol^{-1}	ΔS* / J K^{-1} mol^{-1}	ΔG* / kJ mol^{-1}	pK_a'	χ_R	Rh-O[d, i] / Å
H[a]	47(1)	35(2)	-94.7(1)	63.2(3)	7.04(1)	2.64	-
CH_3[b]	18(1)	29(4)	-120(10)	64.8(4)	10.01(2)	2.38	2.042(6)[e, i]
CH_2CH_3[c]	12.6(4)	16.9(1)	-197(1)	75.6(4)	10.57(1)	2.34	2.048(13)[f]
$CH(CH_3)_2$[c]	6.93(1)	16.7(1)	-197(1)	75.4(5)	10.80(1)	2.29	2.057(6)[g]
$C(CH_3)_3$[c]	4.33(1)	14.4(9)	-197(1)	73(5)	11.47(4)	2.27	2.061(8)[h]

(a) results from reference 3
(b) results from reference 16
(c) this study
(d) Rh-O bond lengths closest to the indicated R group for $[Rh(CF_3COCHCOR)(CO)(PPh_3)]$ complexes
(e) for $[Rh(CF_3COCHCOCH_3)(CO)(PPh_3)]$, reference 17
(f) for $[Rh(CF_3COCHCOCH_2CH_3)(CO)(PPh_3)]$, reference 17
(g) for $[Rh(CF_3COCHCOCH(CH_3)_2)(CO)(PPh_3)]$, reference 18
(h) for $[Rh(CF_3COCHCOC(CH_3)_3)(CO)(PPh_3)]$, reference 19
(i) $Rh\text{-}O^{CF3}$ > 2.07 Å for complexes cited in footnotes e-h, $Rh\text{-}O^{Fc}$ = 2.039 Å and $Rh\text{-}O^{CH3}$ = 2.048 Å for $[Rh(FcCOCHCOCH_3)(cod)]$ from reference 16. Note that although footnotes d-h describe Rh-O bonds for complexes $[Rh(CF_3COCHCOR)(CO)(PPh_3)]$ and not [Rh(FcCOCHCOR)(cod)], the indicated Rh-O bond lengths are not expected to differ much in cod complexes. This is proved by the $Rh\text{-}O^{CH3}$ bond lengths of $[Rh(CF_3COCHCOCH_3)(CO)(PPh_3)]$ (see table) and of $[Rh(FcCOCHCOCH_3)(cod)]$.

The large negative activation entropies clearly indicate that the substitution process proceeds via an associative mechanism (**Equation 3.9**, page 90) and not a dissociative mechanism (**Equation 3.8**). A schematic representation of this mechanism is given in **Scheme 3.7**. The rate-determining step involves the formation of the five-co-ordinated species (b) in **Scheme 3.7**. This step is followed by breakage of one of the two Rh-O bonds of the β-diketone co-ordinated to the rhodium nucleus. To decide which Rh-O bond will most probably break first, a consideration of group electronegativities and Rh-O bond length is instructive. The group electronegativity of the Fc group (χ_{Fc} = 1.87) is substantially lower than those of all the other R groups (**Table 3.10**). Therefore the carbonyl group on the ferrocenyl side of the β-diketonato ligand should be more electron rich than the other carbonyl group, and it should interact strongly with the positively charged rhodium nucleus. This statement is supported by a survey of Rh-O bond lengths. The Rh-O bond length closest to the ferrocenyl group is the shortest of the cited bonds in **Table 3.10** (and footnote i) and thus the strongest. Conversely, the carbonyl group on the other side of the β-diketonato ligand should be relatively more positive in nature (because of the relative high χ_R value). This carbonyl group will, therefore, interact more weakly with the positively charged rhodium nucleus compared with the carbonyl group on the ferrocenyl side of the β-diketonato ligand. This statement is again confirmed by considering Rh-O bond lengths. All the Rh-O^R bond lengths with R = CH_3, CH_2CH_3, $CH(CH_3)_2$ and $C(CH_3)_3$, cited in **Table 3.10** are larger than the Rh-O^{Fc} bond. The Rh-O^R bond strengths are therefore all weaker than Rh-O^{Fc} bond. It is therefore expected that the weaker Rh-O bond nearer to the R group will break first with simultaneous formation of a bond between Rh and the still uncoordinated N atom of phen, forming the five-co-ordinated transitional state (c). This transitional state quickly reacts to form the product of the substitution reaction (d), and the β-diketonato anion, $(FcCOCHCOR)^-$ is liberated.

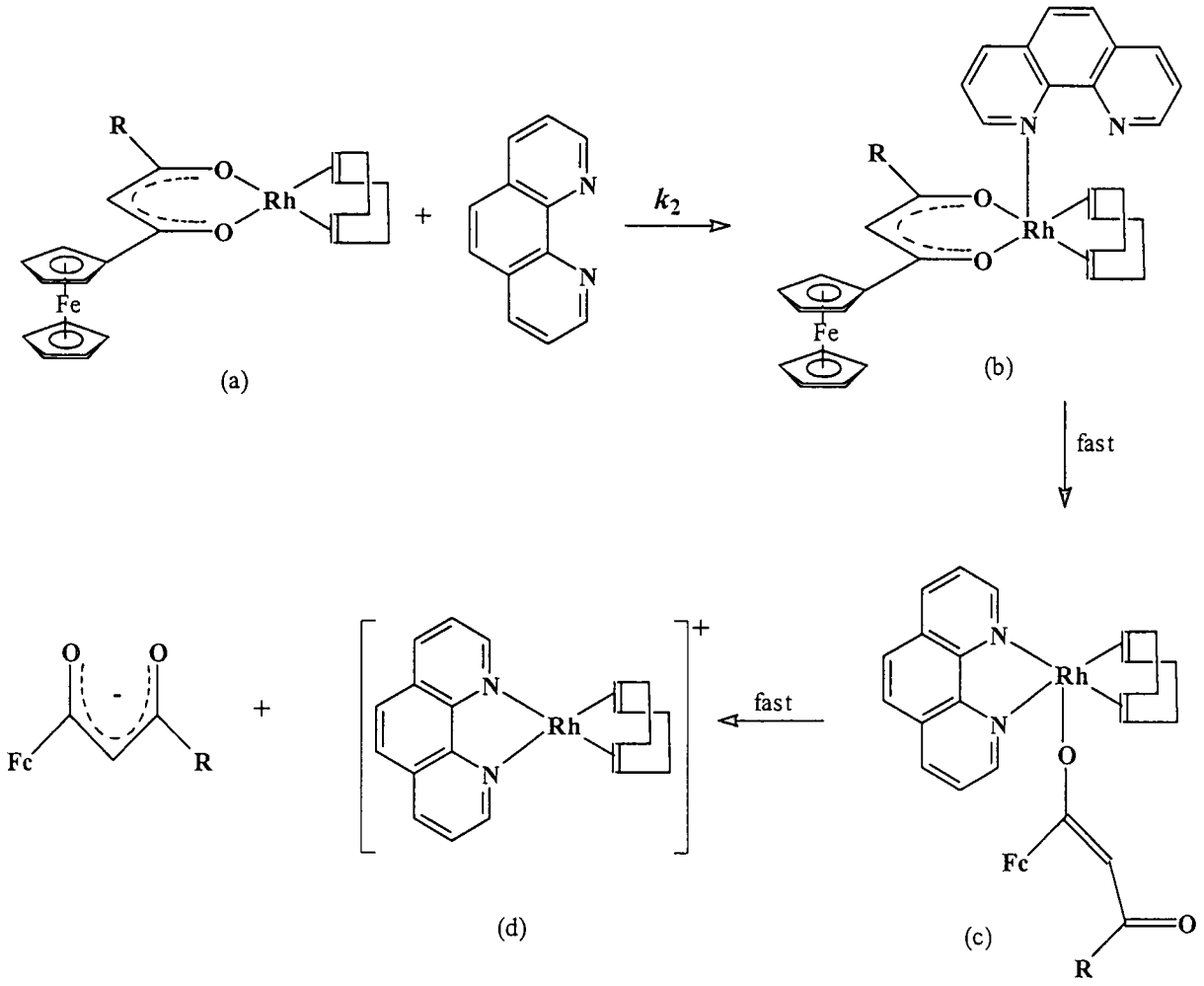

Scheme 3.7: Schematic representation of the associative mechanism of the substitution reaction between [Rh(FcCOCHCOR)(cod)] and 1,10-phenanthroline, with R = H, CH_3, CH_2CH_3, $CH(CH_3)_2$ and $C(CH_3)_3$, Fc = ferrocenyl group. It is expected that the Rh-O bond nearer to the more electronegative substituent (in this case, R group) will break first (see text for explanation).

It has been discussed in chapter 2 that an increasing steric hindrance of ligands co-ordinated to the metal complex slows down the rate of substitution of the incoming ligand (section **2.3.4.7** page 41). This was also found to be the case in this study. Considering the results obtained for the complexes in this study [Rh(FcCOCHCOR)(cod)], (R= H, CH_3, CH_2CH_3, $CH(CH_3)_2$ and $C(CH_3)_3$), these R groups systematically increase in bulkiness, the corresponding second-order rate constants, k_2, (see **Table 3.10**) decrease as R becomes more bulky. **Figure 3.19** illustrates the relationship between second order rate constant and the change in the number of C-atoms on R groups in the complexes of [Rh(FcCOCHCOR)(cod)].

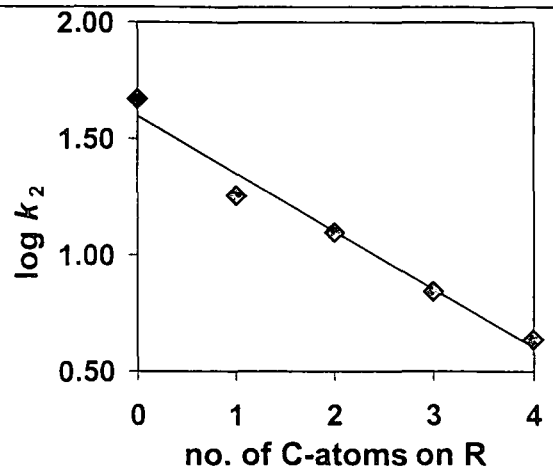

Figure 3.19: Relationship between log k_2, second-order rate constant, and the number of C-atoms on R groups in the complexes [Rh(FcCOCHCOR)(cod)]. R = H, CH_3, CH_2CH_3, $CH(CH_3)_2$ and $C(CH_3)_3$

However, it is **not only** the R group bulkiness that determines the rate of substitution. pK_a' values, substituent group electronegativities and redox potentials also play a role. These relationships were explored in this study. Kinetic data, potentials and pK_a' values that were used for investigation but were not determined from this study may be found in references 3, 10 and 16. The effect of pK_a' values on the reaction rate is shown in **Figure 3.20** (a). From the insert of this graph it can be observed that as the pK_a' values of β-diketones become larger, the rate of substitution becomes slower for the complexes of this study (R = H, CH_3, CH_2CH_3, $CH(CH_3)_2$ and $C(CH_3)_3$). This general trend is also valid when one considers a wider range of β-diketones. The main graph in **Figure 3.20** (a) illustrates the general case for ferrocene containing β-diketones of the type FcCOCHCOR with additional groups of R = CF_3, CCl_3, Ph and Fc (Ph = phenyl and Fc = ferrocenyl). Reference 20 considers this relationship also for β-diketones which do not have a ferrocenyl group. The k_2-pK_a' relationship implies that the more basic the β-diketone becomes, the slower the substitution becomes, and that the rate becomes virtually independent of pK_a' for very basic β-diketones.

Figure 3.20 (b) shows the relationship between k_2 and group electronegativities, χ_R, of R substituents. From the insert in **Figure 3.20** (b), the rate of substitution decreased with decrease in the χ_R value. The insert only considers the complexes that were synthesised in this study. The main graph in **Figure 3.20** (b) also considers complexes with χ_R values over a much wider range. Complexes containing R substituents with larger χ_R values (e.g. χ_{CF3} = 3.01) showed faster substitution of the β-diketonato ligand than those with smaller χ_R values (e.g. χ_{Fc} = 1.87).

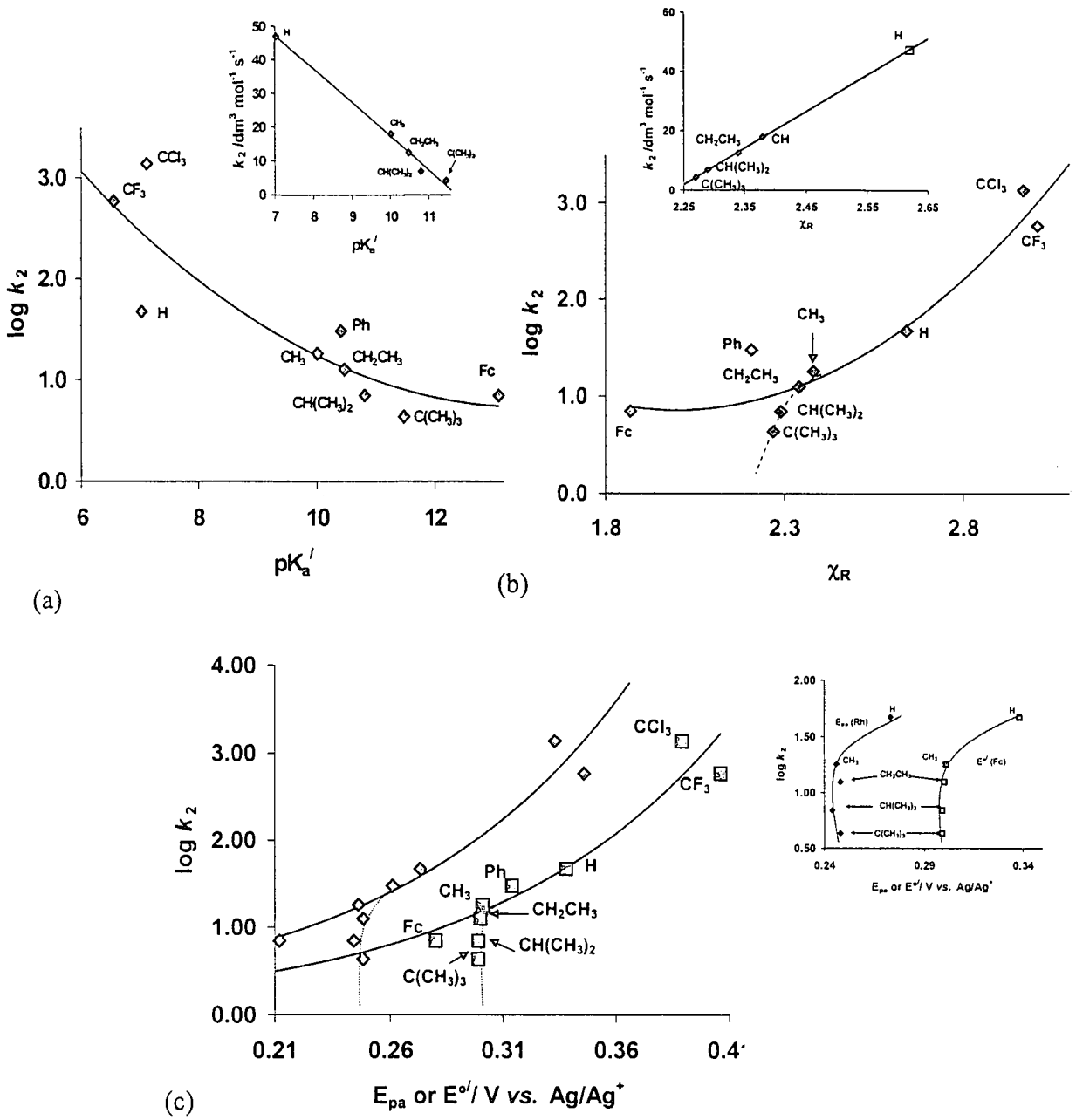

Figure 3.20: (a) The relationship between second-order rate constant, k_2, for the substitution reaction between [Rh(FcCOCHCOR)(cod)] complex and 1,10-phenanthroline in methanol and pK_a' values of the free uncoordinated β-diketones. (b) Relationship between k_2 and group electronegativities of β-diketonato R substituents. (c) The relationship between second-order rate constant, k_2, and $E^{o\prime}$ of the ferrocenyl group, ▣, or E_{pa} of Rh, ◇, *vs.* Ag/Ag^+ in [Rh(FcCOCHCOR)(cod)] complexes. Inserts of these graphs give the mentioned relationships for complexes of this study, that is with R = H, CH_3, CH_2CH_3, $CH(CH_3)_2$ and $C(CH_3)_3$ only.

However, the dependence of k_2 on χ_R becomes less for compounds with substituents having small χ_R values. Again, the main graph in **Figure 3.20** (b) demonstrates the case for ferrocenyl-containing β-diketones, whereas reference 20 addresses the more general case. A small deviation from the

main log k_2-χ_R graph is observed for complexes with R = $CH(CH_3)_2$ and $C(CH_3)_3$ when the broad picture is considered, i.e. for $1.8 \leq \chi_R \leq 3.0$. This implies that the rate of substitution for the complexes in study is not only dependent on the electronegativities of the R groups. Other factors influence the rate as well. This deviation is attributed to the greater steric crowding of the secondary and the tertiary alkyl groups compared to the other R groups. It implies that as 1,10-phenanthroline approaches the rhodium nucleus, these fast rotating bulky substituents (e.g. R = $C(CH_3)_3$) hinder phen from binding with Rh above or below the square planar surface of the molecule. This, therefore, slows the rate determining step of **Scheme 3.7** down. Hence, smaller than expected k_2 values are observed for bulkier alkyl groups.

Therefore, if steric factors did not play a role, the general trend of the relationship between k_2 and $E^{o\prime}$(Fc) or E_{pa}(Rh) of [Rh(FcCOCHCOR)(cod)] (**Figure 3.20** (c)) also shows that fast substitution is observed in complexes where Rh(I) showed the most positive oxidation potential (values in brackets) or where $E^{o\prime}$ (Fc) was more positive, in the following order

(fast substitution) CCl_3 (0.333 V) > CF_3 (0.346 V) > H (0.273 V) > Ph (0.261 V) > CH_3 (0.246 V) ≈ CH_2CH_3 (0.248 V) ≈ $CH(CH_3)_2$ (0.244 V) ≈ $C(CH_3)_3$ (0.248 V) > Fc (0.212 V) (slowest substitution).

As observed in log k_2-χ_R relationship (**Figure 3.20** (b)), bulkier alkyl groups totally deviate from the general trend predicted in **Figure 3.20** (c), see dotted lines. The insert of this graph illustrates that the rate of substitution really becomes independent of Fc formal reduction potentials or Rh oxidation potentials in [Rh(FcCOCHCOR)(cod)] when R = CH_3, CH_2CH_3, $CH(CH_3)_2$ and $C(CH_3)_3$. It implies that for these four complexes, the thermodynamic driving force of the described substitution reaction is equal (because $E^{o\prime}$(Fc) or E_{pa}(Rh) remained constant), but the kinetic driving force becomes smaller as the size of R increases from CH_3 to $C(CH_3)_3$. The lower than expected rate constants for these four complexes are therefore attributed to the steric crowding effect of bulky R groups on the route of access of the rhodium centre an incoming ligand may need. This inter alia means that it becomes more and more difficult for phen to gain access to the Rh centre in substitution reactions involving complexes where R changes from CH_3 through to $C(CH_3)_3$.

From the above results, it is evident that the rate of β-diketonato substitution from [Rh(β-diketonato)(cod)] complexes with 1,10-phenanthroline is not governed by a single factor or variable. Rather, it is governed by the combined superimposed influence of a variety of factors. This

study highlighted at least four parameters that each has an individual effect on the substitution rate. These were steric factors from bulky substituents (**Figure 3.19**), acidity (pK_a' values) of β-diketones (**Figure 3.20** (a)), group electronegativities, χ_R, of the R substituent on the β-diketonato ligand, $(FcCOCHCOR)^-$ (**Figure 3.20** (b)) and the thermodynamic driving force as expressed by the reduction potential of redox active moieties in the [Rh(FcCOCHCOR)(cod)] complexes (**Figure 3.20** (c)).

3.8 Cytotoxic studies

The cytotoxic properties in terms of potential anticancer applications of new ferrocene-containing β-diketones and their rhodium(I) complexes are discussed in this section. It has been shown[21] before that in β-diketones of the type $FcCOCH_2COR$ and rhodium complexes of the type [Rh(FcCOCHCOR)(cod)], the R group drastically influence antineoplastic activity. It was observed that the complex with R = CF_3 was dramatically more active than, for example, R = Ph, in killing cancer cells.

3.8.1 Cytotoxicity of β-diketones, 3-7 and their rhodium complexes 10-14

In this study we determined how antineoplastic activity differ with R = H, CH_3, CH_2CH_3, $CH(CH_3)_2$ and $C(CH_3)_3$. The cytotoxicity of these compounds was determined by observing their effects on cultured HeLa, A_{2780} and A_{2780} platinum resistant cancer cell lines. HeLa is a human cervix epitheloid cancer cell line, while A_{2780} is a human ovarian cancer cell line and A_{2780} (platinum resistant) is a platinum resistant variant of the human ovarian cancer cell line. The author acknowledges Dr. C.E.J. van Rensburg and Mrs. E. Kreft from the University of Pretoria who performed the cytotoxic tests on each cell line. Survival curves (**Figure 3.21** and **Figure 3.22**) indicating percentage cell survival were plotted as a function of drug dose with concentration expressed in μmol dm^{-3}. IC_{50} values (drug dose required for 50% cell death) were estimated by extrapolation and are summarised in **Table 3.11**.

Table 3.11: IC_{50} values of HeLa, A_{2780}, and A_{2780} platinum resistant cancer cell lines, with formal reduction potentials, $E^{o\prime}$, for ferrocene-containing β-diketones and their rhodium complexes. The second-order rate constants, k_2, for the substitution of $FcCOCH_2COR$ in [Rh(FcCOCHCOR)(cod)] with 1,10-phenantrholine are also stated.

Compounds	$E^{o\prime}$(Fc) or Epa (Rh) / V	k_2 / $dm^3\ mol^{-1}\ s^{-1}$	IC_{50} /μmol dm^{-3}		
			HeLa	A_{2780}	A_{2780} platinum resistant
$FcCOCH_2COH$, **3**	0.344	-	73.4	-	-
$FcCOCH_2COCH_3$, **4**	0.308	-	66.6	-	-
$FcCOCH_2COCH_2CH_3$, **5**	0.309	-	62.1	32.5	22.3
$FcCOCH_2COCH(CH_3)_2$, **6**	0.301	-	95.2	32.6	39.1
$FcCOCH_2COC(CH_3)_3$, **7**	0.304	-	67.0	44.2	45.2
[Rh($FcCOCH_2COH$)(cod)], **10**	0.273[(a)], 0.338[(b)]	47(1)	62.4[(c)]	-	-
[Rh($FcCOCH_2COCH_3$)(cod)], **11**	0.246, 0.301	18(1)	64.4[(c)]	-	-
[Rh($FcCOCH_2COCH_2CH_3$)(cod)], **12**	0.248, 0.300	12.6(4)	21.5	9.8	4.68
[Rh($FcCOCH_2COCH(CH_3)_2$)(cod)], **13**	0.244, 0.299	6.9(1)	33.8	24.6	20.8
[Rh($FcCOCH_2COC(CH_3)_3$)(cod)], **14**	0.248, 0.299	4.3(1)	29.1	26.1	19.6

(a) E_{pa} for the irreversible Rh(I) oxidation
(b) $E^{o\prime}$ for the reversible ferrocenium reduction
(c) From unpublished results by J.C. Swarts, with permission.

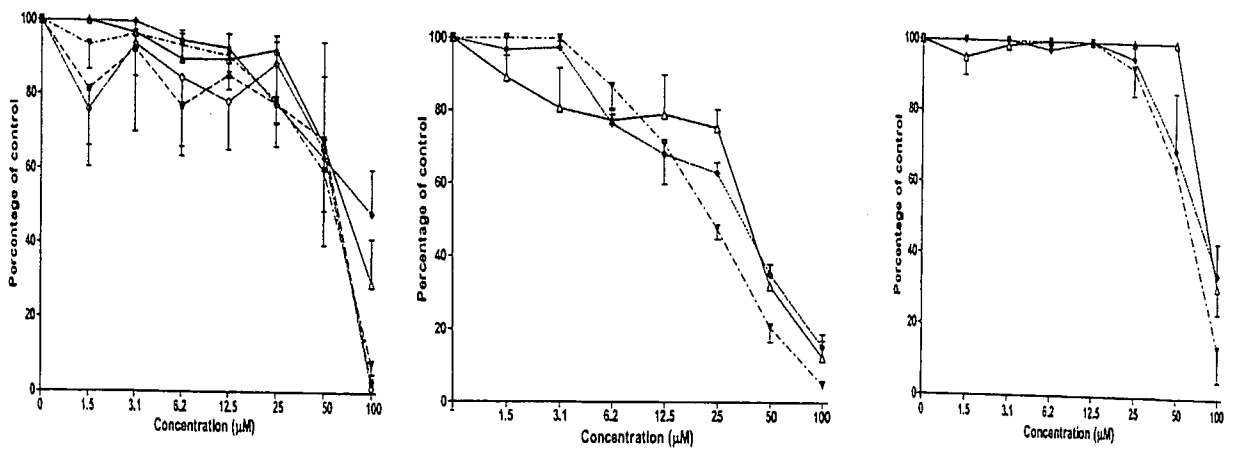

Figure 3.21: Plots of the percentage survival of cells for (a) the HeLa cancer cell line (b) the A_{2780} cancer cell line and (c) the A_{2780} platinum resistant cell line, against concentration (μmol dm^{-3}) of the β-diketones, $FcCOCH_2COR$, 3-7. 3: R = H, ✳; 4: R = CH_3, ◇; 5: R = CH_2CH_3, ▼; 6: R = $CH(CH_3)_2$, ◆ and 7: R = $C(CH_3)_3$, Δ. (The author acknowledges Mrs. E. Kreft from the University of Pretoria for compilation of the survival curves).

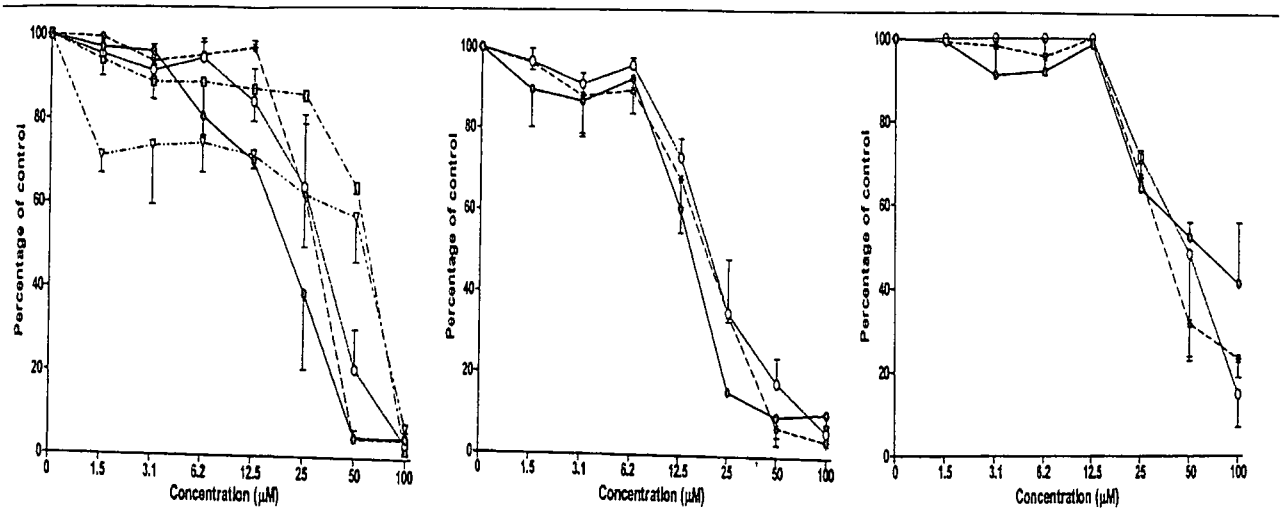

Figure 3.22: Plots of percentage survival of cells for (a) the HeLa cancer cell line (b) the A_{2780} cancer cell line and (c) the A_{2780} platinum resistant cell line, against concentration (μmol dm^{-3}) of [Rh(FcCOCHCOR)(cod)] complexes 10-14. 10: R = H, ■; 11: R = CH_3, ▽; 12: R = CH_2CH_3, ●; 13: R = $CH(CH_3)_2$, ○ and 14: R = $C(CH_3)_3$, ✳. (The author acknowledges Mrs. E. Kreft from the University of Pretoria for compilation of the survival curves).

β-Diketones and rhodium complexes with R = H and CH_3 were not tested against A_{2780} and A_{2780} platinum resistant cancer cell lines, because at the time of testing these cells were not available. From the survival plots and IC_{50} values tabulated in **Table 3.11**, it is clearly observed that rhodium complexes are more cytotoxic than the free β-diketones for each cancer cell line. This was expected as the same trend was observed for other ferrocene-containing rhodium complexes studied in this laboratory.[21] The rhodium complexes were also more effective in destroying A_{2780} and A_{2780} platinum resistant cell lines than HeLa cells. Particularly striking is the observation that the rhodium complexes are more effective in killing the platinum resistant A_{2780} cancer cell line. A graph of amount of C-atoms on the R group compared to the IC_{50} values for the rhodium complexes is shown in **Figure 3.23** (a). It is clear from the results that the ethyl-containing derivative, [Rh(FcCOCHCOCH$_2$CH$_3$)(cod)] is slightly more active in killing cancer cells (smaller IC_{50} values) than the other R groups *viz.* H, CH_3, $CH(CH_3)_2$ and $C(CH_3)_3$.

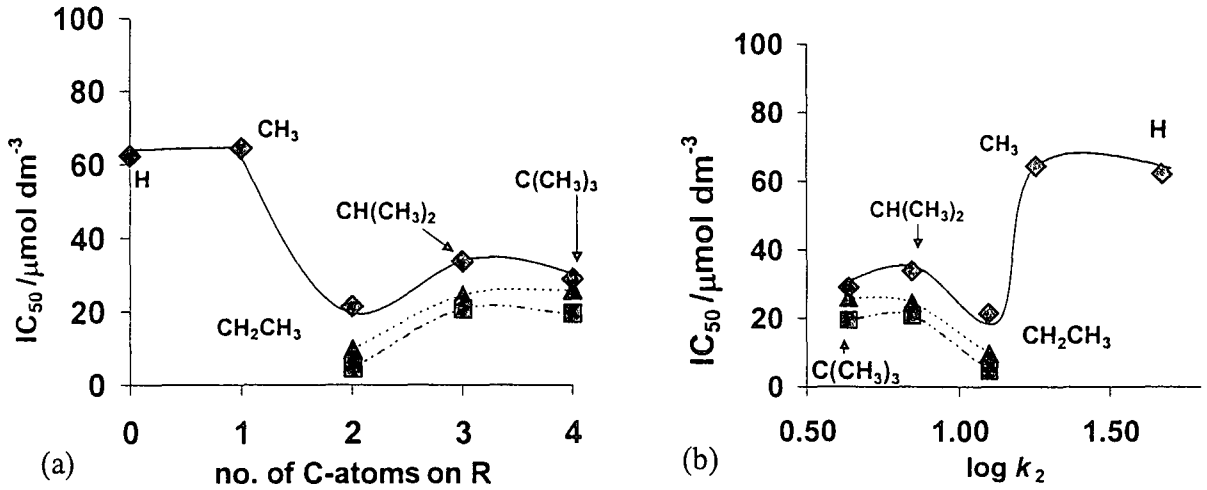

Figure 3.23: (a) Relationship between the IC_{50} of the rhodium complexes [Rh(FcCOCHCOR)(cod)] with R indicated on the graph, for the HeLa cancer cell line (—— and ◆), the A_{2780} cancer cell line (..... and ▲) and the A_{2780} platinum resistant cancer cell line (-..-..-.. and ■) and the number of C-atoms on R. (b) Relationships between IC_{50} values for HeLa (◆), A_{2780} cancer cell line (▲) and A_{2780} platinum resistant cancer cell line (■) and second-order rate constant, k_2, for the substitution of $(FcCOCHCOR)^-$ from [Rh(FcCOCHCOR)(cod)] with 1,10-phenanthroline.

The mechanism of action of rhodium complexes in chemotherapy is assumed to involve at least in part a substitution reaction between Rh-containing drug and DNA. A relationship between the second-order rate constant, k_2, for the substitution of $(FcCOCHCOR)^-$ from [Rh(FcCOCHCOR)(cod)] with 1,10-phenantrholine and IC_{50} values is given in **Figure 3.23** (b). The mechanism of action of the ferrocenyl moiety in chemotherapy is based on electron transfer see chapter 2, page 51). In contrast to what was found for ferrocene-containing acids of the type $Fc(CH_2)_nCOOH$, no clear-cut relationship is observable between IC_{50} and reduction potential of the ferrocenyl group in compounds **3-7** and **10-14**. This means the driving force that makes the ethyl derivative the most antineoplastic material is not thermodynamic in origin, or even a kinetic driving force. Rather, it appears to be a physical effect in that, for example, the ethyl derivatives are more successful in crossing intercellular membranes than any of the other derivatives.

3.9 References

[1] Lowrey, A.H., D'Antonio, P.D. and Karle, J., *J. Amer. Chem. Soc.*, **93,** 6399 (1971).

[2] Chatt, J. and Venanzi, L.M., *J. Chem. Soc.*, **(A),** 4735 (1957).

[3] Conradie, J., *Chemical kinetics, electrochemistry and structural aspects of ferrocene-containing* β-*diketonato complexes of rhodium(I) and iridium(I),* PhD Thesis, UOFS, p 211, 1999.

[4] Barrow, G.M., *Physical Chemistry,* McGraw-Hill, New York International student edition, Chapter 7, p 155, 1961.

[5] Espenson, J.H., *Chemical Kinetics and Reaction Mechanisms,* McGraw-Hill International Editions, 2nd ed., Chapter 3, p 46, 1995.

[6] Helm, L., MINSQ, Non-linear parameter estimation and model development, least squares parameter optimisation V3.12, MicroMath Scientific Software, Salt Lake City, UT (1990).

[7] Syzmanski, H.A., *Infrared Band Handbook,* Plenum press, New York, 1963.

[8] Wells, P.R., *Prog. Phys. Org. Chem.*, **6,** 112 (1968).

[9] Du Plessis. W.C., Erasmus, J.J.C., Lamprecht, G.J., Conradie, J., Cameron, T.S., Aquino, M.A.S. and Swarts, J.C., *Can. J. Chem.*, **77,** 378 (1999).

[10] Du Plessis, W.C., Vosloo, T.G. and Swarts, J.C., *J. Chem. Soc., Dalton Trans.*, 2507 (1998).

[11] Kagarise, R.E., *J. Am. Chem. Soc.*, **77,** 1377 (1955).

[12] Martell, A.E., *Stability Constants of Metal-Ion Complexes*, The Chemical Society, London, Special Publication No. 25, 3rd Ed., part II, p 365, 1971.

[13] Swarts, J.C., Neuse, E.W. and Lamprecht, G.J., *J. Inorg. Organomet. Polym.*, **4,** 143 (1994).

[14] Maron, S.H. and Lando, J.B., *Fundamentals of Physical Chemistry,* Macmillan Publishing Co. Inc., New York, Chapter 14, p 573, 1974.

[15] Maron, S.H. and Lando, J.B., *Fundamentals of Physical Chemistry,* Macmillan Publishing Co. Inc., New York, Chapter 16, p 677, 1974.

[16] Vosloo, T.G, Du Plessis, W.C. and Swarts, J.C., *Inorg. Chim. Acta,* **331,** 188 (2002).

[17] Steynberg, E.C., Lamprecht, G.J. and Leipoldt, J.G., *Inorg. Chim. Acta,* **133,** 33 (1987).

[18] Basson, S.S., Leipoldt, J.G. and Nel, J.T., *Inorg. Chim. Acta*, **84,** 167 (1984).

[19] Leipoldt, J.G., Basson, S.S. and Potgieter, J.H., *Inorg. Chim. Acta,* **117,** L3 (1986).

[20] Vosloo, T.G., *Sintetiese, Kinetiese en Strukturele Aspekte van* β-*diketoonkomplekse met 'n Potensiële Mediese Toepassing,* MSc Thesis, UOFS, p 125, 1991.

[21] Swarts, J.C., unpublished results, with permission.

CHAPTER 4

EXPERIMENTAL

4.1 Materials

Solid reagents (Merck, Aldrich) were used without further purification. Solvents were distilled prior to use and water was double distilled. THF was dried by refluxing over sodium wire under nitrogen. Flash column chromatography was performed on Silica gel 60 (particle size 0.040-0.063m, eluent hexane-ether 1:1 by volume unless otherwise stated). Melting points (m.p.) were determined with a Reichert Thermopan microscope with a Koffler hot-stage and are uncorrected. Liquid reactants (esters) were purchased from Aldrich without further purification.

4.2 Spectroscopy, equilibrium constants, K_c and pK_a' measurements

NMR measurements at 292 K were recorded on a Bruker Advance DPX 300 NMR spectrometer. The chemical shifts are reported relative to $SiMe_4$ at 0.00 ppm. IR spectra (KBr pellets or chloroform solutions) were recorded on a Hitachi model 270-50 spectrometer with data processor. UV spectra of [Rh(FcCOCHCOR)(cod)] and $[Rh(phen)(cod)]^+$ were recorded in a Cary 50 Probe UV/Visible spectrophotometer.

4.2.1 Calculation of % keto isomer and determination of K_c

^1H NMR spectra of β-diketones, $FcCOCH_2COR$ were recorded at 292 K with concentrations ranging between 1.3 and 1.7 mmol dm^{-3} in $CDCl_3$. Integration of spectra was done in such a way that the methine proton, Fc-CO-C**H**=C(OH)-R at ca. 5.73 – 5.80 ppm was always assigned an integral value of one. The % keto was calculated from the relationship

$$\% \text{ keto isomer} = (I \text{ of keto signal})/\{(I \text{ of keto signal}) + (I \text{ of enol signal})\} \times 100$$

with I = integral value. Once the % keto isomer was known, the equilibrium constant

$$K_c = \frac{[Fc\text{–}CO\text{–}CH\text{=}C(OH)\text{–}R]}{[Fc\text{–}CO\text{–}CH_2\text{–}CO\text{–}R]}$$

$= k_1/k_{-1}$, applicable to equilibrium

$$Fc\text{-}CO\text{-}CH_2\text{-}CO\text{-}R \overset{K_C}{\rightleftharpoons} Fc\text{-}CO\text{-}CH\text{=}C(OH)\text{-}R$$

was obtained from the relationship

K_c = (% enol isomer)/ (% keto isomer)

= (100 - % keto isomer)/ (% keto isomer).

4.2.2 Observed acid dissociation constant, pK_a', determination

The pK_a' values were obtained by measuring the absorbance at different pH during an acid-base titration in acetonitrile-water mixtures 1:9 by volume, μ = 0.100 mol dm^{-3} ($NaClO_4$) at 25.0 (1)°C with β-diketone concentrations less than 0.12 x 10^{-3} mol dm^{-3}. A linear response by the pH meter (Hanna instruments model HI 9321), fitted with a glass electrode, was ensured by calibration with buffers at pH = -log α_H = 4.00, 7.02 and 12.00 respectively, α_H = activity of H^+. A test pK_a' determination was performed by titrating Hfca, which was previously characterised.[1] The titrations were performed with $HClO_4$ from high pH, adjusted with NaOH to low pH. The least squares fit of the obtained UV absorbance/pH data for this titration using equation

$$A_T = \frac{A_{HA}10^{-pH} + A_A 10^{-pK_a}}{10^{-pH} + 10^{-pK_a}}$$

by utilising the fitting program MINSQ,[2] resulted in a pK_a' of 9.98 ± 0.05. This was within experimental error of the published pK_a' of 10.01 ± 0.02. It was therefore concluded that our electrode system was calibrated to measure hydrogen ion activity under the conditions used.

4.3 Substitution kinetics

The Beer-Lambert law, $A = \varepsilon Cl$ with A = UV/Vis absorbance, ε = molar extinction coefficient, C = concentration and l = path length = 1 cm, were found to be valid for all complexes in the concentration range utilised for the kinetic studies. Pseudo-first-order rate constants, k_{obs}, were

determined by monitoring the disappearance of [Rh(FcCOCHCOR)(cod)] at wavelengths 480 nm for R = CH_2CH_3 (C = 4.07 x 10^{-4} mol dm^{-3}), 460 nm for R = $CH(CH_3)_2$ (C = 4.04 x 10^{-4} mol dm^{-3}) and 480 nm for R = $C(CH_3)_3$ (C = 4.02 x 10^{-4} mol dm^{-3}) on a 05-109 pbp Spectrakinetic stopped flow spectrometer. 1,10-Phenanthroline concentrations were between 4.02 x 10^{-3} and 0.16 mol dm^{-3}. Absorbance-time data was collected and k_{obs} values were determined from a linear fit of data according to:

$$\ln (A_o/A_t) = k_{obs}\, t$$

A_o indicates initial absorbance and A_t is the absorbance at time t. The second-order rate constant, k_2, was determined (slope) from the relationship between the k_{obs} and different phen concentrations according to the following equation

$$k_{obs} = k_2[\text{phen}] + k_s$$

It was found that k_s = 0 for all complexes. The activation parameters ΔH*, ΔS* and ΔG* were obtained from fitting second order kinetic data between 10 and 35°C to the following equations:

$$\ln \frac{k}{T} = -\frac{\Delta H^*}{RT} + \frac{\Delta S^*}{R} + \ln \frac{R}{Nh}$$

$$\Delta G^* = \Delta H^* - T\Delta S^*$$

Utilising the fitting program MINSQ.[2] Temperatures were kept constant to within 0.01°C.

4.4 Cyclic Voltammetry

Measurements on ca. 1 mmol dm^{-3} β-diketone solutions in acetonitrile with 0.10 mol dm^{-3} tetra-*n*-butylamonium hexafluorophosphate (Fluka, electrochemical grade) as supporting electrolyte were conducted under a blanket of purified argon at 25.0°C utilising BAS model CV-27 voltammograph interfaced with a personal computer. A three-electrode cell, which utilised a Pt auxiliary electrode, a Pt (surface area = 0.03142 cm^2) or a glassy carbon (surface area = 0.0707 cm^2) working electrode, and a Ag/Ag^+ (0.010 mol dm^{-3}, $AgNO_3$) reference electrode[3] mounted on a Luggin capillary was employed.[4] Data, uncorrected for junction potentials, were collected with an Adalab-PC™ and Adapt™ data acquisition kit (Interactive Microwave. Inc.) with locally developed software, and

analysed with Hyperplot (JHM International, Inc.). All temperatures were kept constant to within 0.2°C.

4.5 Cytotoxic results

The author acknowledges Mrs. E. Kreft from the University of Pretoria for performing these experiments.

4.5.1 Sample preparation

β-Diketones **3-7** and rhodium complexes **10-14** were dissolved in DMSO to give stock concentration of 10 mg cm^{-3}. These were then diluted in the appropriate growth medium supplemented with fetal calf serum to give final DMSO concentrations not exceeding 0.5% and drug concentrations of 1-3000 μg cm^{-3} prior to cell experiments.

4.5.2 Cell cultures

Human ovarian cancer cell line, A_{2780}, and its platinum resistant variant cell line were grown as suspended culture in RPMI 1640. The human cervix epitheloid cancer cell line, HeLa, was grown as a monolayer culture in MEM. Growth medium was incubated at 37°C under 5% CO_2 and fortified with 10% FCS, and 1% penicillin and streptomycin. Appropriate solvent control systems were included. Cells were seeded at 2000 cells/well for 24 h incubation experiments and 400 cells/well for 7 day incubation experiments in 96 well microtiter plates in a final volume of 200 μl of growth medium in the presence or absence of different concentrations of experimental drugs. Wells without cells and with cells but without drugs were included as controls. After incubation at 37°C for 1 day or 7 days, survival was measured by means of the colometric 3-(4,5-dimethylthiazol-2-yl)-diphenyltetra sodium bromide (MMT) assay.

4.6 Synthesis

4.6.1 Acetylferrocene (2)

A mixture of ferrocene (9.3 g, 0.05 mol), acetic anhydride (25 cm^3) and 85% phosphoric acid (2 cm^3) was heated at 100°C for 10 minutes. Care was taken to maintain the internal temperature[5] of the reaction mixture between 100 and 105°C. The reaction mixture was cooled slightly and poured onto ice. After standing overnight, the mixture was neutralised with sodium carbonate monohydrate (20 g) in 20 cm^3 of water. The resulting brown pasty product was cooled on an ice bath and filtered. The tan product was washed four times with 100 ml portions of water and filtered. The granular product was dried in a vacuum dessicator over phosphoric anhydride. Recrystallisation from hexane gave a sufficiently pure product (81% yield) for β-diketone synthesis. Characterisation data: m.p. 85°C; R_f = 0.38 (ether: hexane = 1:1) ν_{max}(KBr)/ cm^{-1} 1662 (C=O), δ_H (80 MHz, $CDCl_3$) 2,40 (3H, s, CH_3), 4.21 (5H, s, C_5H_5), 4.52 (2H, t, C_5H_4), 4.78 (2H, t, C_5H_4).

4.6.2 β-Diketones

All the β-diketones were synthesised from a general procedure as described for Hfca.

4.6.2.1 1-Ferrocenylbutane-1,3-dione (Hfca, 4)

Nitrogen was flushed through a flask equipped with acetylferrocene (1.0 g, 4.38 mmol) for an hour and then dissolved in dry THF (5 cm^3). $LiNPr^i_2$ (2 ml) was added at 0°C and the solution was stirred for 30 minutes before a solution of ethyl acetate (0.4478 g, 0.5 cm^3 and 4.38 mmol) in 1 ml dry THF was added. The resulting dark red suspension was stirred under nitrogen for 16 hours, followed by treatment with HCl (100 cm^3, 0.5 mol dm^{-3}). After extraction of the product with ether, purification was effected by column chromatography on silica gel with hexane as the eluent yielding dark red oil, which was recrystallized with hexane and ether. Two weeks storage in the freezer and solvent removal under reduced pressure afforded dark red crystals of Hfca (0.384 g, 28%), m.p. 98°C, R_f = 0.78 (ether: hexane = 1:1). δ_H (300 MHz, $CDCl_3$) 2.10 (3H, s, enol CH_3), 2.32 (3H, s, keto CH_3), 3.85 (2H, s, keto CH_2), 4.22 (5H, s, enol C_5H_5), 4.25 (5H, s, keto C_5H_5),

4.52 (2H, t, enol C_5H_4), 4.60 (2H, t, keto C_5H_4), 4.80 (2H, t, C_5H_4), 4.81 (2H, t, keto C_5H_4) and 5.74 (1H, s, enol CH).

4.6.2.2 1-Ferrocenylpentane-1,3-dione (Hfcp, 5)

Hfcp was prepared in yields up to 24% as described for Hfca by replacing ethyl acetate with ethyl propionate. Characterisation data: m.p. 41°C, R_f = 0.85 (ether: hexane = 1:1). δ_H (300 MHz, $CDCl_3$) 1.22 (3H, t, enol $CH_2C\underline{H}_3$), 1.34 (3H, t, keto $CH_2C\underline{H}_3$), 2.37 (2H, q, enol $C\underline{H}_2CH_3$), 2.67 (3H, q, keto $C\underline{H}_2CH_3$), 3.84 (2H, s, keto CH_2), 4.20 (5H, s, enol C_5H_5), 4.25 (5H, t, keto C_5H_5), 4.51 (2H, t, C_5H_4), 4.49 (2H, t, C_5H_4), 4.79 (2H, t, C_5H_4) and 5.73 (1H, s, enol CH).

4.6.2.3 1-Ferrocenyl-4-methylpentane-1,3-dione (Hfcdma, 6)

Hfcdma was prepared in yields up to 21% as described for Hfcp by replacing ethyl propionate with ethyl isobutyrate. Characterisation data: m.p. 50°C, R_f = 0.80 (ether: hexane = 1:1). δ_H (300 MHz, $CDCl_3$) 1.15 (6H, d, keto $CH(C\underline{H}_3)_2$), 1.23 (6H, d, enol $CH(C\underline{H}_3)_2$), 2.53 (1H, m, enol $C\underline{H}(CH_3)_2$),2.86 (1H, m, keto $C\underline{H}(CH_3)_2$), 3.90 (2H, s, keto CH_2), 4.20 (5H, s, enol C_5H_5), 4.26 (5H, s, keto C_5H_5), 4.51 (2H, t, enol C_5H_4), 4.58 (2H, t, keto C_5H_4), 4.80 (2H, t, C_5H_4) and 5.74 (1H, s, enol CH).

4.6.2.4 1-Ferrocenyl-4,4-dimethylpentane-1,3-dione (Hfctma, 7)

Hfcdma was prepared in yields up to 17% as described for Hfcp by replacing ethyl propionate with ethyl trimethylacetate. Characterisation data: m.p. 58°C, R_f = 0.72 (ether: hexane = 1:1). δ_H (300 MHz, $CDCl_3$) 1.19 (9H, s, keto $C(CH_3)_3$), 1.21 (9H, s, enol $C(CH_3)_3$), 3.91 (2H, s, keto CH_2), 4.16 (5H, s, enol C_5H_5), 4.24 (5H, t, keto C_5H_5), 4.47 (2H, t, enol C_5H_4), 4.52 (2H, t, keto C_5H_4), 4.77 (2H, t, C_5H_4) and 5.79 (1H, s, enol CH).

4.6.2.5 2-Ferrocenoyletan-1-al (Hfch, 3)

This product fixated on a silica gel column and therefore was purified mainly by crystallisation. Characterisation data: m.p. 104°C, δ_H (300 MHz, $CDCl_3$) 3.79 (2H, d, keto CH_2), 4.23 (5H, s, enol C_5H_5), 4.24 (5H, t, keto C_5H_5), 4.53 (2H, t, keto C_5H_4), 4.57 (2H, t, enol C_5H_4), 4.59 (2H, t, keto C_5H_4), 4.81 (2H, t, enol C_5H_4), 5.77 (1H, d, enol CH), 7.75 (1H, m, enol H) and 9.91 (1H, t, keto H).

4.6.3 Di-μ-chloro-bis(η-cycloocta-1,5-diene)dirhodium(I) $[Rh_2Cl_2(cod)_2]$ (9)

$RhCl_3.H_2O$ (0.50 g, 2.2 mmol) was dissolved with few drops of water and ethanol (11 cm^3) was added while stirring the solution. Cyclooctadiene (3.25 cm^3) was added dropwise and the dark red solution was refluxed at 78°C for $2^1/_2$ hours. The mixture was cooled down on an ice bath. The yellow precipitate was filtered off and washed with cold methanol. The product (73% yield) was then left overnight in a dark place to dry. Characterisation data: m.p. 256°C δ_H (300 MHz, $CDCl_3$) 1.30 (4H, m, half of $4CH_2$), 2.08 (4H, m, half of $4CH_2$) and 4.42 (4H, m, 4CH).

4.6.4 [Rh(β-diketone)(cod)] complexes

The general procedure for all rhodium complexes was as follows. $[Rh_2Cl_2(cod)_2]$ (0.5 g, 1 mmol) was dissolved in 4 cm^3 DMF. The base $NaHCO_3$ (2 mmol) was added followed by the addition of the β-diketone (2 mmol). After 4 minutes of stirring the product was precipitated with an excess of ice cold water, filtered off and then dissolved ether. The ether solution was washed with water, dried with $MgSO_4$ and evaporated to dryness. Column chromatography gave the pure products with yields above 80%.

4.6.4.1 (η^4-1,5-cyclooctadiene)(1-ferrocenyl-1,3-propanedionato-κ^2 *O,O*)rhodium(I) [Rh(fch)(cod)] (10)

This product was purified by recrystallisation, as it could not be eluted from a silica gel column. Characterisation data: m.p. 173°C, δ_H (300 MHz, $CDCl_3$), 1.85 (4H, m, half of aliphatic C_8H_{12} protons), 2.49 (4H, m, other half of aliphatic C_8H_{12} protons), 4.07-4.25 (9H, m, four olefinic protons of C_8H_{12} and 5H of C_5H_5), 4.36 (2H, t, C_5H_4), 4.65 (2H, t, C_5H_4), 5.55 (1H, d, CH) and 7.88 (1H, d, CH).

4.6.4.2 (η^4-1,5-cyclooctadiene)(1-ferrocenyl-1,3-pentanedionato-κ^2 *O,O*)rhodium(I) [Rh(fca)(cod)] (11)

Characterisation data: 80% yield, m.p. 92°C, R_f = 0.79 (ether: hexane = 2:3); δ_H (300 MHz, $CDCl_3$) 1.87 (4H, m, half of aliphatic C_8H_{12} protons), 2.02 (3H, t, CH_3), 2.51 (4H, m, other half of aliphatic C_8H_{12} protons), 4.12 (4H, four olefinic protons of C_8H_{12}), 4.16 (5H, s, C_5H_5), 4.34 (2H, t, C_5H_4), 4.64 (2H, t, C_5H_4) and 5.62 (1H, s, CH)

4.6.4.3 (η^4-1,5-cyclooctadiene)(1-ferrocenyl-1,3-pentanedionato-κ^2 *O,O*)rhodium(I) [Rh(fcp)(cod)] (12)

Characterisation data: 85% yield, m.p. 92°C, R_f = 0.78 (ether: hexane = 2:3); δ_H (300 MHz, $CDCl_3$) 1.07 (3H, t, $CH_2C\underline{H}_3$), 1.83 (4H, m, half of aliphatic C_8H_{12} protons), 2.22 (2H, q, $C\underline{H}_2CH_3$), 2.48 (4H, m, other half of aliphatic C_8H_{12} protons), 4.05 (9H, four olefinic protons of C_8H_{12}), 4.12 (5H, s, C_5H_5), 4.29 (2H, t, C_5H_4), 4.60 (2H, t, C_5H_4) and 5.59 (1H, s, CH)

4.6.4.4 (η^4-1,5-cyclooctadiene)(1-ferrocenyl-4-methyl-1,3-pentanedionato-κ^2 *O,O*)rhodium(I) [Rh(fcdma)(cod)] (13)

Characterisation data: 82% yield, m.p. 102°C, R_f = 0.81 (ether: hexane = 2:3). δ_H (300 MHz, $CDCl_3$) 1.08 (6H, d, $CH(C\underline{H}_3)_2$), 1.82 (4H, m, half of aliphatic C_8H_{12} protons), 2.42 (1H, m,

C<u>H</u>$(CH_3)_2$), 2.47 (4H, m, other half of aliphatic C_8H_{12} protons), 4.04 (9H, four olefinic protons of C_8H_{12}) 4.11 (5H,s, C_5H_5), 4.28 (2H, t, C_5H_4), 4.60 (2H, t, C_5H_4) and 5.60 (1H, s, CH)

4.6.4.5 (η^4-1,5-cyclooctadiene)(1-ferrocenyl-4,4-dimethyl-1,3-pentanedionato-κ^2 *O,O*)rhodium(I) [Rh(fctma)(cod)] (14)

Characterisation data: 88% yield, m.p. 148°C, R_f = 0.80 (ether: hexane = 1:1). δ_H (300 MHz, $CDCl_3$) 1.11 (9H, s, $C(CH_3)_3$), 1.82 (4H, m, half of aliphatic C_8H_{12} protons), 2.47 (4H, m, other half of aliphatic C_8H_{12} protons), 4.08 (9H, four olefinic protons of C_8H_{12}), 4.11 (5H, s, C_5H_5), 4.28 (2H, t, C_5H_4), 4.59 (2H, t, C_5H_4) and 5.77 (1H, s, CH).

4.7 References

[1] Du Plessis, W.C., Vosloo, T.G. and Swarts, J.C., *J. Chem.Soc., Dalton Trans.*, 2507 (1998).

[2] Helm, L., MINSQ, Non-linear parameter estimation and model development, least squares parameter optimisation V3.12, MicroMath Scientific Software, Salt Lake City, UT (1990).

[3] Sawyer, D.T. and Roberts, Jr., J.L., *Experimental electrochemistry for chemists,* Wiley, New York, p 54, 1974.

[4] (a) Evans, D.H., O'Connell, K.M., Peterson, R.A. and Kelly, M.J., *J. Chem. Educ.*, **60,** 291 (1983). (b) Mabbott, G.A., *J. Chem. Educ.*, **60,** 697 (1983).

[5] Van Ryswky, H. and Van Hecke, G.R., *J. Chem. Educ.*, **68,** 878 (1991).

CHAPTER 5

SUMMARY AND FUTURE PERSPECTIVES

In this study, six new compounds were synthesised. These were β-diketones $FcCOCH_2COR$ and their rhodium (I) complexes, [Rh(FcCOCHCOR)(cod)], with R = CH_2CH_3, $CH(CH_3)_2$ and $C(CH_3)_3$ and Fc = ferrocenyl. The newly synthesised β-diketones were characterised by several techniques in order to differentiate their activities and compare them to β-diketones and rhodium complexes with R = H and CH_3. Group electronegativities, χ_R, of the R substituents were determined from the IR carbonyl stretching frequencies of their ethyl esters. There was an inconsistency with the group electronegativity of H before. The IR carbonyl stretching frequency data gave χ_H values of 2.11[1] and 2.13[2] and electrochemical studies gave a value of 2.55.[3] Utilising pK_a'-χ_R relationship, χ_H was found to be 2.64, which is mutual consistent with the electrochemically determined value of 2.55. It was observed that as the group electronegativities of the R substituents decreased, the β-diketones become more basic. The keto-aldehyde, $FcCOCH_2COH$ was found to be the most acidic of the series in this study with β-diketone $FcCOCH_2COC(CH_3)_3$ being the most basic. The pK_a' values and group electronegativities of R substituents were found to be (pK_a', R, χ_R) = (7.04, H, 2.64), (10.01, CH_3, 2.38), (10.57, CH_2CH_3, 2.34), (10.80, $CH(CH_3)_2$, 2.29) and (11.47, $C(CH_3)_3$, 2.27).

All β-diketones exist in principle as a mixture of keto and enol isomers as given by

$$\text{Fc-C(OH)=CH-CO-R} \rightleftharpoons \text{Fc-CO-CH}_2\text{-CO-R} \rightleftharpoons \text{Fc-CO-CH=C(OH)-R}$$

(A) **(B)**

^{1}H NMR studies on $FcCOCH_2COR$ indicated that enolisation in a direction away from the ferrocenyl group, i.e. isomer **B,** always dominates. This observation was explained in terms of resonance stabilisation of canonical forms. The formation of different canonical forms of isomer **B** lower the energy of this isomer enough to allow it to dominate the existence of the isomer **A**. Proof of the resonance stabilising effect of canonical forms are presented in the discussion of the crystal structure of $FcCOCH_2COCH_3$.[4]

From electrochemical studies, utilising cyclic voltammetry, it was found that free β-diketones exhibited an electrochemical reversible Fc/Fc^+ couple. It was also observed that the oxidation of ferrocenyl group of $FcCOCH_2COR$ was independent of the different R groups for R = CH_3 (0.308 V), CH_2CH_3 (0.309 V), $CH(CH_3)_2$ (0.301 V) and $C(CH_3)_3$ (0.304 V). Values in brackets are the formal reduction potential, $E^{o'}$ *versus* Ag/Ag^+, for each β-diketone. When R = H, ferrocene was much more difficult to oxidise with the $E^{o'}$ value about 40 mV more positive than if R = alkyl

group. This is consistent with H having a much larger group electronegativity (more electron withdrawing) than the alkyl groups. The H group withdraws more electron density from the ferrocene, causing the ferrocene to be oxidised at a more positive potential. All rhodium complexes, [Rh(FcCOCHCOR)(cod)], exhibited an electrochemical reversible Fc/Fc^+ couple at $0.299\ V < E^{o\prime} < 0.338\ V$ and an electrochemically irreversible Rh^I oxidation wave at $0.248\ V < E_{pa} < 0.273\ V$. The formal reduction potentials of the ferrocenyl group, $E^{o\prime}(Fc)$ and anodic potential of the rhodium, $E_{pa}(Rh)$, were again independent of R, provided R = alkyl group. The rhodium nucleus of the complex with R = H was oxidised at potentials of 15 mV more positive than those with alkyl groups.

The kinetic study of the substitution of the β-diketonato ligand, $(FcCOCHCOR)^-$, from [Rh(FcCOCHCOR)(cod)] with 1,10-phenanthroline (phen) was conducted utilising UV/Visible stopped-flow kinetic techniques. All rhodium(I) complexes obeyed the Beer-Lambert law, which allowed substitution kinetics to be studied by optical methods. The general rate law applicable to this substitution was found to be

$$\text{Rate} = k_2[\text{phen}][\text{Rh(FcCOCHCOR)(cod)}]$$

Second-order rate constants, measured in $dm^3\ mol^{-1}\ s^{-1}$, were found to be k_2 = 47 (H), 18 (CH_3), 12.6 (CH_2CH_3), 6.9 ($CH(CH_3)_2$) and 4.3 ($C(CH_3)_3$). All substitution reactions did not show a noticeable solvent related pathway. The substitution reaction was found to be proceeding via an associative mechanism due to large negative entropies of activation, ΔS^*. The rate-determining step involved the attack by the 1,10-phenanthroline ligand on the rhodium centre. The rate of substitution was found to be decreasing as the number of C-atoms on the R group increased. This implies that the rate is retarded when bulkier R groups are present on the β-diketonato ligand as they hinder the approach of phen to an appropriate rhodium binding site. Other factors that influence the rate of substitution other than steric hindrance were also explored. It was inter alia found that the rate of substitution decreased with increasing pK_a' values of the β-diketones, it increases with an increase in the group electronegativities of R substituents, for the complexes of this study. An independence of the rate of substitution on the formal reduction potentials of the rhodium complexes was observed. Further reactions like oxidative addition and carbonyl insertion reactions are still to be investigated for rhodium complexes of the type [Rh(β-diketonato)(CO)(PPh_3)] containing the new β-diketonato ligands of this study.

The cytotoxic properties in terms of potential anticancer applications of these newly synthesised β-diketones and their rhodium(I) complexes were studied. HeLa, A_{2780} and A_{2780} platinum resistant cancer cell lines were utilised to determine how cytotoxicity differ with R = H, CH_3, CH_2CH_3, $CH(CH_3)_2$ and $C(CH_3)_3$. It was observed that rhodium complexes are more effective in killing cancer cells than the free β-diketones. The rhodium complex with R = CH_2CH_3 was also found to be more cytotoxic than other complexes. The compounds of this study were found to be less effective in killing cancer cells as compared to complexes with R = CF_3.

In this laboratory, fairly detailed studies involving different R groups have been performed. Future studies on similar systems may include varying the ferrocenyl group with a variety of other metallocenes including ruthenocene, osmocene and cobaltocene. Other metallic centres than rhodium may also be considered. These include iridium, platinum and palladium. Applications of these novell complexes in terms of catalysis should also be addressed. These would include carbon-carbon bond formation utilising palladium complexes in, for example, typical Heck reactions, and the conversion of methanol to acetic acid utilising the rhodium based Monsanto process or the iridium based Cativa process.

References

[1] This study.

[2] Du Plessis, W.C., Erasmus, J.C., Lamprecht, G.J., Conradie, J., Cameron, T.S., Aquino, M.A.S. and Swarts, J.C., *Can. J. Chem.*, 77, 378 (1999).

[3] Conradie, J., *Chemical kinetics, electrochemistry and structural aspects of ferrocene-containing β-diketonato complexes of rhodium(I) and iridium(I),* PhD Thesis, UOFS, p 211, 1999.

[4] Du Plessis, W.C., Vosloo, T.G. and Swarts, J.C., *J. Chem. Soc., Dalton Trans.*, 2507 (1998).

APPENDIX

^{1}H NMR SPECTRA

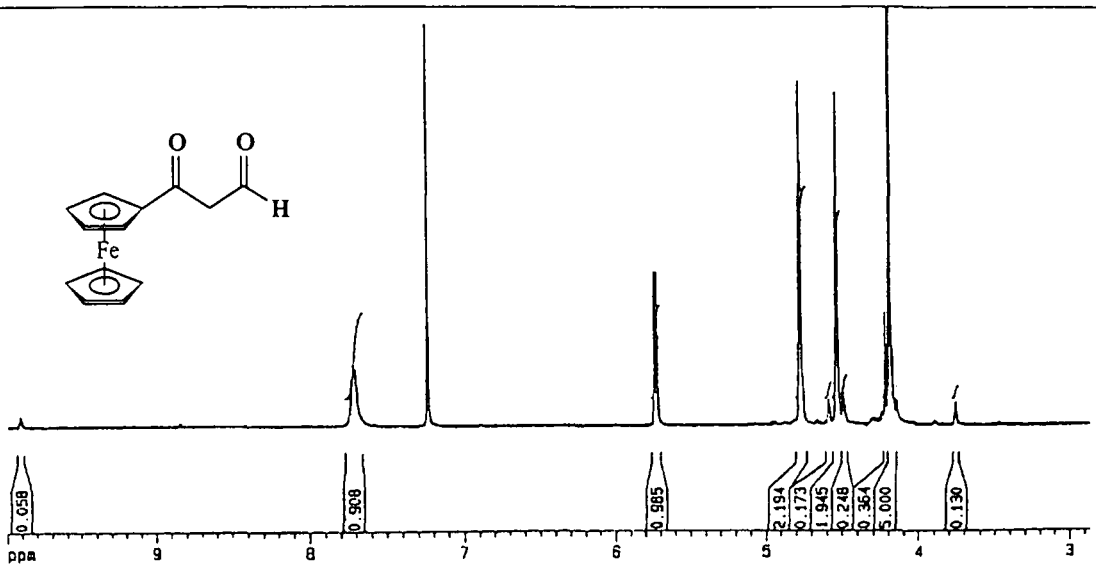

Spectrum 1: Hfch, 3

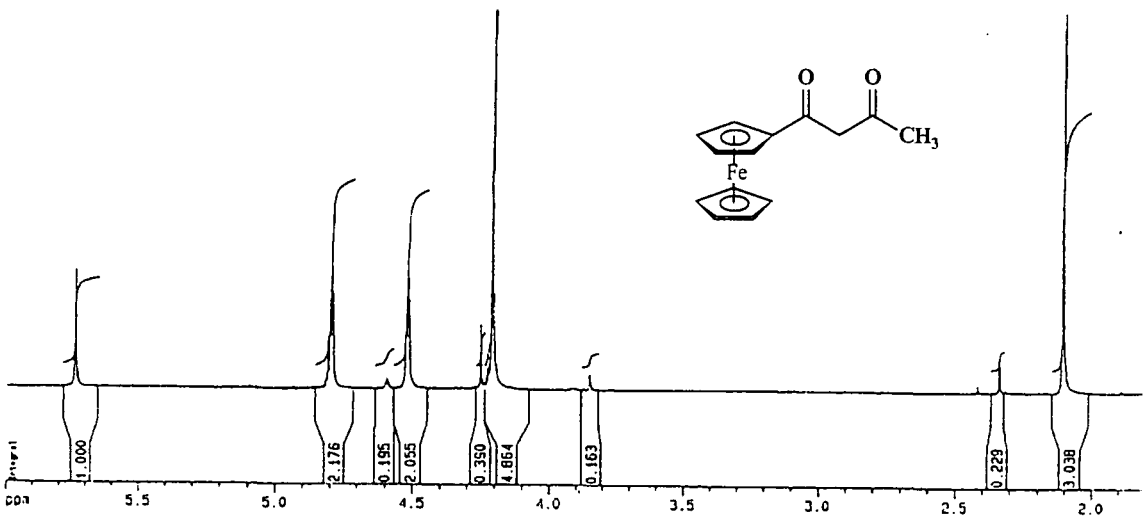

Spectrum 2: Hfca, 4

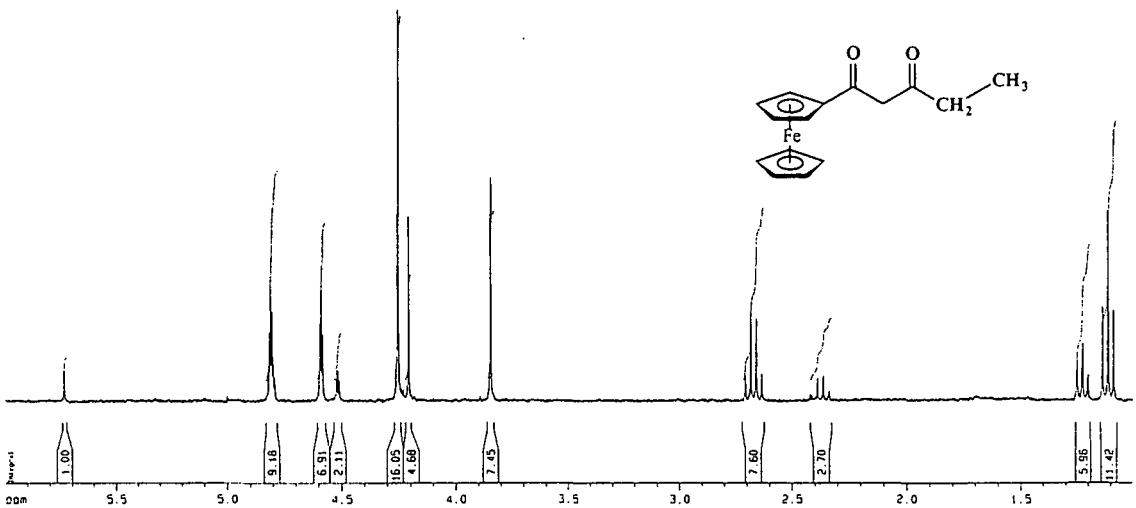

Spectrum 3: Hfcp, 5

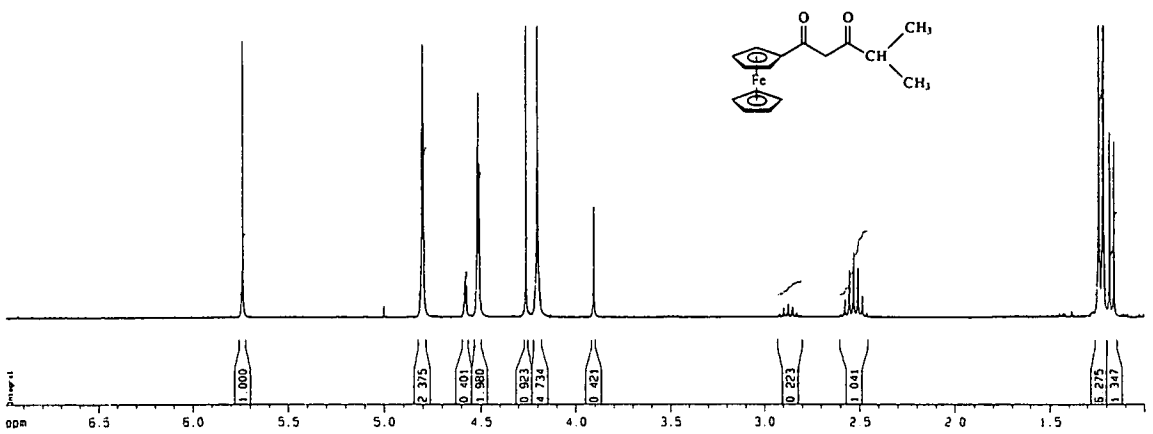

Spectrum 4: Hfcdma, 6

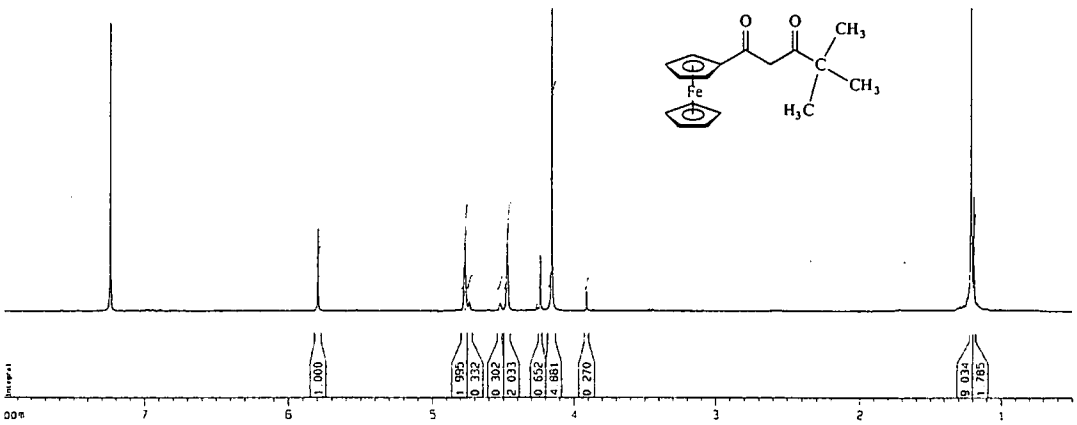

Spectrum 5, Hfctma, 7

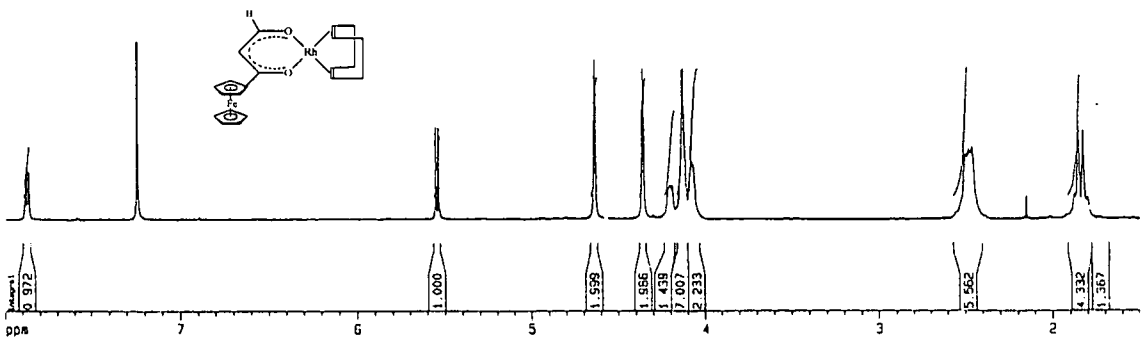

Spectrum 6: [Rh(fch)(cod)], 10

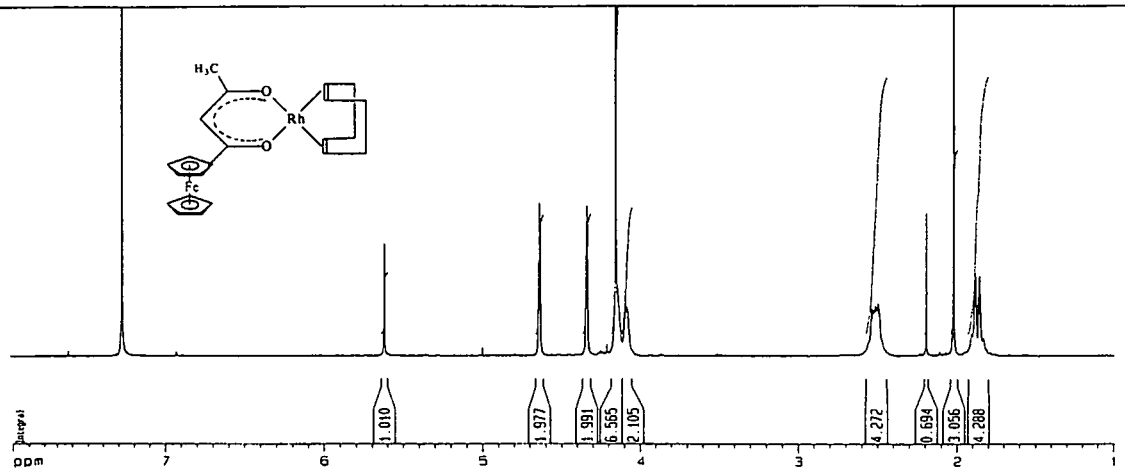

Spectrum 7: [Rh(fca)(cod], 11

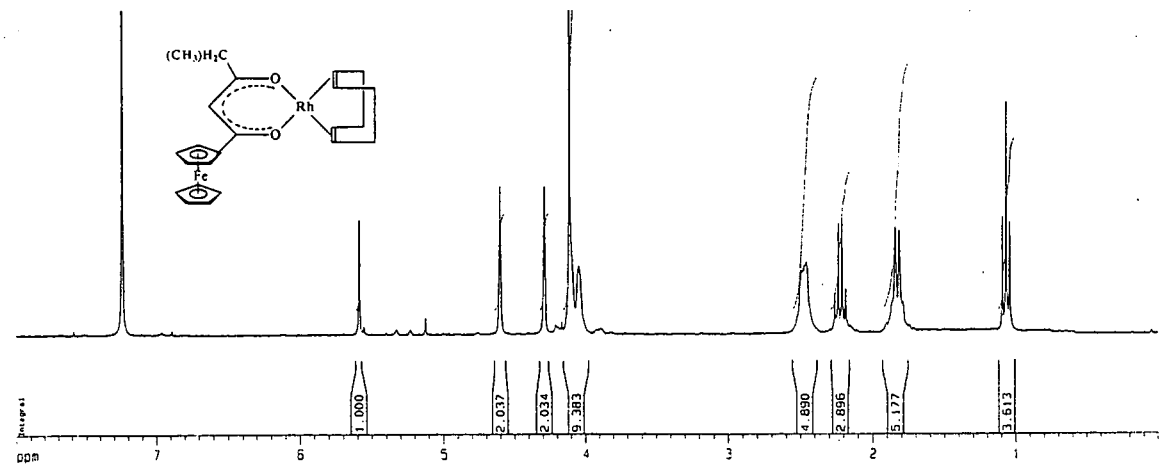

Spectrum 8: [Rh(fcp)(cod)], 12

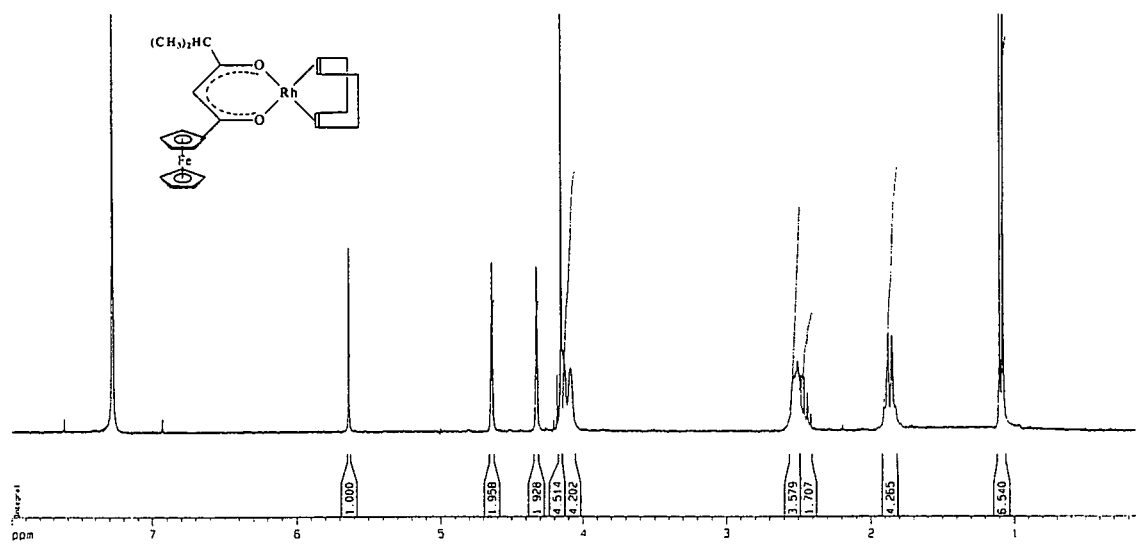

Spectrum 9: [Rh(fcdma)(cod)], 13

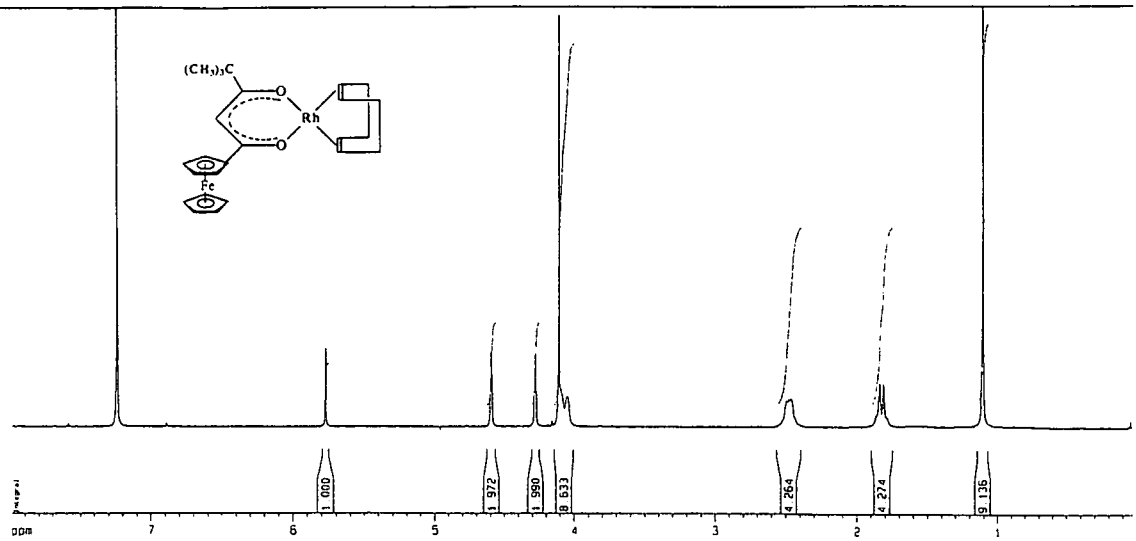

Spectrum 10: [Rh(fctma)(cod)], 14

ABSTRACT

Synthetic routes to prepare new ferrocene-containing β-diketones, $FcCOCH_2COR$, with Fc = ferrocenyl, R = H, CH_3, CH_2CH_3, $CH(CH_3)_2$ and $C(CH_3)_3$, have been developed. Rhodium complexes of the type [Rh(FcCOCHCOR)(cod)] were obtained in yields approaching 80% by treating these β-diketones with $[Rh_2Cl_2(cod)_2]$. Group electronegativities χ_R of R substituents were determined from a linear relationship between ethyl ester IR carbonyl stretching frequencies of the type $RCOOCH_2CH_3$ and group electronegativities of known R groups. pK_a' values of new β-diketones were determined. ^1H NMR studies on $FcCOCH_2COR$ indicated that enolisation in the direction furthest from the ferrocenyl group always dominate. This finding is considered to be the result of resonance driving force rather than inductive electronic effects of substituents on the pseudo-aromatic β-diketone core.

Formal reduction potentials ($E^{o'}$ values *vs.* Ag/Ag^+) of the iron core in the free β-diketones, $FcCOCH_2COR$, and in [Rh(FcCOCHCOR)(cod)] complexes as well as the peak anodic oxidation potentials, E_{pa}, of the rhodium(I) nucleus were determined. The roles of pK_a' and group electronegativities on redox potentials are also discussed.

Second-order rate constants, k_2, for the substitution of the β-diketonato ligand, $(FcCOCHCOR)^-$, from the complexes [Rh(FcCOCHCOR)(cod)] with 1,10-phenanthroline at 25°C in methanol were determined. Large negative values obtained for entropy of activation suggested an associative substitution mechanism. All substitution reactions were independent of a solvent step.

Cytotoxic properties in terms of potential anticancer applications of these newly synthesised β-diketones and their rhodium complexes on cancer cells are described. Cytotoxicity was tested on HeLa, A_{2780} and A_{2780} platinum resistant cancer cells lines. Rhodium complexes were observed to be more effective in killing cancer cells than the free β-diketones.

Keywords: Ferrocene, β-diketones, rhodium, group electronegativities, cyclic voltammetry, substitution kinetics and cytotoxicity.

OPSOMMING

Sintetiese prosedures ter bereiding van nuwe ferroseenbevattende β-diketone, $FcCOCH_2COR$, met Fc = ferroseniel, R = H, CH_3, CH_2CH_3, $CH(CH_3)_2$ en $C(CH_3)_3$, is ontwikkel. Rodiumkomplekse van die tipe [Rh(FcCOCHCOR)(cod)] in opbrengste van bykans 80% is verkry deur hierdie β-diketone met $[Rh_2Cl_2(cod)_2]$ te reageer. Groep elektronegatiwiteite, χ_R, van die R-substituente is bepaal vanaf direkte verwantskappe tussen etielester IR-karboniel strekkingsfrekwensies van die tipe $RCOOCH_2CH_3$ en groep elektronegatiwiteite van bekende R-groepe. pK_a'-waardes van nuwe β-diketone is bepaal. ^1H KMR studies van $FcCOCH_2COR$ het deurgaans gedui op dominante enolisasie in die rigting verste van die ferroseniel groep. Hierdie bevinding word beskou as die resultaat van resonansdryfkragte eerder as induktiewe elektroniese effekte van substituente op die pseudo-aromatiese β-diketoon kern.

Formele reduksiepotensiale ($E^{o\prime}$ waardes *vs.* Ag/Ag^+) van die yster kern in die vry β-diketone, $FcCOCH_2COR$, en in [Rh(FcCOCHCOR)(cod)] komplekse, sowel as die piek anodiese oksidasiepotensiale, E_{pa}, van rodium(I)kerne was bepaal. Die rol wat pK_a' en groep elektronegatiwiteite op redokspotensiale speel is ook bespreek.

Tweede-orde tempokonstantes, k_2, vir die substitusie van die β-diketonato ligand $(FcCOCHCOR)^-$, van komplekse [Rh(FcCOCHCOR)(cod)] met 1,10-fenantrolien by 25°C in metanol was bepaal. Die groot negatiewe waardes wat verkry is vir die aktiveringsentropie dui op 'n assosiatiewe substitusie meganisme. Alle substitusiereaksies was onafhanklik van 'n oplosmiddel stap.

Sitotoksiese eienskappe in terme van potensiële antikanker toepassings van hierdie nuut gesintetiseerde β-diketone en hulle rodiumkomplekse op kankerselle is beskryf. Sitotoksisiteit op HeLa, A_{2780} en A_{2780} platinum weerstandbiedende kankerselbelynings is getoets. Daar is bevind dat rodiumkomplekse meer effektief is as β-diketone in die vernietiging van kankerselle.

I, Palesa Klaas, declare that the dissertation hereby submitted by me for the Magister Scientiae degree at the University of Free State is my own independent work and has not previously been submitted by me at another university/faculty. I therefore cede copyright of the dissertation in favour of the University of the Free State.

Signed..... Date.....